A unifying framework for the modelling and analysis of STR DNA samples arising in forensic casework

Robert G. Cowell

February 28, 2018

Abstract

This paper presents a new framework for analysing forensic DNA samples using probabilistic genotyping. Specifically it presents a mathematical framework for specifying and combining the steps in producing forensic casework electropherograms of short tandem repeat loci from DNA samples. It is applicable to both high and low template DNA samples, that is, samples containing either high or low amounts DNA. A specific model is developed within the framework, by way of particular modelling assumptions and approximations, and its interpretive power presented on examples using simulated data and data from a publicly available dataset.

The framework relies heavily on the use of univariate and multivariate probability generating functions. It is shown that these provide a succinct and elegant mathematical scaffolding to model the key steps in the process. A significant development in this paper is that of new numerical methods for accurately and efficiently evaluating the probability distribution of amplicons arising from the polymerase chain reaction process, which is modelled as a discrete multi-type branching process. Source code in the scripting languages Python, R and Julia is provided for illustration of these methods. These new developments will be of general interest to persons working outside the province of forensic DNA interpretation that this paper focuses on.

Keywords: DNA profiles; forensic statistics; polymerase chain reaction; branching process; probability generating functions; Fast Fourier Transform.

Contents

Introduction

Genetic fingerprinting, also called DNA profiling, has grown to be an indispensable tool for identification of individuals in the investigative and judicial process associated with criminal cases. Judiciaries throughout the world have built up large databases of DNA profiles of convicted, and additionally in some cases non-convicted, individuals. These databases are based, in the main, upon short-tandem-repeat (**STR**) loci. Although newer DNA identification techniques based upon genomic sequencing (next generation sequencing) are being actively developed, the size of the currently existing databases, and the comparative low cost and reliability of the laboratory process for dealing with **STR** loci means that **STR** DNA profiling will remain in use for several years to some.

Ever since the pioneering work instigated by Jeffreys et al. (1985), advances of techniques in the collection and processing of crime scene DNA samples have led to forensic laboratories routinely processing small amounts of DNA, for example as may be contained in just a few cells extracted from a fingerprint. Indeed, current technology allows for the amplification of even as little DNA as is contained within one cell (Findlay et al., 1997). Such *low template DNA* (**LTDNA**) samples can present challenges to the forensic scientist in their interpretation. Such examples typically show signs of containing DNA from two or more persons. These **LTDNA** mixtures are also subject to various artefacts such as degradation, drop-in, drop-out and stutter which further exacerbate the problems of their interpretation. Over the years a variety of methods have been developed and applied to provide interpretation in court.

It is convenient to distinguish two phases of DNA processing. The first is the laboratory processing of the physical DNA. This part is described in detail in (Butler, 2011). The end result of this is one or more *electropherograms* (**EPG**s), described further in Section 1.2 below. Each **EPG** is then subject to interpretation by the forensic statistician; interpretation issues are described in detail in (Butler, 2014).

In recent years *probabilistic genotyping* models have been gaining acceptance within the forensic science community and in court for interpreting challenging DNA mixtures. These models typically describe themselves as *fully continuous*, by which is meant (at least as understood by the author) that they model the peak heights seen in the **EPG** as realisations of continuous random variables in statistical models for evaluating the *weight of evidence* of competing hypotheses presented to a court.

It is perhaps fair to say that that such models begin their interpretation with the

1

EPG, or **EPG**s in case of the analysis of multiple replicates from a sample, and that much of the information contained in the processing of the DNA sample that lead to the **EPG** is not used. It is the contention of this paper that, particularly for low template analyses, these steps need to be explicitly or implicitly incorporated into any statistical model for analysing **STR** DNA single source samples and mixtures. To not do so is to lose important information that could lead to biases or incorrect inferences. This paper presents a framework in which such information can readily be incorporated.

An early model for the whole process from sample to **EPG** was given by Gill et al. (2005). Their model was used only to simulate **EPG** peaks, in order to relate some of the parameters of their model to the procedures in their laboratory and observed values from **PCR** runs. The model was not concerned interpreting given **EPG**s. An **R** package (R Core Team, 2016) called `forensim` (Haned, 2013), implements the simulation model. Recently, another model for simulating **EPG**s has been proposed (Duffy et al., 2016).

The framework presented in this book can be thought of as an extensive elaboration of the simulation model of Gill et al. (2005). We say *framework* rather than *model* as many models may be derived from the framework; in addition the framework may be extended to cover other aspects of the processing not covered in this paper. One key elaboration, described in more detail below, is that the Gill et al. (2005) model starts the branching process simulation using amplicons; it ignores the fact that the **PCR** processing of real DNA samples starts with genomic strands. A second elaboration is that it does not take account of the tagging of amplicons with dyes so that they can be observed for the **EPG**. We incorporate explicitly such the tagging in our framework. We also extend the Gill et al. (2005) model to include forward and double backward stutters. Higher order stutters could also be included if desired, but because of their smallness relative to other peaks in the **EPG** they are not considered important (as they would be indistinguishable from noise).

However, not only can our framework be used to make simulated **EPG**s, but it can also be used for statistical interpretation. A key part of this is the use of *multivariate probability generating functions* to model the steps in the laboratory process leading to the **EPG**s. This provides a compact and elegant probability model, or rather set of models based on approximations that are assumed. Using standard techniques, means and variances of peak height distributions may be found from these generating functions, and these may be used to model peak height distributions using standard distributions, such as normal, lognormal or gamma distributions via moment matching. Such distributions have been used

in fully continuous models as simple and convenient distributions: in part this has been because there is no analytic form the for full distribution of amplicons arising in the **PCR** branching process. However, this paper shows that such full branching process distributions may be obtained efficiently from the probability generating functions; there is therefore no need for probabilistic genotyping software to assume simple standard distributions for peak height distributions. We show in examples that they do not capture the intricate *multi-modal* distributional behaviour of the full branching process that can occur for **LTDNA** samples.

This paper consists of three main parts. The first introduces background information to the objectives and problems of interpreting forensic DNA samples. The second part introduces elements of the mathematical approach used in the paper, and shows how full distributions can be efficiently computed for the branching processes by combining a specification in terms of probability generating functions with their evaluation using discrete Fourier transforms. The third part presents a detailed comprehensive framework for modelling forensic DNA problems, from which specific models may be formed by specialisation and approximations. It describes a particular model specialisation based on the general framework. The efficacy of the model is exhibited with simulated and real data.

Part I

Background

In this part of the paper we introduce background information to the problems we are addressing with the framework developed here.

1 DNA background

In this section some background information on DNA is introduced, sufficient for the remainder of the paper; readers unfamiliar with this background are recommended to consult (Butler, 2011, 2014) for more details.

1.1 Short Tandem Repeat (STR) markers

Forensic scientists encode an individual's genetic profile using the composition of DNA at various positions on the chromosomes. A specific position on a chromosome is called a *locus*, or *marker*. Human DNA has twenty three pairs of chromosomes: twenty two autosomal chromosome pairs and a sex-linked pair, the *X* and *Y* chromosomes.

The information at each (autosomal) locus consists of an unordered pair of *alleles*[1] which forms the *genotype* at that locus; a pair because chromosomes come in pairs, one inherited from the father and one from the mother, and unordered because it is not recorded from which chromosome of the pair each allele originates.

The loci used for forensic identification have been chosen for various reasons. Among these, we point out the two.

The first is that at each locus there is a wide variability between individuals in the alleles that may be observed. This variability can therefore be exploited to differentiate people.

The second reason is that, at least until recently, each (autosomal) locus is either on a distinct chromosome, or if a pair of loci are on the same chromosome then they are widely separated. When this occurs, the alleles at the various loci may be treated as mutually independent, thus simplifying the statistical analysis.

---

[1]This is also true for the Amelogenin locus which occurs on both X and Y chromosomes. However for other sex-linked loci the alleles might also possibly occur singly or not at all. For example a female does not have a Y chromosome, and so will not have an allele in any Y-linked locus.

However in recent years the numbers of loci used has increased, so that there are now some pairs loci that are close together on the same chromosome. We return to this issue of *genetic linkage* later.

The alleles of a marker are sequences of the four amino acid nucleotides *adenine, cytosine, guanine* and *thymine*, which we represent by the letters A, C, G and T. Each amino acid is also called a *base*, and because the DNA molecule has a double helix structure, each amino acid on one strand is linked to a complementary amino acid on the other strand; a complementary pair of amino acids is called a *base pair*.

An allele is typically named by its *repeat number*, usually an integer. For example, consider the allele with repeat number 5 (commonly also referred to as allele 5 for brevity) of the marker TH01. This allele includes the sequence of four nucleotides AATG repeated consecutively five times. It can be designated by the formula $[AATG]_5$. Likewise allele 8 of TH01 has eight consecutive repetitions of the AATG sequence, which may be denoted by $[AATG]_8$. Repeat numbers are not always integers. For example, allele 8.3 of TH01 has the chemical sequence $[AATG]_5ATG[AATG]_3$, in which '8' refers to the eight complete four-word bases $[AATG]$ and the '.3' refers to the three base-long word sequence ATG in the middle. Repeat numbers with decimal '.1' and '.2' endings are also possible, indicating the presence of a word of one or two bases. Note that the integer part of the repeat number counts how many complete words of four bases make up the allele sequence but the words need not be all identical and may vary even within loci. For example, allele 11 of the marker vWA has the base sequence $TCTA[TCTG]_3[TCTA]_7$. Also, some markers are based on tri- or pentanucleotide motifs rather than tetranucleotides as above. The base-letter sequences for many alleles may be found in Butler (2005).

When the repeat numbers of the two alleles of an individual at a marker are the same, then the genotype for that marker is said to be *homozygous*; when the repeat numbers differ, the genotype for that marker is said to be *heterozygous*.

The repetitive structure in the alleles gives rise to the term *short tandem repeat* (**STR**) marker to describe these loci; they also go by the name of *microsatellites*. Note that for other purposes of genetic analysis it is common to use single-nucleotide polymorphisms (SNPs) which are defined as DNA sequence variations that occur when a single nucleotide (A, T, C, or G) in the genome sequence is altered.

Forensic identification using **STR**s is based upon the size of the allele. However, for some loci, different people might not have the same nucleotide sequence for one or more alleles of a specific repeat number. This information is not used

by the framework developed in this paper, but is the basis of finer genetic discrimination available to the next-generation sequencing methods currently being developed that were mentioned in the introduction.

Within a population the various alleles of **STR** markers do not occur equally often, some can be quite common and some quite rare. When carrying out probability calculations based on DNA, forensic scientists use estimates of probabilities based on allele frequencies in profiles of a sample of individuals. The sample sizes typically range from a few hundred to thousands of individuals. For example, Butler et al. (2003) presents tables of US-population **STR**-allele frequencies for Caucasians, African-Americans, and Hispanics based on sample sizes of 302, 258 and 140 individuals. These are used to estimate the genetic profile probabilities of an individual: for the autosomal loci and the locus Amelogenin, independence of loci expressed through the lack of genetic linkage means that they may be found by multiplying probabilities across the loci. Although the **PCR** process described below applies to other sex-linked loci, the linkage of loci on the sex-linked loci presents special problems in estimating genetic profile probabilities. This issue will be addressed in another paper, although some of the discussion below will not be specific to autosomal loci.

1.2   The PCR process

The DNA collected from a crime scene for forensic analysis consists of a number of human cells from one or more individuals. Note that each cell of an individual will contain two alleles (diploid cells) for each autosomal marker, whereas sperm cells have only one allele (haploid cells). This means that in a mixture, a particular individual will contribute the same number of alleles for each marker. In order to identify the alleles that are present, a DNA sample is first subjected to chemical reagents that break down the cell walls so that the individual chromosomes are released into a solution. A small amount of this solution is used to quantify the concentration of DNA; the typical unit of measurement is picograms per microlitre, the DNA in a single human cell having a mass of between six and seven picograms. Having determined the density of DNA in the sample, a volume is extracted that is estimated to contain a certain quantity of DNA, typically around 0.5 nanograms, equivalent to around 75 human cells. The DNA in the extract is then amplified using the *polymerase chain reaction* (PCR) process. This involves adding *primers* and other biochemicals to the extract, and then subjecting it to a number of rapid heating and cooling cycles. Heating the extract has the effect of splitting apart the two complementary strands of DNA, the cooling phase then al-

lows free floating primers and amino acids to bind with these individual strands in such a way that the DNA is copied. By the action of repeated heating and cooling cycles, typically around 28 altogether, an initially small amount of DNA is amplified to an amount large enough for quantification. Mathematically, the amplification process may be modelled as a branching process (Sun, 1995; Stolovitzky and Cecchi, 1996a). The amplification process is not 100% efficient, that is, not every allele gets copied in each cycle. This means that if two distinct alleles in a marker are present in the extract in the same amount prior to amplification, they will typically occur in different amounts at the end of the PCR process.

Note that after breaking down the cell walls to release the genomes, there could be sufficient DNA in the sample to carry out several independent PCR amplifications with sub-extracts. When this is done it is called a *replicate run*.

To understand the quantification stage of the post PCR amplified DNA, it is important to know that the amplification process does not copy only the repeated DNA word segment of a marker, it also copies DNA at either end. These are called *flanking regions*, and their presence is important in performing the PCR process. Regions at either end of the flanking region, called *primer binding regions*, are where the primers bind to the DNA to initiate copying. These regions are labelled as 5' and 3'; there is one for each of the two strands making up the double helix of the DNA. During the heating cycle the double helix separates into two strands, which for reasons that will become apparent later we denote by the two genomic strands by g and g_d. During the cooling phase one of the strands primers will bind at the 5' end, and on the other at the 3' end. After the primers have attached the Taq polymerase adds individual bases to complete the copying. This leads to two strands that we call h and h_d, (with h for $h$alf-strand).

The process is illustrated in the following sequence of figures. In the first figure we have a fragment of DNA consisting of two complimentary joined strands g and g_d which are long enough to contain the repeat structure of an allele of interest and primer binding regions on either side of the allele. The 'teeth' in the figure indicates the individual bases making up each strand.

Heating breaks the bonds of the base-pairs of the DNA molecule, so separating the strands. During cooling primers,indicated by the smaller sets of teeth. bind to

each of the 5' ends of the strands. Note that the sequences of bases in the primers attaching to the two ends are in general different, because of the differences in the base sequence in the primer-binding regions of the two strands.
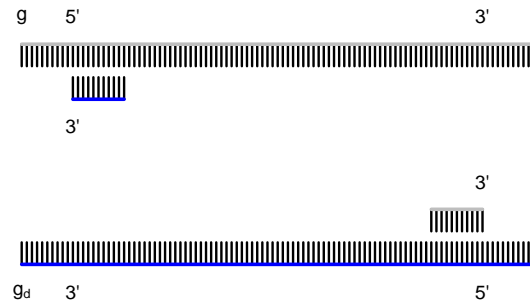
After the primer binds at one end the Taq polymerase extends to copy to beyond the primer region at the other end. The g strand generates the h_d strand for its copy, and the g_d strand the h strand for its copy.
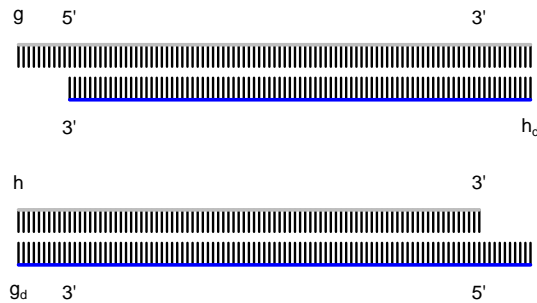
During the next heating cycle the g/h_d strand pair separate, and the g_d/h pair separate. The g and g_d strands repeat the process as above. During the cooling phase, primers bind to the 5' ends of the h and h_d strands,
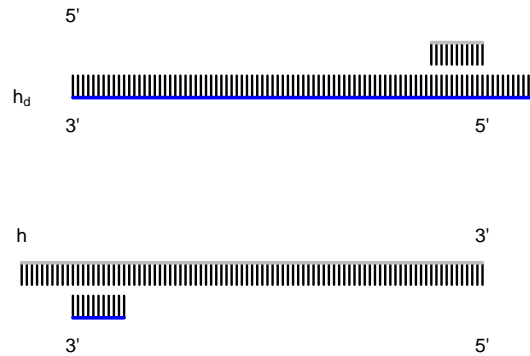
and the Taq polymerase adds bases to the ends, thus making with the *h* strand a complementary a_d strand, and with the h_d strand, a complementary *a* strand.
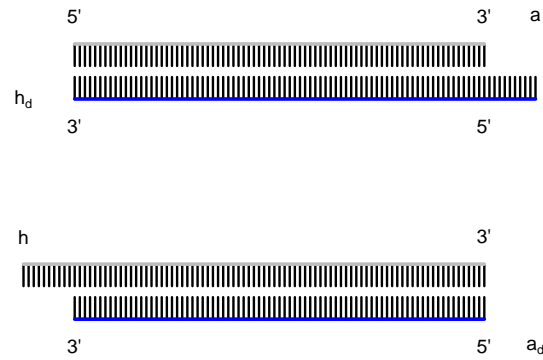
During the next heating cycle the h/a_d strand pair separate, as does the h_d/a strand pair. The *h* and h_d strands behave as above (as the *g* and g_d strands continue to do so as well). Primers bind at the 5' ends of the *a* and a_d strands,
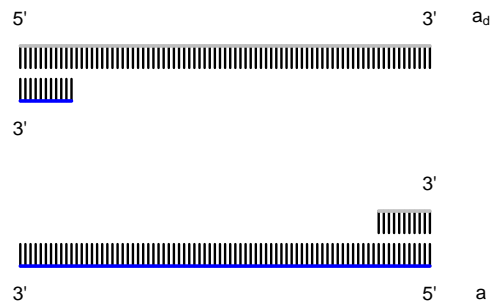
and the Taq polymerase completes the copy, so that the *a* strand makes a complimentary a_d strand, and the a_d strand makes a complimentary *a* strand.

Thus an amplified allele will consist of the allele word repeat sequence region and two flanking regions, and will have a length associated with it which is

measured in the total number of base pairs included in the word sequence and the flanking regions. This is called an *amplicon*.

Repeat region

5' 3' a_d

3' 5' a
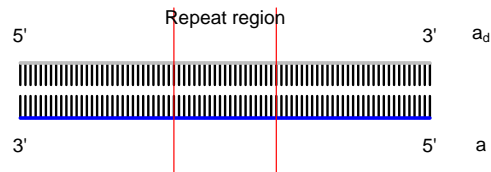
Further heating cycles lead to an exponential growth in the number of *a* and a_d strands with the number of cycles. After around 28 or 29 cycles there is a sufficient number of amplicons to measure their amount.

For each marker, the DNA sequence (hence the size) forming each of the two flanking regions is constant, but different across markers. Thus quantifying a certain allele is equivalent to measuring how much DNA is present of a certain size. This is carried out by the process of *electrophoresis*, as follows.

During the binding of primers a fluorescent dye is also attached. We said earlier that the primers for the two ends of the strand are different. Typically dyes are attached to only of the two types or primers: we can now reveal that the *d* subscript used in the description indicates the presence of a dye tag, thus a_d represents the strand in the complementary pair of strands making up the dye-tagged amplicon, and *a* other strand that is not tagged with a dye. (Note that h_d represents a dye-tagged half-strand, but that g_d strands are not dye tagged. However it simplifies notation to treat the g_d as if they are, rather than introduce another symbol to distinguish the *g* strand from its compliment.) For brevity in the remainder of the paper, we shall refer to a_d as a dye-tagged amplicon, and *a* and an untagged amplicon.

Hence we wish to measure the number of dye-tagged amplicons, a_d. The description above has assumed 100% efficiency in the amplification process. However, not every strand will get a primer attached in each cycle, and the **PCR** process will operate at less than 100% efficiency. Typical amplification efficiencies are in the range 0.8-0.9.

Several colours of fluorescent dyes are used to distinguish similarly sized alleles from different markers. The amplified DNA is drawn up electro-statically through a fine capillary to pass through a light detector, which illuminates the DNA with a laser and measures the amount of fluorescence generated. The latter is then an indication of the number of alleles tagged with the fluorescent marker. The longer alleles are drawn up more slowly than the shorter alleles, however alleles of the same length are drawn up together. This means that the intensity of the

detected fluorescence will sharply peak as a group of alleles of the same length passes the light detector, and the value of the intensity will be a measure of the number of alleles that pass. The detecting apparatus thus measures a time series of fluorescent intensity, but it converts the time variable into an equivalent base pair length variable. The data may be presented to a forensic scientist as an *electropherogram* (**EPG**) as illustrated by the simulated **EPG** shown in Figure 1. Each panel in the EPG corresponding to a different dye. The horizontal axes indicate the base pair length, and the vertical axis the intensity.
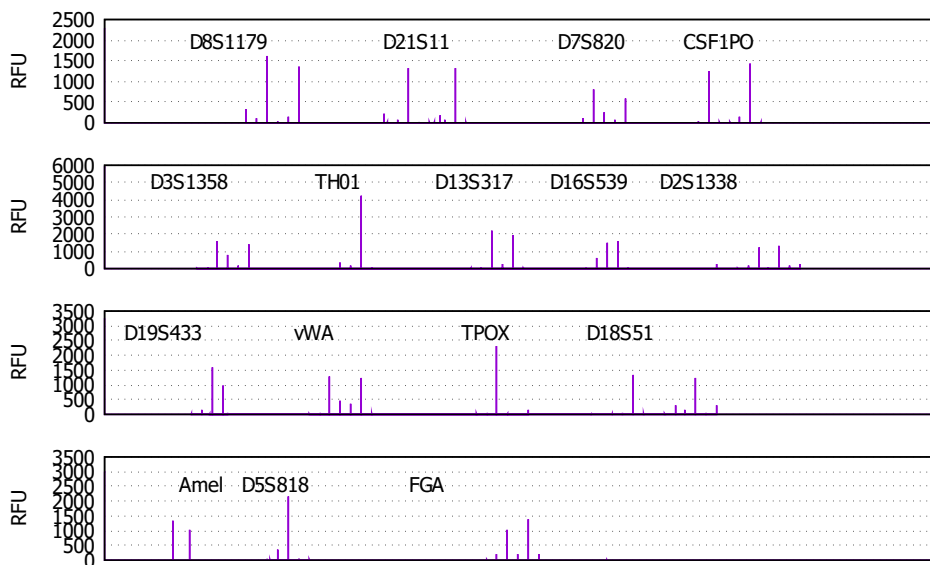
Figure 1: Schematic of an electropherogram plot for a simulated 3-person mixture, for the Identifiler Plus[TM] STR kit of the Amelogenin locus and 15 autosomal loci. Each of the four panels represents a dye. On the left-hand side of each panel the scale of RFU is indicated. The horizontal scale (not shown) is in units of base-pairs, with a range of between 50 to 450 for the plots. Each vertical spike represents an allele.

In the absence of artefacts, a peak in the **EPG** indicates presence of an allele in the sample before amplification. The peak height is a measure of the amount of the allele in the amplified sample expressed in *relative fluorescence units* (RFU). The area of the peak is another measure of the amount, but this is highly correlated with the height (Tvedebrink et al., 2010). Both peak height and peak area are determined by software in the detecting apparatus.

We shall call the peak size information extracted from the **EPG** the *profile of the DNA sample*, or more briefly, the DNA profile. Commonly, DNA profile also refers to the combined genotype of a person across all markers.

In measuring the peak heights, low level noise give rise to small spurious peaks. A *peak amplitude threshold*, called the *analytic threshold*, may be set by the forensic analyst whereby peaks below the analytic threshold level are ignored. Thus an allele present in the DNA sample will not be recorded as observed if the peak it generates is below the analytic threshold; when this happens a *dropout* of the allele is said to have occurred. A dropout of an allele can also occur if no genomic strands containing the allele are selected for amplification. Dropout is an artefact that can make the analysis of DNA samples difficult. Another common artefact is *stutter*, whereby an allele that is present in the sample is mis-copied at some stage in the PCR amplification process, and (for a tetraneucleotide marker) a four base pair word segment is omitted. This damaged copy itself takes part in the amplification process, and so yields a peak located four base pairs[2] below the allele from which it arose. More rarely, two repeats are omitted during a **PCR** cycle, which is called *double stutter*, or an extra repeat is inserted, which is called *forward stutter*; once formed these artefacts can themselves replicate in subsequent cycles.

Another artefact is known as *dropin*, referring to the occurrence of small unexpected peaks in the EPG. This can for example be due to sporadic contamination of a sample either at source or in the forensic laboratory.

Finally, a mutation in the flanking region can result in the allele not being picked up at all by the PCR process, in which case we say that the allele is *silent*. An allele can also be undetectable and thus *de facto* silent because its length is off-scale and the peak does therefore not appear in the **EPG**. Note that an allele might be silent for a kit made by one manufacturer but not another; this is because different manufacturers of kits for performing **PCR** use different primer binding regions.

2   From sample to EPG

In this section we give a description of the process of going from a DNA sample, recovered for example from a crime scene, to the electropherogram (**EPG**) that is used to make inferences about the constitution of the DNA in the sample. For a

---

[2]For tetrameric loci.

much more detailed account of the laboratory processes please see (Butler, 2011).

We start with a descriptive summary, and follow this with a more detailed mathematical specification.

2.1 Steps in the process

The following is a summary of the sequence of steps taken to obtain an **EPG** from a DNA sample, recovered for example at a crime scene; Figure 2 illustrates the sequence of steps involved.

1. Collect sample of DNA. The sample might be a single source trace, that is, it contains DNA from a single individual, or it could be a mixture, that is a trace with DNA originating from two or more people.

2. Take a sub-sample of the sample and using bi-chemical reagents extract nuclear DNA to create an aliquot (solution of extracted DNA- check this is the correct meaning). Typically this will be in a mini-tube of a volume of between $50\mu L$ to $100\mu L$, depending on laboratory standard operating procedures.

3. Take a small extract of the aliquot, typically around $2\mu L$, to determine the concentration of DNA in the aliquot. Usually this will be carried out using **qPCR** (Butler, 2011), so that (if possible) an optimal amount DNA can be used for the **PCR** step.

4. Based upon the estimated density of DNA in the aliquot, take enough of the aliquot for **PCR** amplification so that there is an optimal amount of genomic DNA in the mini-tube for the **PCR** amplification is to be carried. For **LTDNA** samples, obtaining a sufficient amount might not be possible. Typically a maximum volume of $20\mu L$ is taken from the aliquot, so that there is sufficient volume left in the PCR mini-tubes for the PCR primers. In some cases the aliquot is split into several parts called *replicates* and each is separately amplified via **PCR**.

5. Carry out the **PCR** amplification of each replicate using some kit and protocol. Usually, but not always, the same manufacturer kit is used for all of the replicates when more than one replicate is made.

6. An **EPG** is then produced from each replicate by capillary electrophoresis.
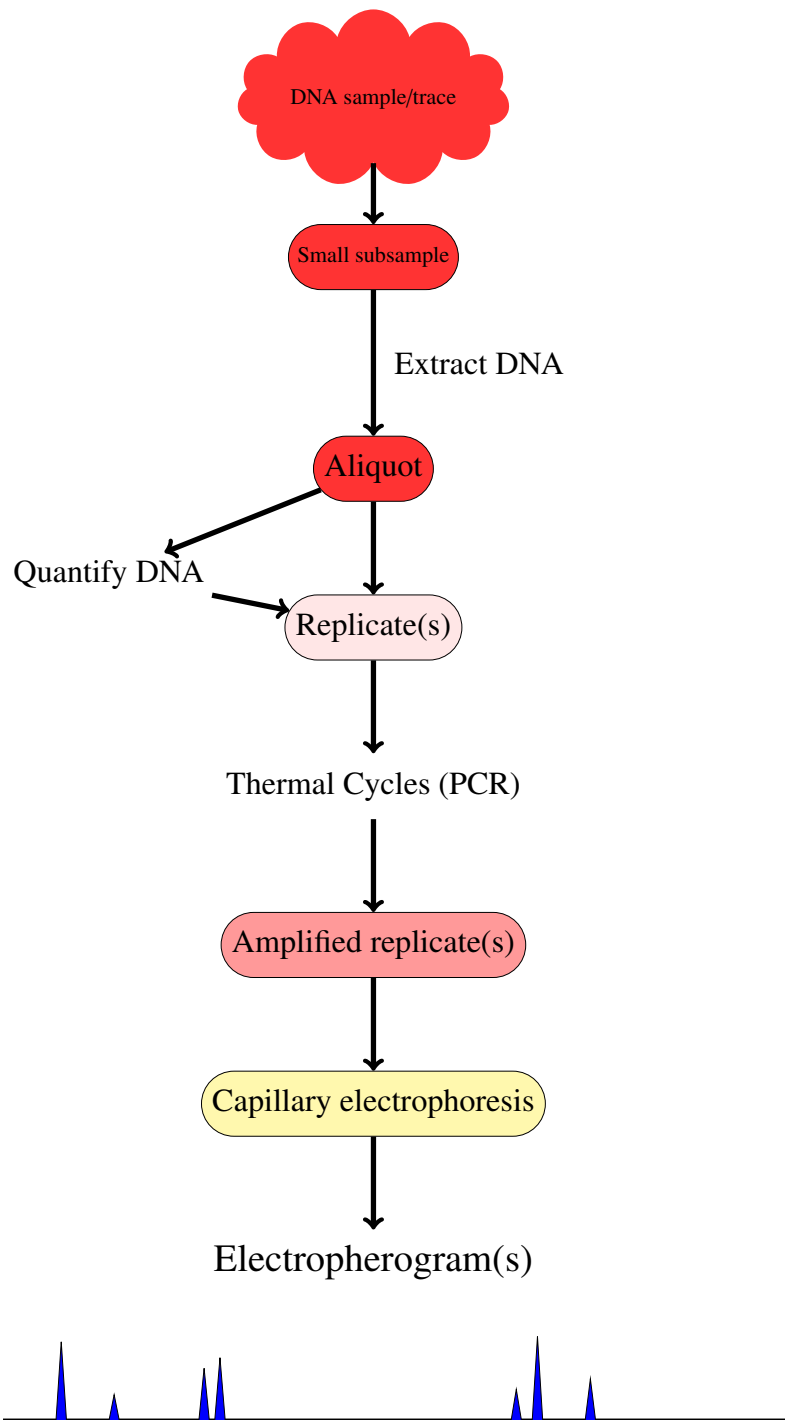
Figure 2: Overview of the sequence of steps to produce an electropherogram from a DNA sample.

3 The objectives of an EPG analysis

In the previous sections we have given a brief qualitative description of how we obtain an **EPG** from a DNA sample. In this section we describe the information a forensic scientist wishes to obtain from an **EPG**. In later sections we develop a mathematical framework to help realise those aims.

A forensic scientist may wish to use the information in an **EPG** to calculate the *weight of evidence* for two competing hypotheses regarding the contributors to the DNA sample; another objective is to try and identify the likely genotypes of contributors (Perlin and Szabady, 2001; Wang et al., 2006; Tvedebrink et al., 2012b), a process known as *deconvolution*.

We consider each of these objectives in turn.

Weight of evidence In an adversarial court setting, we have two competing hypotheses, one argued for by the prosecution, called the *prosecution hypothesis* $\mathcal{H}_p$, the other called the *defence hypothesis* $\mathcal{H}_d$. Note that the defence is not obliged to propose an alternative to the prosecution hypothesis $\mathcal{H}_p$; usually the defence hypothesis is proposed by the prosecution for comparative purposes. The available *evidence E* in the case consists of the peak heights as observed in the **EPG** as well as the set of genotypes of some known individuals; denote the known genotype information by G. The prosecution and defence hypotheses differ in their assumptions as to whose DNA is in the sample that produced the **EPG**. In most cases where a suspect S is on trial, the prosecution case would be that S contributed to the sample and the defence case that S did not. However this is not always the case. For example, a DNA sample might be recovered from a swab of an area of skin of the suspect where physical contact is alleged to have been made during an assault on a victim V. Under this scenario, the presence of S's DNA in the sample is not disputed, it is the presence of the victim's DNA offered by the prosecution as proof of the assault that is disputed.

The strength of the evidence (Good, 1950; Lindley, 1977; Balding, 2005) is normally represented by the *likelihood ratio*:

$$LR = \frac{L(\mathcal{H}_p)}{L(\mathcal{H}_d)} = \frac{\Pr(E \,|\, \mathcal{H}_p)}{\Pr(E \,|\, \mathcal{H}_d)}.$$

This may be expressed on a base-10 log scale of units called the *ban*, introduced by Alan Turing (Good, 1979) so that one ban represents a factor 10 on the likelihood ratio. Then the *weight of evidence* is WoE $= \log_{10} LR$ in bans (Balding, 2013).

The numerator and denominator in the likelihood ratio are calculated based on models having the form

$$\Pr(E \,|\, \mathcal{H}, G) = \sum_{\mathbf{g}} \Pr(E \,|\, \mathbf{g}) \Pr(\mathbf{g} \,|\, \mathcal{H}, G), \tag{1}$$

so that the model for the conditional distribution $\Pr(E \,|\, \mathbf{g})$ of the evidence given the genotypes $\mathbf{g}$ of all contributors is the same for both hypotheses, whereas the hypotheses differ concerning the distribution $\Pr(\mathbf{g} \,|\, \mathcal{H}, G)$ of genotypes of the contributors. Note that the genotypes $\mathbf{g}$ that are summed over may include those of one or more *unknown contributors*, that is, individuals whose genetic profiles are not known (not included in G).

Note that $\Pr(E \,|\, \mathbf{g})$ has a dependence, not shown, on the amount of DNA from each contributor in the sample, and other factors such as sample degradation: this implies a similar implicit dependence for the left hand side.

Deconvolution of DNA mixtures In the deconvolution of a DNA sample, typically a mixture, we assume that there are one or more genetically untyped contributors to the DNA sample. We then wish to find the genotypes of these untyped individuals. Typically how this is done is that for each individual separately a ranked list of genetic profiles ordered by their likelihood is produced. The potential profiles having high likelihood could, for example, be checked against an offender database for a match. However, sometimes a ranking of the joint genotypes of two or more individuals may also be of interest.

Part II
Mathematical formulation

In this part of the paper we give the mathematical notation underpinning the framework of this paper. From the right hand side of (1) we see that there are two components of the framework that require specification. One part is specifying the (conditional) probability for the **EPG** data, $\Pr(E\,|\,\mathbf{g})$, the other specifying the genetic profile probabilities, $\Pr(\mathbf{g}\,|\,\mathcal{H},G)$. As the latter is relatively uncontroversial, and is common to all models for the $\Pr(E\,|\,\mathbf{g})$ distribution, we discuss that first. We then discuss the simulation model of Gill et al. (2005), and show how the full distribution may be obtained without simulation. We then extend the analysis to finding the distribution for the more realistic model in which we start with genomic strands and we find the distribution of dye-tagged amplicons. We then elaborate this in stages leading to the general framework that includes background noise, drop-in, forward and double-reverse stutters, degradation and inhibition, for possibly multiple replicates analysed with possibly multiple kits from possibly multiple independent samples.

4   Specifying genetic profile probabilities

Given the genotypes of contributors, the framework formulated in this paper for specifying peak-height likelihoods is applicable to any type of STR locus, that is for evaluating $\Pr(E\,|\,\mathbf{g})$. However, if there are untyped contributors, evaluation of $\Pr(\mathbf{g}\,|\,\mathcal{H},G)$ can be problematic for sex-linked loci. In this paper we shall assume that the set of loci are all autosomal loci plus, optionally, Amelogenin. We shall also assume that all contributors are unrelated. With these assumptions (1) simplifies to a product over the loci L, with $\mathbf{g_l}$ denoting a genotype in the set G_l of genotypes on the locus $l \in L$:

$$\Pr(E\,|\,\mathcal{H},G) = \prod_{l \in L}\left(\sum_{\mathbf{g_l}} \Pr(E\,|\,\mathbf{g}) \Pr(\mathbf{g_l}\,|\,\mathcal{H},G_l) \right), \qquad (2)$$

We assume that the population from which each contributor comes from is known, and that allele frequency estimates are available. We do not assume that the contributors all come from the same population. It is assumed that populations substructure correction parameters are known for each population. Optionally, the

finite size database correction of (Cowell, 2016) may be applied. We do not have to be concerned with linkage between autosomal loci because of the assumption that contributors are unrelated. Relatedness amongst contributors could be incorporated, but at the cost of complicating the presentation presented here, especially if there are linked loci. For a detailed discussion of these issues relating to populations and genotype probability estimation, as they relate to forensic applications, see (Evett and Weir, 1998; Balding and Steele, 2015; Egeland et al., 2015). A companion paper by the author is planned that proposes solutions to the twin problems of Y-STR haplotype probability estimation and the resolution of Y-STR mixtures.

5 The simulation model of Gill et al. (2005): the amplicon model

In this section we summarise the simulation model of Gill et al. (2005), for further details please see the original paper. We shall refer to this model as the *amplicon model*.

The model presented in Gill et al. (2005) has variants for diploid cells and haploid cells. As mentioned earlier, their model fails to take account of the fact that the process starts with genomic material rather than amplicons, and it also ignores the dye-tagging of the amplicons during the **PCR** process. Despite these short-comings, the model provides a convenient starting point for the more realistic models presented later. We start off with the case of no stutters;

5.1 Simulating the process without stutters

The model of Gill et al. (2005) is a simulation model. It assumes that initially we have a number n_c of cells in our small subsample of Figure 2. We concentrate on just one allele from one locus. If the cell is diploid, and the individual is homozygous, then there will be $2n_c$ such amplicons within the cells to start with; otherwise if the individual is heterozygous on the locus, or the cell is haploid, then there will be n_c such amplicons in the cells to start with. For whichever case holds, denote by N the total number of amplicons initially.

In the first stage the amplicons are extracted from the cells. This process is not 100% efficient, more typically only between 10-30% are extracted intact (Gill et al., 2005). Following Gill et al. (2005), let π_{eff} denote the extraction probability

that an individual amplicon is released intact into the aliquot. Assuming independence of the release of the distinct amplicons, the total number of intact amplicons in the aliquot is therefore binomially distributed with distribution $\text{Binom}(N, \pi_{eff})$.

A fraction of the aliquot $\pi_{aliquot}$ is then taken for **PCR**. If we let $\phi = \pi_{eff}\pi_{aliquot}$, then the total number of amplicons intact and selected for amplification will be Binomially distributed as $\text{Binom}(N, \pi_{eff}\pi_{aliquot}) \equiv \text{Binom}(N, \phi)$.

These are now subject to **PCR** amplification, where it is assume that in each cycle, each amplicon makes a copy of itself with probability π_{pcr} If we assume that there are K cycles, then the total number of amplicons can be simulated using the following algorithm, starting with N amplicons:

Algorithm 5.1 [SIMPLE AMPLICON **PCR** SIMULATION]

- Randomly sample n from $\text{Binom}(N, \phi)$.

- For K times do:

    - Sample m from $\text{Binom}(n, \pi_{pcr})$
    - Update $n := n + m$
    $\square$

This algorithm is very simple to implement. If it is run many times, a histogram, or kernel density estimate, plot may be made of the distribution of the number of amplicons.

Python code presented in Appendix E.1.1 produced the kernel density plot shown in Figure 3, based on a million simulations. The parameter values used were $\pi_{eff} = 0.6$, $\pi_{aliquot} = 20/66$, $\pi_{PCR} = 0.8$ and $K = 28$ cycles (values taken from the Gill et al. (2005) paper), for a single starting amplicon, $N = 1$. Note that for each simulation there is a probability $\phi = 0.6 \times 20/66 = 2/11$ that the amplicon is selected for amplification , so that we have a total dropout probability of $9/11$. As this will dwarf the rest of the plot, these zeros have been removed before the kernel density has been estimated.

5.2 Generating the full distribution (without stutters)

We now show how the simulation model can be represented by using probability generating functions, following the approach of (Good, 1949) based on Galton-Watson cascade processes. Consider an initial single amplicon. In the first PCR cycle it can either amplify with probability π_{PCR}, or fail to amplify with probability
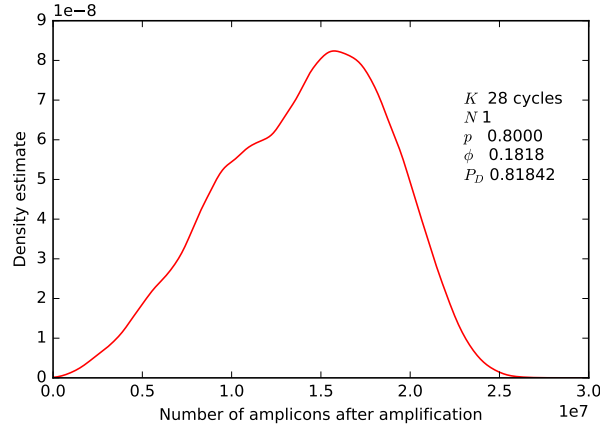
Figure 3: Kernel density estimate, based on 1 million simulations, of the final number of amplicons, starting with a single amplicon selected with probability $\phi = 2/11$ for **PCR**, and amplified for 28 cycles with amplification probability of 0.8 per cycle if selected. The estimated total drop-out probability is 0.81842, compared to the theoretical value of $9/11 = 0.81818\cdots$. Note that the zero amplicon values have been removed prior to the kernel density estimate, hence the kernel density estimate is for the conditional probability of the number of amplicons after the 28 amplification cycles, *given* that one is selected for amplification.

$1 - \pi_{PCR}$. The probability distribution of the number of alleles after one cycle can therefore be represented by the *probability generating function* (**PGF**):

$$F_1(t) = f(t) = (1 - \pi_{PCR})t + \pi_{PCR}t^2.$$

After two **PCR** cycles the number of alleles has the **PGF**

$$F_2(t) = f(f(t)),$$

and after 3 cycles it has the **PGF**

$$F_3(t) = f(f(f(t))).$$

More generally, we have

Theorem 5.1 *The **PGF** for the number of molecules after r **PCR** cycles, given that there is exactly one prior to any amplification cycle, is*

$$F_r(t) = f(f(f(\ldots f(t)\ldots))) \tag{3}$$

20

where

$$F_1(t) = f(t), \quad F_{s+1}(t) = f(F_s(t)), \quad (s = 1, 2, 3, \ldots). \tag{4}$$

This is Theorem 1 of Good Good (1949) (but here specialised to $F(t)$ given above).

The above gives the **PGF** for a single starting amplicon: if there are K cycles the **PGF** will be a polynomial in t of degree 2^K. However, for the simulation model we start not with a amplicon, but with N initial amplicons, that are each sampled independently for amplification with probability ϕ. The **PGF** taking into account the initial number and the pre-**PCR** sampling is (Cowell, 2009)

$$(1 - \phi + \phi F_K(t))^M$$

a polynomial of degree $M \times 2^K$. This is simply the functional composition of the Binomial **PGF** $(1 - \phi + \phi t)^N$ for the pre-**PCR** sampling of the amplicons with the **PGF** of the number of amplicons arising from a single amplicon in the **PCR** branching process.

Let us rewrite the recursion in (4) on substituting $f(t)$; for later convenience we also replace π_{PCR} by p_t, thus the recurrence relation becomes:

$$F_{s+1}(t) = (1 - p_t)F_s(t) + p_t F_s(t)^2.$$

with initial value $F_0(t) = t$. It is in principle possible to find the polynomial $F_K(t)$ quite simply by iteration using a computer algebra package, however the growth in the numbers of terms in the polynomials means that there is a relatively small limit to the number of iterations that can be carried out before computer memory is exhausted of the order of $K = 10$ or so, even if numerical values for p_t are used. In addition in the later stages, the brute force evaluation of the quadratic term $F_s(t)^2$ grows quadratically in complexity, thus making the later stages of iterations slower and slower.

There is however another way to evaluate the **PGF** numerically, by noting that the quadratic expression $F_s(t)^2$ is simply the **PGF** of the convolution of two (identical) probability distributions. The convolution can be carried out using a *Discrete Fourier Transform* (**DFT**), which may be done efficiently using a *Fast Fourier Transform* (**FFT**). Moreover, as we shall show, the binomial sampling composition can also be carried out using the **FFT**. Before given the details, the reader may care to look at Figure 4, which shows the exact distribution for a single starting amplicon evaluated using the **FFT**.
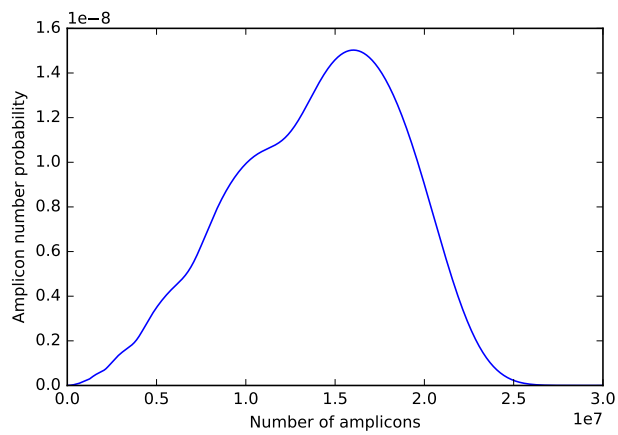
Figure 4: Exact probability distribution for the total number of amplicons, starting with a single amplicon selected with probability $\phi = 2/11$ for **PCR**, and amplified for 28 cycles with amplification probability of 0.8 per cycle if selected. The complete drop-out probability value of $9/11$ at 0 is off the scale of the plot. Unlike Figure 3, the plot shown here is not conditional on selection, which is why the vertical scales of the two plots differ.

The discrete Fourier transform

Before presenting the algorithm for generating the full distribution using the **FFT**, we first give a brief review of the **DFT**. Suppose that a sequence of (real) numbers $(x_0, x_1, x_2, \ldots, x_{n-1})$ is given, and an integer $N \geq n$. Then the sequence of numbers defined by

$$X_k = \sum_{j=0}^{N-1} x_j e^{-2\pi i jk/N},$$

where $i = \sqrt{-1}$, is the discrete Fourier transform of the sequence $(x_0, x_1, x_2, \ldots, x_{n-1})$. There is an inversion formula:

$$x_k = \frac{1}{N} \sum_{j=0}^{N-1} X_j e^{2\pi i jk/N}$$

The key result that we use is that multiplication of two large polynomials may be done efficiently using the **DFT**, which may be calculated efficiently using the **FFT**. Suppose that $x(t)$ is a polynomial of degree n in t with coefficients $(x_0, x_1, x_2, \ldots, x_n)$, and that $y(t)$ is a polynomial of degree m in t with coefficients $(y_0, y_1, y_2, \ldots, y_m)$. Let $z(t) = x(t)y(t)$; this is a polynomial of degree $m + n$ with coefficients $(z_0, z_1, \ldots z_{n+m})$ where

$$z_k = \sum_{j=0}^{k} x_j y_{k-j},$$

(defining $x_j = 0$ for $j > n$ and $y_{k-j} = 0$ for $k - j > m$). Let N be an integer such that $N \geq n + m + 1$. if we extend the sequence $(x_0, x_1, x_2, \ldots, x_n)$ with zeros to create a new sequence $(x_0, x_1, x_2, \ldots, x_{N-1})$, and similarly extend the sequence $(y_0, y_1, y_2, \ldots, y_m)$ with zeros to create a new sequence $(y_0, y_1, y_2, \ldots, y_N)$, then we may form the **DFT** of these extended sequences:

$$X_k = \sum_{j=0}^{N-1} x_j e^{-2\pi i jk/N}$$

$$Y_k = \sum_{j=0}^{N-1} y_j e^{-2\pi i jk/N}$$

23

If the sequence $(z_0, z_1, \ldots z_{n+m})$, extended with zeros if required to make the sequence $(z_0, z_1, \ldots z_{N-1})$, then the **DFT** of this sequence is

$$Z_k = \sum_{j=0}^{N-1} z_j e^{-2\pi i jk/N}$$

and we have that

$$Z_k = X_k Y_k \quad \text{for all } k \in \{0, N-1\}.$$

so that

$$z_k = \frac{1}{N} \sum_{j=0}^{N-1} X_j Y_j e^{2\pi i jk/N}$$

Hence to multiple the polynomials $x(t)$ and $y(t)$, we choose N sufficiently large, take the **DFT**s of the coefficients of $x(t)$ and of $y(t)$, multiply the two **DFT**s termwise, and then take the inverse **DFT**. The computation of the forward and backward **DFT** may be carried out efficiently using the **FFT** algorithm, an algorithm by Gauss that dates back to 1805 (see (Heideman et al., 1984) for an interesting history of the **FFT**, and (Rao et al., 2011) for a recent monograph on **FFT** algorithms.).

We can now present an algorithm for generating the full distribution using the **DFT**. It is given in Algorithm 5.2 for the case of a single starting amplicon and no binomial presampling. Let $F[]$ be a vector with indices starting from zero, such that $F[n]$ denotes the coefficient of t^n in the **PGF**. With K cycles, the number of amplicons will range up to 2^K, hence $F[]$ must be a vector of size at least $2^K + 1$.

Algorithm 5.2 [Single amplicon distribution using the **DFT**]

- Initialise $F[]$ to be a vector of size at least $2^K + 1$, with all entries 0 except $F[1] = 1$.

- Let $\mathcal{F}[]$ denote the **DFT** of $F[]$.

- For K times do:

    - for each element $\mathcal{F}[f]$ of $\mathcal{F}[]$ update $\mathcal{F}[f] := (1 - p_t)\mathcal{F}[f] + p_t\mathcal{F}[f]^2$

- Set $F[]$ equal to the inverse **DFT** of $\mathcal{F}[]$. $\qquad\qquad\square$

Note that taking the **DFT** is a linear operator; denote it by L and its inverse by L^{-1}. Hence we may write (with $\times$ denoting element wise multiplication)

$$
\begin{aligned}
F_{s+1}(t) &= (1 - p_t)F_s(t) + p_t F_s(t)^2 \\
&= (1 - p_t)F_s(t) + p_t L^{-1}(L(F_s(t)) \times L(F_s(t))) \\
&= (1 - p_t)L^{-1}(L(F_s(t)) + p_t L^{-1}(L(F_s(t)) \times L(F_s(t))) \\
&= L^{-1}\left((1 - p_t)L(F_s(t)) + p_t L(F_s(t)) \times L(F_s(t))\right),
\end{aligned}
$$

thus justifying Algorithm 5.2.

Taking account of starting with M amplicons, and binomially sampling them with probability ϕ is almost trivial. We have, using the linearity of L and its inverse:

$$
\begin{aligned}
(1 - \phi + \phi F_K(t))^M &= L^{-1}L\left((1 - \phi + \phi F_K(t))^M)\right) \\
&= L^{-1}\left((L(1 - \phi) + \phi L(F_K(t))^{\times M}\right)
\end{aligned}
$$

where the superscript $^{\times M}$ denotes taking the M-th power of each element in the transform. Hence to take this into account we modify Algorithm 5.2 thus, (extending the initial size of $F[]$ for the higher number of amplicons that could result):

Algorithm 5.3 [AMPLICON DISTRIBUTION WITH BINOMIAL PRE-SAMPLING USING THE **DFT**]

- Initialize $F[]$ to be a vector of size at least $M(2^K + 1)$, with all entries 0 except $F[1] = 1$.

- Let $\mathcal{F}[]$ denote the **DFT** of $F[]$.

- For K times do:

  - for each element $\mathcal{F}[f]$ of $\mathcal{F}[]$ update $\mathcal{F}[f] := (1 - p_t)\mathcal{F}[f] + p_t \mathcal{F}[f]^2$

- for each element $\mathcal{F}[f]$ of $\mathcal{F}[]$ update $\mathcal{F}[f] := (1 - \phi + \phi \mathcal{F}[f])^M$.

- Set $F[]$ equal to the inverse **DFT** of $\mathcal{F}[]$. $\qquad\square$

Now the extreme right-hand tail of the amplicon distribution has very low probabilities, and for all practical intents and purposes can be taken to be zero. Hence we may take the $F[]$ vector to have size $M2^K$ which makes finding the **DFT** using the **FFT** much more computationally efficient, especially if M itself is a power of 2. Using this approximation, Algorithm 5.3 is readily implemented. Appendix E.2.1 presents the seven(!) lines of code R code for this, repeated here.

```
N = M*2**K
F = rep(0,N)
F[2] = 1                          # F[] now corresponds to F(t) = t
F = fft(F,inverse=FALSE)
for (k in 1:K) F = (1 - p)*F + p*F*F     # K amplifications cycles
F = (1-phi + phi*F)**M                   # binomial sampling
F = Re(fft(F,inverse=TRUE)) /N           # real part of inverse
```
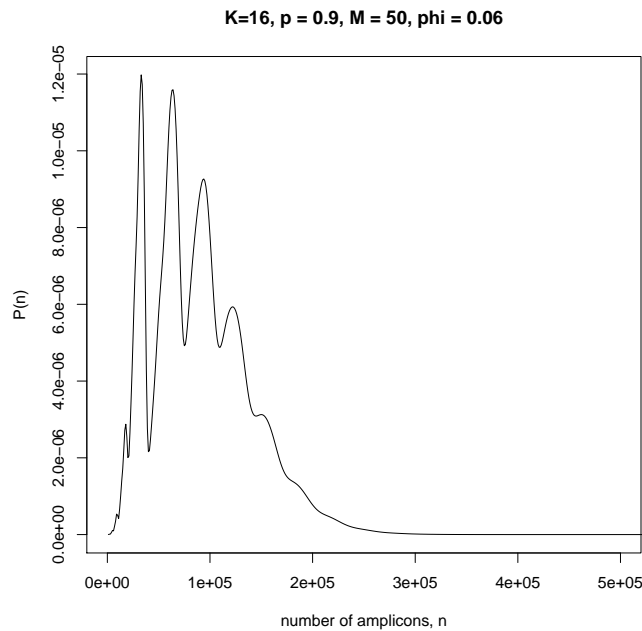

Figure 5: A marginal target distribution computed with the R implementation of Algorithm 5.3 given in Appendix E.2.1 .

Figure 5 shows the amplicon distribution obtained using the code given above for a low template amount, in which multimodality is clearly present, and would be missed by current probabilistic genotyping software based assuming a unimodal probability distribution (such as lognormal or gamma) for peaks heights.[3]

It is also worth emphasising that the model naturally includes dropout, and that the full distribution calculated using Algorithm 5.3 enables the means to assess dropout probabilities –there is no need to posit a separate additional model for allelic dropout, such as the logistic regression model (or variants thereof) of Tvedebrink et al. (2009). Indeed, in a follow-up paper, (Tvedebrink et al., 2012a) refine their logistic regression approach with a probit model based on and compared with the amplicon model of Gill et al. (2005).

To illustrate this, we consider an amplification probability of $p = 0.85$. To keep computations manageable we take the number of cycles to be $K = 15$, take $\phi = 0.1$, and set the analytic threshold to be 40000 amplicons. Figure 6 shows the dropout probabilities $P(D)$ as a function of the number of starting cells - note that the horizontal axis is on a log-scale for comparison with Figure 1 of Tvedebrink et al. (2012a). The plot shows two curves, with the red corresponding to a homozygous individual, and the black to a heterozygous individual. (R code to generate this plot is given in Appendix E.2.2.)

---

[3]Equivalent Python code, used for generating Figure 4 is given in Appendix E.1.2. Running the Python code for the full 28 cycles took around 3 minutes on a laptop with an Intel i7[TM] processor, and used around 30Gb of ram.
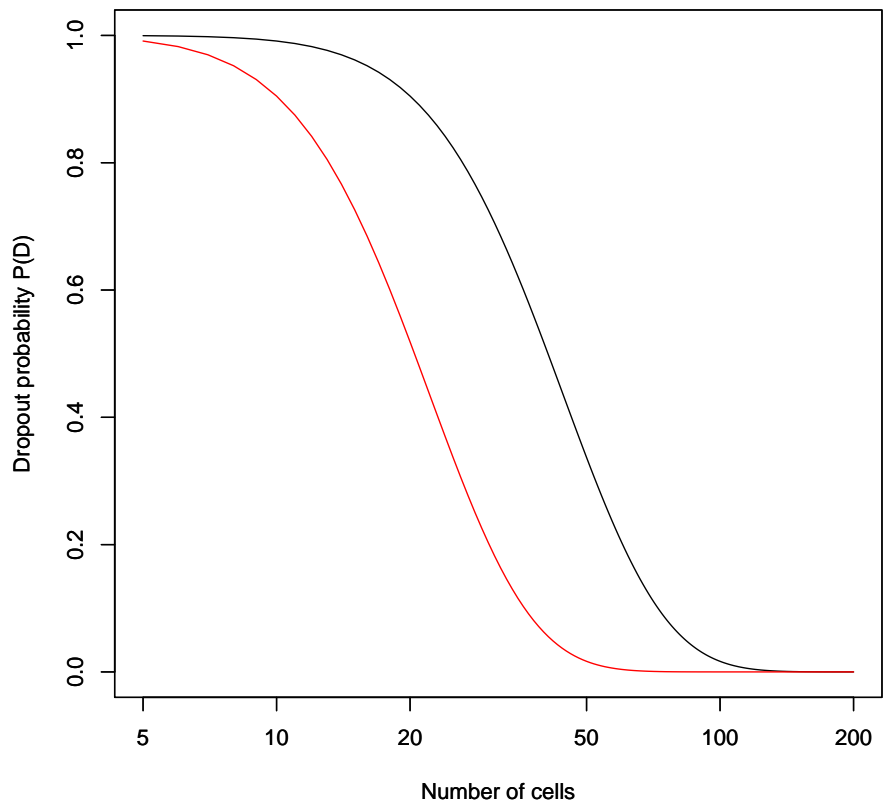
Figure 6: Dropout probabilities for homozygous (red) and heterozygous (black) individuals, using $K = 15$ amplification cycles, pre-amplification sampling probability of $\phi = 0.1$, an amplification probability of $p = 0.85$ on each cycle, and a threshold of 40000 amplicons.

5.3 Alternative derivation of the distribution probabilities

There is another way to extract the probabilities from the probability generating function $(1 - \phi + \phi F_K(t))^M$. Note that this is a finite degree polynomial in t. The coefficient of t^n gives the probability $F[n]$ of exactly n amplicons. Instead of generating the full distribution using the **DFT**-based algorithms above, we can extract this single value by using Cauchy's residue theorem with a contour in the complex plane that contains the origin,

$$F[n] = \frac{1}{2\pi i} \oint \frac{(1 - \phi + \phi F_K(t))^M}{t^{n+1}} dt.$$

If we take the contour to be the unit circle in the complex plane centred at the origin, we may make a change of variable, $t = \exp(-2\pi i\theta)$, so that θ ranges over $[0, 1]$, and the contour integral becomes

$$F[n] = \int_0^1 (1 - \phi + \phi F_K(\exp(-2\pi i\theta)))^M \exp(2\pi n\theta) d\theta$$

We may evaluate this numerically by splitting the range up into a large number N of equal sized intervals (with size $d\theta = 1/N$) and using the trapezoidal approximation. Note that the beginning and the end point values are identical because we are evaluating the closed circular contour, so that as the approximation we have

$$F[n] \approx \frac{1}{N} \sum_{j=0}^{N-1} (1 - \phi + \phi F_K(\exp(-2\pi i j/N)))^M \exp(2\pi n j/N)$$

This is fully equivalent to using the DFT above if the same value of N is used, and hence is <u>exact</u> if N is sufficiently large.

The advantage of this formulation is that if only a single value from the distribution is required, it may be found without the large overhead in computer memory that using the **FFT** incurs in storing the arrays $F[]$ and $\mathcal{F}[]$.

There is another use for this approach. When evaluating a likelihood for a peak height of an allele, it may be that no peak is observed at the allele position in the **EPG**, or one is observed but is not above the analytic threshold. In such cases we need to find the cumulative probability to the threshold. Suppose that the threshold corresponds to n amplicons. Then the cumulative probability is

$$\sum_{m=0}^{n} F[n] = \sum_{m=0}^{n} \frac{1}{2\pi i} \oint \frac{(1 - \phi + \phi F_K(t))^M}{t^{m+1}} dt$$

$$= \frac{1}{2\pi i} \oint (1 - \phi + \phi F_K(t))^M \left(\sum_{m=0}^{n} \frac{1}{t^{m+1}} \right) dt$$

$$= \frac{1}{2\pi i} \oint (1 - \phi + \phi F_K(t))^M \frac{1 - t^{-n-1}}{t - 1} dt$$

Again, the trapezoidal rule may be used to evaluate this with line integral on the unit circle in the complex plane.

5.4   Simulating the process with stutters

The paper of Gill et al. (2005) also included a model for stutters. There is a slight error in their paper that was pointed out in (Cowell, 2009). Their corrected model is as follows. During an amplification an amplicon may make a copy of itself, with probability p_t, or make a stutter copy with probability p_s. Thus neither a stutter nor an exact copy is made with probability $1 - p_t - p_s$. It is assumed that when a stutter amplicon is made it will make a copy of itself in each subsequent cycle with probability p_t. Let n_k denote the number of amplicons and m_k the number of stutter amplicons after k cycles. Assuming N_0 starting amplicons sampled binomially with probability ϕ for amplification, a simulation for the number of amplicons and stutters may be expressed as in Algorithm 5.4. In this, the draw of J simulates the total number of new amplicons and stutters produced in the k-th cycle by the existing amplicons. The J_t draw then samples from these new products to simulate how many are copies of the target amplicon, with the remainder being stutters. The J_s draw simulates how many new stutter amplicons are produced by currently existing stutter products.

Algorithm 5.4 [SIMPLE AMPLICON **PCR** SIMULATION WITH STUTTERS]

- Sample n_0 from Binom(N_0, ϕ), and set $m_0 = 0$.

- for k in 1 to K do

    - Sample J from Binom($n_{k-1}, p_s + p_t$)
    - Sample J_t from Binom($J, p_t/(p_s + p_t)$)

- Sample J_s from $\mathrm{Binom}(m_{k-1}, p_s + p_t)$
- Set $n_k = n_{k-1} + J_t$
- Set $m_k = m_{k-1} + (J - J_t) + J_s$ □

In (Gill et al., 2005) a value of $p_s = 0.002$ was estimated from experimental data. However, after correcting their error (which was to use $\mathrm{Binom}(n_{k-1}, p_t)$ for the number of copies of amplicons generated, and $\mathrm{Binom}(n_{k-1}, p_s)$ for the number of stutter products generated from amplicons, hence allowing the possibility for an amplicon to generate both a copy of itself and also a stutter in a single cycle) it appears that a value of around 0.004 would be more appropriate.

Figure 7 shows a scatterplot of 10000 simulated (n_K, m_K) values for K cycles starting from a single amplicon, $n_0 = 1$ (so no pre-sampling) using $p_t = 0.8$ and $p_s = 0.004$. The plot indicates some correlation between the two values — for the data in the plot the correlation coefficient is around 0.22, a theoretical value will be given later. Weusten and Herbergs (2012) also found such correlations in their analysis.
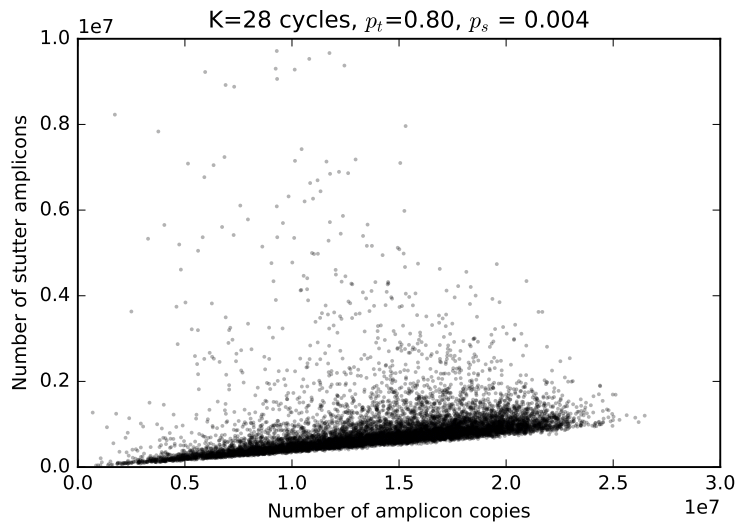
Figure 7: Scatterplot of main and stutter amplicon numbers for simple amplicon mode, for a simulation of size 10000.

From the simulated data we may also estimate the marginal distribution for stutter amplicons, a density estimate is shown in Figure 8.
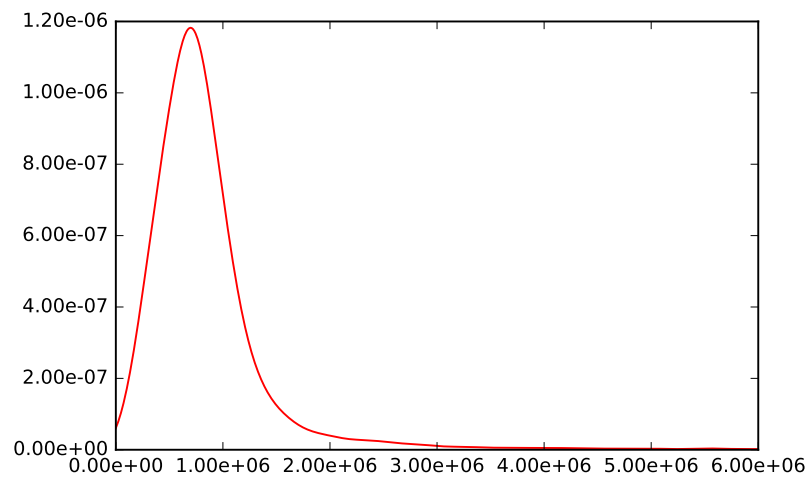
Figure 8: Kernel density estimate of the marginal distribution of the number of stutter amplicons from the simulation data plotted in Figure 7.

We may also find the fraction of the number of amplicons generated that are stutters, that is the ratio of the number of stutter amplicons to the total number of amplicon and stutter amplicons, and generate a kernel density estimate. (The values of this ratio are therefore between 0 and 1, unlike the stutter proportion which is the ratio of stutter amplicons to amplicons, which can grow very large.) A kernel density estimate is shown in Figure 9.
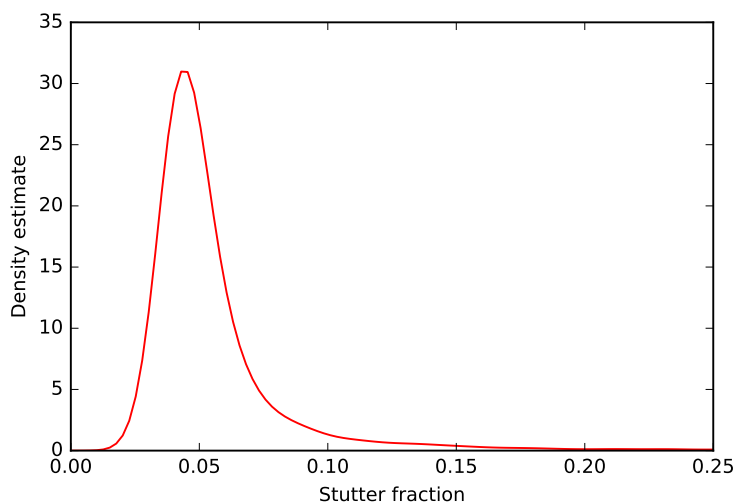
Figure 9: Kernel density estimate of the stutter fraction in the simulation data plotted in Figure 7.

5.5 Generating the full joint distribution

We now show how to find the full joint- distribution of amplicon copies and stutter amplicons, at least theoretically. To do this we combine a 2-dimensional **FFT** analysis with bivariate probability generating functions. A bivariate **PGF** is appropriate here, as we have both main amplicons and stutter amplicons, that is in the amplification cycles we have a multi-type branching process of the sort that was formulated by Good (1955) in terms of vectorial generating functions.

We shall refer to the main, or initial, type of amplicon as a *target* amplicon, and use the symbol t in the bivariate **PGF** to represent their number. We shall use the symbol s to represent the stutter amplicon number. As for the simple (no-stutter) model, we may express the **PGF** by functional iteration. However, because we have two types of amplicons, we need to use coupled equations to express the amplifications of single target and single stutter amplicons:

$$t \rightarrow (1 - p)t + p(1 - \xi)t^2 + p\xi ts$$
$$s \rightarrow (1 - p)s + ps^2$$

Here we let p denote the probability that an amplicon (of either type) makes a product in a cycle; ξ is the conditional probability that a target amplicon produces a stutter given either a target or stutter is produced. In terms of the previous notation we have $p_s = p\xi$ and $p_t = p(1 - \xi)$. Let $F_0(s, t) = t$ and $G_0(s) = s$. Let $F_n(t, s)$ denote the bivariate **PGF** of the joint distribution for the number of target and stutter amplicons after n amplification cycles, arising from a single initial target amplicon, and let $G_n(s)$ denote the number of stutter amplicons that (would) arise from an initial single stutter amplicon.

Then for $n > 0$ we have the iteration scheme:

$$F_n(t, s) = (1 - p)F_{n-1}(t, s) + p(1 - \xi)F_{n-1}^2(t, s) + p\xi F_{n-1}(t, s)G_{n-1}(s) \quad (5)$$
$$G_n(s) = (1 - p)G_{n-1}(s) + pG_{n-1}^2(s). \quad (6)$$

To see this is the case we argue as follows (the reader may find it helpful to draw a probability tree). Initially we have one target allele with **PGF** $F_0(s, t) = t$. In the first cycle there are three possible outcomes.

In the first outcome, with probability $(1 - p)$ we still have just the one target amplicon. Hence with a further $n - 1$ cycles the bivariate **PGF** for the number target and stutter amplicons conditional on this outcome is $F_{n-1}(t, s)$.

The second possible outcome from the first cycle is that the original target makes a target copy. This happens with probability $p(1 - \xi)$, and the **PGF** conditional on this outcome is t^2 representing the two targets. Now in the subsequent $(n - 1)$ cycles each of these targets will independently give rise to set of target and stutter amplicons. The **PGF** for the descendants from each target will each be $F_{n-1}(t, s)$. Because the amplifications arising from each of the two targets are independent, the **PGF** representing the total number of target and stutter amplicons from these two targets will be the product of each of their **PGF**s, that is $F_{n-1}^2(t, s)$.

The third outcome is that the initial target produces a stutter. This happens with probability $p\xi$, and we have the joint **PGF** conditional on this outcome is st. In the subsequent $n - 1$ amplifications the number of target and stutter amplicons generated by the target will have **PGF** $F_{n-1}(t, s)$. Independently the stutter amplicon will generate further stutter amplicons with **PGF** $G_{n-1}(s)$. The bivariate **PGF** for the total number of target and stutter amplicons generated from the single target and amplicon is, because of the independence of amplification, the product of their **PGF**s, that is $F_{n-1}(t, s)G_{n-1}(s)$.

Adding these three possibilities together with their probability weights yields the coupled **PGF** of (5): note that the recurrence relation for $G_n(s)$ is that presented in Theorem 5.1 for the non-stutter amplification process.

Now $F_n(t, s)$ given above is for a single starting amplicon. If we start with M amplicons that are pre-sampled binomially with probability ϕ, then the final distribution is given by

$$(1 - \phi + \phi F_n(t, s))^M \tag{7}$$

5.6   FFT implementation of target and stutter distribution

We now show how the recurrence relations (5) and (6) may be evaluated numerically using **FFTs**, at least in principle. (In practice the memory requirements to carry this out will be excessive for the number of cycles used in forensic **PCR** analyses.) The extension is to use a 2-dimensional **DFT**. Algorithm 5.5 gives the details (a Python implementation is given in Appendix E.1.3).

Algorithm 5.5 [Joint distribution for target and stutter amplicons **DFT**]

- Set $N = M2^K$

- Initialize $F[,]$ to be a two dimensional $N \times N$ array, (with lowest index $[0, 0]$) initialized such that all entries are zero except $F[1, 0] = 1$.

- Initialize $G[]$ to be an N dimensional array such that all entries are zero except $G[1] = 1$.

- Set $\mathcal{F}[,]$ equal to the 2-dimensional **DFT** of $F[,]$.

- Set $\mathcal{G}[]$ denote the one-dimensional **DFT** of $G[]$.

- For K times do:

  - for each element $\mathcal{F}[f, g]$ of $\mathcal{F}[f, g]$
    * update $\mathcal{F}[f, g] := (1 - p)\mathcal{F}[f, g] + p(1 - \xi)\mathcal{F}[f, g]^2 + p\xi\mathcal{F}[f, g]$.
  - for each element $\mathcal{G}[g]$ of $\mathcal{G}[]$ update $\mathcal{G}[g] := (1 - p)\mathcal{G}[g] + p\mathcal{G}[g]^2$.

- for each element (f, g) of $\mathcal{F}[]$ update $\mathcal{F}[f, g] := (1 - \phi + \phi\mathcal{F}[f, g])^M$

- Set $F[,]$ equal to the inverse **DFT** of $\mathcal{F}[]$. $\square$

Although the use of the Algorithm 5.5 is not practical for large K and or M, it can be used for small K and M values. Figure 10 shows a contour plot of the joint distribution for a single amplicon with subject to $K = 13$ amplification cycles, with $p = 0.85$ and $\xi = 0.005$ on each cycle, and Figure 11 a surface plot. From the figures we can see quite clearly the correlation between the number of target and stutter amplicons. Multi-modality of the distribution is also clearly evident. The reader may care to compare these figures to Figure 7.
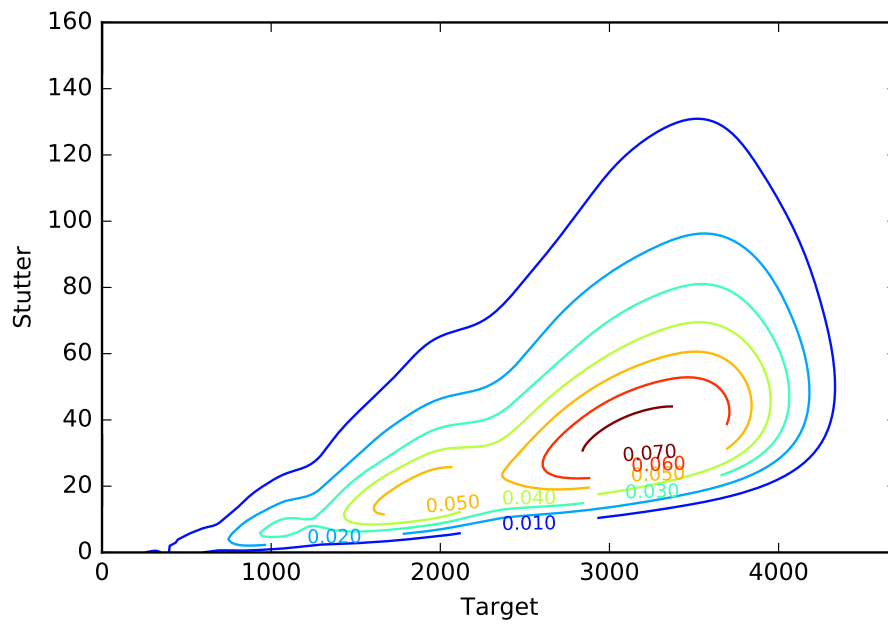
Figure 10: Contour plot of the joint distribution of the number of target and stutter amplicons, arising from an single amplicon amplified for $K = 13$ amplification cycles, with $p = 0.85$ and $\xi = 0.005$ on each cycle. Note that the numerical probabilities shown on the contours are the true values multiplied by a factor of 10000.
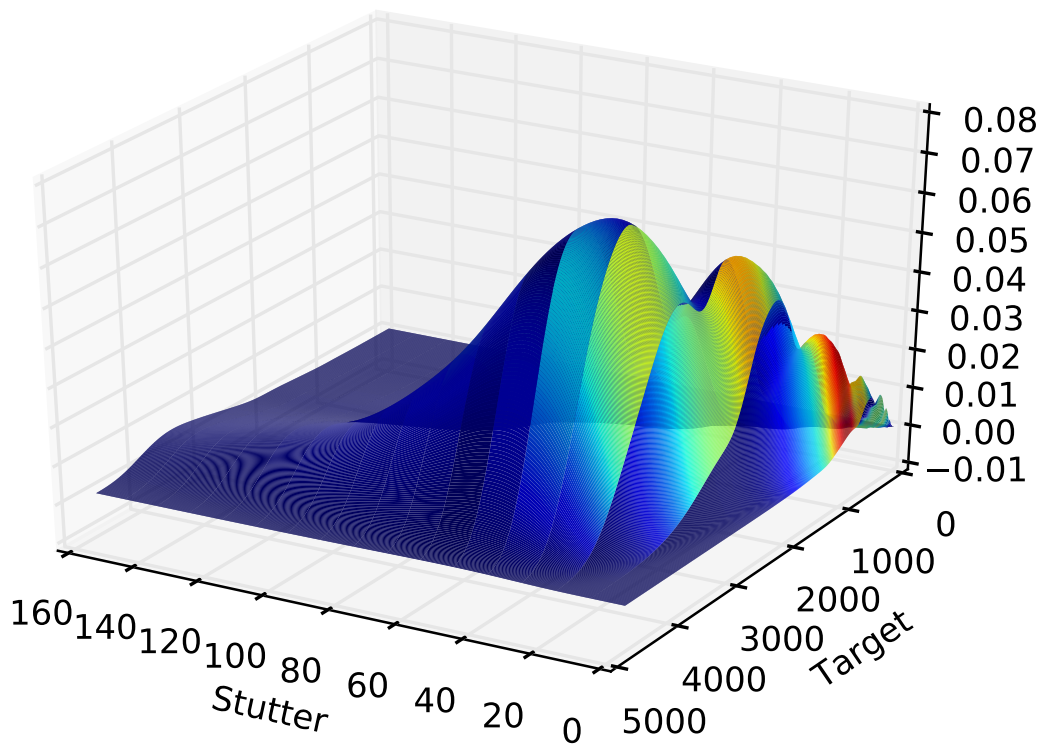
Figure 11: Surface plot of the joint distribution of the number of stutter and target amplicons, using the same values used for Figure 10.

5.7 Stutter marginal distribution

From the joint **PGF** $F(t, s)$ of target and stutter amplicons, we may obtain the marginal distribution of the target amplicon simply by substituting $s = 1$. Similarly we may obtain the **PGF** of the marginal distribution of the number of stutter amplicons by substituting $t = 1$. It is the latter we are interested in here. Recall that the iterative equations finding the joint **PGF** are

$$F_n(t, s) = (1 - p)F_{n-1}(t, s) + p(1 - \xi)F_{n-1}^2(t, s) + p\xi F_{n-1}(t, s)G_{n-1}(s)$$
$$G_n(s) = (1 - p)G_{n-1}(s) + pG_{n-1}^2(s).$$

with initial values $F_0(t, s) = t$ and $G_0(s) = s$. Rather than iterate to find $F_n(t, s)$ and then substituting $t = 1$ to find the stutter marginal, we may instead first make the substitution and then iterate: the equations then simplify to

$$F_n(s) = (1 - p)F_{n-1}(s) + p(1 - \xi)F_{n-1}^2(s) + p\xi F_{n-1}(s)G_{n-1}(s)$$
$$G_n(s) = (1 - p)G_{n-1}(s) + pG_{n-1}^2(s).$$

with initial values $F_0(s) = F_0(1, s) = 1$ and $G_0(s) = s$.

These can be evaluated numerically using a pair of 1-dimensional **FFTs**, the algorithm is almost identical to Algorithm 5.5, (a Python implementation is given in Appendix E.1.4).

Algorithm 5.6 [Joint distribution for target and stutter amplicons **DFT**]

- Set $N = M2^K$

- Initialize $F[]$ to be an N dimensional array such that all entries are zero except $F[0] = 1$.

- Initialize $G[]$ to be an N dimensional array such that all entries are zero except $G[1] = 1$.

- Set $\mathcal{F}[,]$ equal to the **DFT** of $F[,]$.

- Set $\mathcal{G}[]$ equal to the **DFT** of $G[]$.

- for each index g of $\mathcal{F}[]$

– For K times do:

   * update $\mathcal{F}[g] := (1 - p)\mathcal{F}[g] + p(1 - \xi)\mathcal{F}[g]^2 + p\xi\mathcal{F}[g]\mathcal{G}[g]$
   * update $\mathcal{G}[g] := (1 - p)\mathcal{G}[g] + p\mathcal{G}[g]^2$.

   update $\mathcal{F}[g] := (1 - \phi + \phi\mathcal{F}[g])^M$

- Set $F[]$ equal to the inverse **DFT** of $\mathcal{F}[]$. $\qquad\qquad\square$

Figure 12 shows the marginal distribution of the number of stutter amplicons arising from a single initial target amplicon, and amplified for $K = 22$ cycles with $p = 0.8$ and $\xi = 0.004$ on each cycle. The long right-hand tail of the distribution is evident.
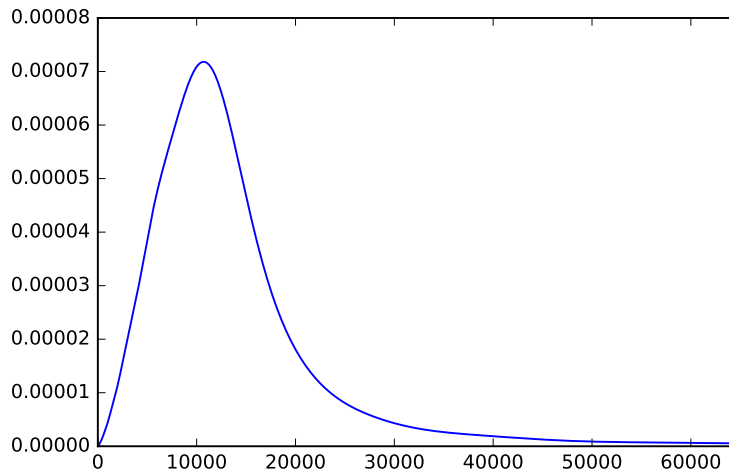
Figure 12: Marginal distribution of the number of stutter amplicons arising from a single target amplicon amplified for $K = 22$ cycles, with $p = 0.80$ and $\xi = 0.004$ on each cycle.

Figure 13 shows the marginal distribution of the number of stutter amplicons arising from an initial set of 83 target amplicons, sampled binomially with selection probability $\phi = 2/11$, and amplified for $K = 18$ cycles with $p = 0.8$ and $\xi = 0.004$ on each cycle.

40
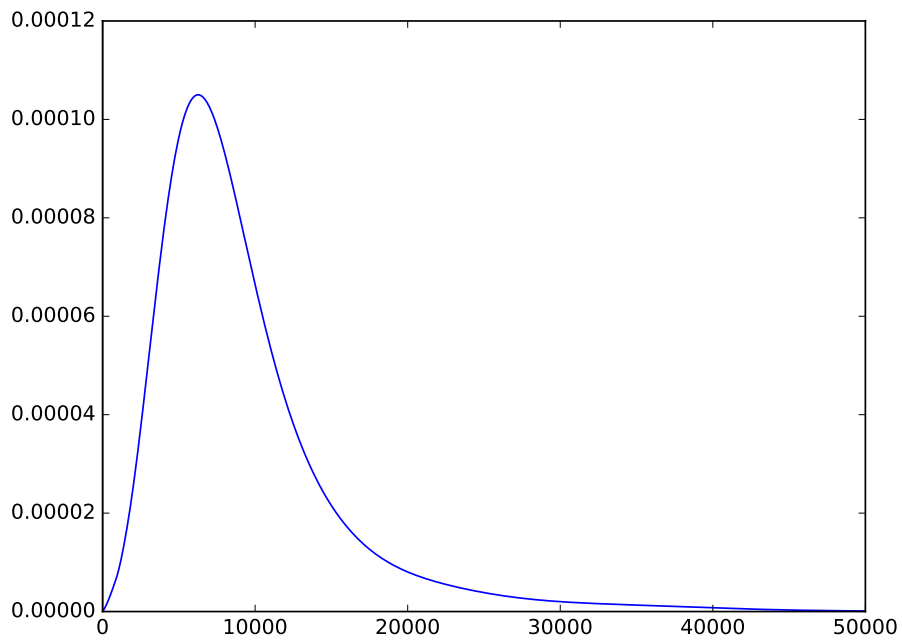
Figure 13: Marginal distribution of the number of stutter amplicons arising from $M = 83$ amplicons pre-sampled with probability $\phi = 1/11$ prior to amplification, and amplified for $K = 18$ cycles, with $p = 0.8$ and $\xi = 0.004$ on each cycle.

5.8 Moment analysis

The previous sections have shown how the full joint distribution of target and stutter amplicons may be found numerically by evaluating the **PGFs** the **DFT**. Up to now, probabilistic genotyping software packages, lacking this evaluative ability, assume some simple distributional assumption— the most common distributions used are the normal, lognormal of gamma. However, it is straightforward to derive, from the **PGF**, expressions for the means and variances of the full distribution. These moments may be used for finding a 'best fitting' simple distribution based on moment matching.

Let T denote the number of target amplicons, and S the number of stutter amplicons, arising from the amplification of a single target amplicon. We have that

$$\mathbb{E}T \,|\, n = \frac{\partial F_n(t,s)}{\partial t}\Big|_{t=1,s=1}$$

$$\mathbb{E}T(T-1)\,|\, n = \frac{\partial^2 F_n(t,s)}{\partial t^2}\Big|_{t=1,s=1}$$

$$\mathbb{E}S \,|\, n = \frac{\partial F_n(t,s)}{\partial s}\Big|_{t=1,s=1}$$

$$\mathbb{E}S(S-1)\,|\, n = \frac{\partial^2 F_n(t,s)}{\partial s^2}\Big|_{t=1,s=1}$$

$$\mathbb{E}TS \,|\, n = \frac{\partial^2 F_n(t,s)}{\partial s\partial t}\Big|_{t=1,s=1}$$

from which the variances $\mathbb{V}T$ and $\mathbb{V}T$ and the correlation $\mathrm{Cor}(N,M)$ may be found. (Derivations of algebraic solutions are given in Appendix A using different notation.) We have (variance formulae are given in the appendix)

$$\mathbb{E}T \,|\, n = (1 + p(1-\xi))^n$$

$$\mathbb{E}S \,|\, n = (1+p)^n - (1 + p(1-\xi))^n$$

$$\mathbb{E}TS \,|\, n = (1 + p*(1-x))^{n-1}\left([1-(1+p)^n]x + 2*[(1+p)^n - (1 + p*(1-x))^n]\right)$$

$$\mathrm{Cov}(T,S \,|\, n) = (\mathbb{E}TS \,|\, n) - (\mathbb{E}T \,|\, n)(\mathbb{E}S \,|\, n)$$

$$= (1 + p(1-\xi))^{n-1}\left[(1 - p(1-\xi))[(1+p)^n - (1 + p(1-\xi))^n] - \xi((1+p)^n - 1)\right]$$

As an alternative to using the analytic formula, instead one could fix numerical values for p, ξ and K and solve the recurrence relations numerically and very simply. It is interesting to examine how the correlation varies with p and ξ and

the number of cycles. In Figure 14 we show the dependence for 28 and 34 cycles, in the form of contour plots. For forensic applications we expect that p will be in the range $0.75 - 0.95$, with ξ in the range $0.004 - 0.01$. Thus we see that there can be quite high correlation between the number of amplicons (which is proportional to the peak heights in the **EPG**) of stutter and target alleles. This is apparently at variance with the experimental results of (Bright et al., 2013)— we shall return to this point later.

Figure 14:
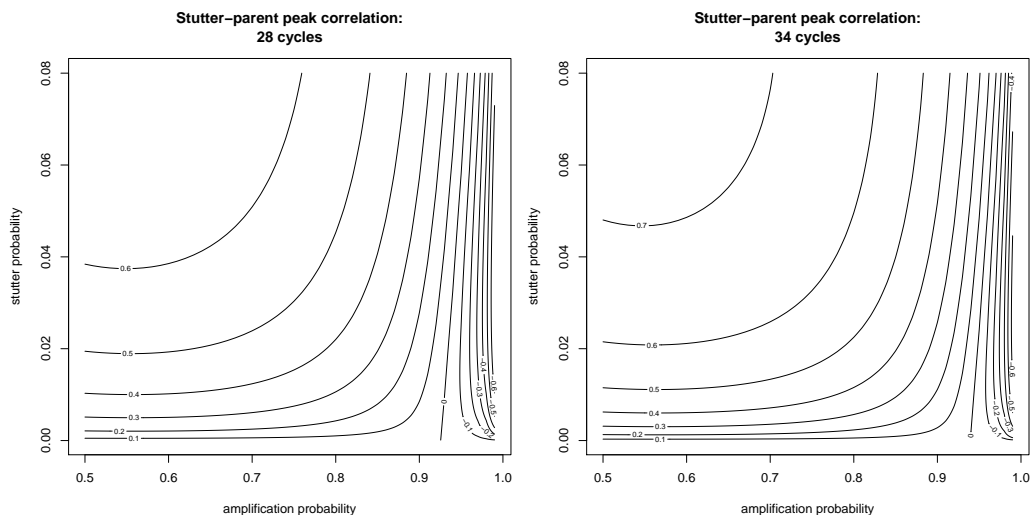
The moment formulae above assume a single initial amplicon, but they are readily extended to take account of binomial pre-sampling. There are two ways to proceed. One way is to write down the **PGF** to include the sampling; this is given by

$$(1 - \phi + \phi F_n(t, s))^M.$$

This can then be differentiated to find the moments.

Another, simpler way, is to use conditional expectation:

$$EY = E[EY \,|\, X]$$
$$VY = E[VY \,|\, X] + V[EY \,|\, X]$$

43

for the means and variances of T and S, where in our case $X \sim \text{Binom}(M, \phi)$ having mean $M\phi$ and variance $M\phi(1 - \phi)$. Let $\mathcal{T}$ denote the total number of amplicons arising from pre-sampling M target amplicons and then amplifying the sample, and let $\mathcal{S}$ denote the number of stutter amplicon products.

With this we obtain

$$
\begin{aligned}
\mathbb{E}\mathcal{T} &= M\phi\mathbb{E}[T \mid n] \\
\mathbb{V}\mathcal{T} &= M\phi(\mathbb{V}[T \mid n] + (1 - \phi)E[T \mid n]^2) \\
\mathbb{E}\mathcal{S} &= M\phi\mathbb{E}[S \mid n] \\
\mathbb{V}\mathcal{S} &= M\phi(\mathbb{V}[S \mid n] + (1 - \phi)E[S \mid n]^2)
\end{aligned}
$$

and for the covariance we have

$$
\text{Cov}(\mathcal{T}, \mathcal{S}) = M\phi\left(\text{Cov}(T, S \mid n) + (1 - \phi)\mathbb{E}[T \mid n]\mathbb{E}[S \mid n]\right)
$$

from which we deduce that the correlation between T and S does not depend on the initial number of target amplicons, but does depend on the sampling probability ϕ:

$$
\text{Cor}(\mathcal{T}, \mathcal{S}) \frac{\text{Cov}(T, S \mid n) + (1 - \phi)(\mathbb{E}T \mid n)(\mathbb{E}S \mid n))}{\sqrt{(\mathbb{V}[T \mid n] + (1 - \phi)(\mathbb{E}[T \mid n])^2}\sqrt{(\mathbb{V}[S \mid n] + (1 - \phi)(\mathbb{E}[S \mid n])^2}} \tag{8}
$$

In many forensic laboratory experiments DNA samples are prepared by high dilution of large template DNA. For such scenarios a Poisson distribution would appear to be more appropriate. Let us assume that the total number of target amplicons selected for **PCR** has a Poisson distribution with rate λ with $\lambda > 0$. If $X \sim \text{Poisson}(\lambda)$, then the **PGF** of X has the form

$$
\exp(\lambda(t - 1))
$$

To obtain the **PGF** for the total number of amplicons we simply substitute $F_n(t, s)$ for t in this Poisson **PGF**

$$
\exp(\lambda(F_n(t, s) - 1))
$$

and take derivatives as appropriate, Alternatively, we may use conditional expectation noting the mean and variance of a Poisson(λ) random variable is λ. Either way we obtain

$$\text{Cor}(\mathcal{T}, \mathcal{S}) = \frac{\mathbb{E}[TS \mid n]}{\sqrt{(\mathbb{E}[T \mid n]^2)(\mathbb{E}[S \mid n]^2)}} \tag{9}$$

Surprisingly, the correlation $\text{Cor}(\mathcal{T}, \mathcal{S})$ does not depend on λ (see Appendix A). Note also that (8) reduces to (9) with $\phi = 0$, which corresponds to the double limit $M \to \infty, \phi \to 0$ with $M\phi = \lambda$ fixed.

The correlations can get very high, for example with $p = 0.8$, $\xi = 0.005$ and $k = 28$ cycles, the correlation is approximately 0.74.

6 Amplifying genomic strands: a genomic model

The previous section examined the simple amplicon model of (Gill et al., 2005), and showed how by using **PGFs** and the **FFT** is it possible to extract, in a very simple manner, the full probability distributions for the number of target and stutter amplicons. Two simplifications in the model are that it starts from amplicons, and not genomic strands, and it does not take into account the dye-tagging of the amplicons. We shall now remove these limitations; we shall also add in the artefacts of forward and double stutter, drop-in and baseline noise, and show how they may all be expressed in a unified manner using **PGF**s, and evaluated using **DFT**s. We being by considering the genomic strand model without stutters.

6.1 The basic model described

The basic difference between the model developed here and the simplified model of Gill et al. (2005) is that the latter assumed that we start the branching process with amplicons; in reality we start the branching process with samples of genomic strands. As pointed out by Butler (2011), this means that amplicons are not formed until at least the end of the second thermal amplification cycle as we show in Section 6.2.

Consider starting from a single genomic strand, and let us assume that amplification is 100% efficient in all stages. We are interested in a particular locus.

- In the first thermal cycle, the genomic strand is melted, and primers attach to the flanking regions, one on each of the two strands of the melted genome. The TAQ polymerase lays down dNTRs along each strand from the primer to past the complimentary flanking region. Call these generated sequences

half-genomes. Then on cooling we have two separate strands, each consisting of one of the complementary strands making up the genomic strand bound to a half-genome.

- In the second thermal cycle these two hybrid genomes melt, and we have the two parts of the genome and also the two half-genome strands in solution. In this cycle the genomic strands behave as in the first thermal cycle, but the half-genome strands, which were not there then, attach primers to their complimentary flanking regions, and then the TAQ lays down dNTRs along it all the way to the (far) end of original flanking region, where the process stops because that is the end of the molecule. Each half-genome strand now has a complementary amplicon strand attached to it.

- In the third thermal cycle the two complementary amplicon strands separate from the half-genomes and make complementary copies of themselves, and so the exponential growth in the number of amplicons with further thermal cycles begins.

The above description is not quite complete, again as described by Butler (2011), in that in addition to making the amplicons, the amplicons have attached to them a fluorescent dye at one of the flanking regions, say the 5' region (so that it can be seen in the capillary electrophoresis (CE) equipment). When measuring the amplicons in the CE equipment, the amplicons are heated to separate them out into individual complementary strands, only one each of each complement has a dye attached.

Weusten and Herbergs (2012) included initial genomic strands and amplicons in their analysis of **PCR**, but did not include the intermediate half-strands. They also did not consider direct double stutter or forward stutter, or the tagging of amplicons with fluorescent dyes.

6.2 Initial mathematical formulation : no stutters

We may denote the original double-helix genomic strand by the pair g and g_d The half-genomic strands may be denoted by h and h_d, and the amplicons by a and a_d. The d subscript denotes a florescence dye attached. (The original genomic DNA does not have a dye attached to it, but we use g_d to avoid introducing a special notation; the half-genomes and amplicons do have such dyes attached.)

The branching process is then summarized by the following processes on the various components:

$$g \rightarrow g, h_d$$
$$g_d \rightarrow g_d, h$$
$$h \rightarrow h, a_d$$
$$h_d \rightarrow h_d, a$$
$$a \rightarrow a, a_d$$
$$a_d \rightarrow a_d, a$$

and we are interested in the final number of tagged amplicons, a_d after the n cycles.

It is also simpler to break the process up into two independent branching process, one that result in products from the g strand, and one from the g strand:

$$g \rightarrow g, h_d$$
$$h_d \rightarrow h_d, a$$
$$a \rightarrow a, a_d$$
$$a_d \rightarrow a_d, a$$

and from the g_d strand:

$$g_d \rightarrow g_d, h$$
$$h \rightarrow h, a_d$$
$$a_d \rightarrow a_d, a$$
$$a \rightarrow a, a_d$$

The following two tables show how the numbers of each type increase in each cycle for these two processes treated independently, assuming 100% efficiency in each cycle. The second table follows the pattern of the first.

cycle	g	h_d	a	a_d
0	1	0	0	0
1	1	1	0	0
2	1	2	1	0
3	1	3	3	1
4	1	4	7	4
5	1	5	15	11
6	1	6	31	26
7	1	7	63	57
8	1	8	127	120
9	1	9	255	247
10	1	10	511	502

cycle	g_d	h	a_d	a
0	1	0	0	0
1	1	1	0	0
2	1	2	1	0
3	1	3	3	1
4	1	4	7	4
5	1	5	15	11
6	1	6	31	26
7	1	7	63	57
8	1	8	127	120
9	1	9	255	247
10	1	10	511	502

Of interest is the number of tagged amplicons, which is obtained from adding up the row entries for a_d in each of the two tables above:

cycle n	a_d
0	0
1	0
2	1
3	4
4	11
5	26
6	57
7	120
8	247
9	502
10	1013

It is readily verified numerically that these totals are the numbers $2^n - n - 1$ for each number of cycles n. (They form the sequence A000225, called the *Eulerian numbers*, in the The On-Line Encyclopedia of Integer Sequences.) We can verify this algebraically by induction as follows. Let us consider the g sequence. It clear that after k cycles the number of h_d is equal to k, as the g has had k opportunities to make and h_d. We see that the values in the third column are (for $k > 0$) the integers $2^{k-1} - 1$, and those in the fourth column are the Eulerian numbers k reduced by 1, that is $2^{k-1} - k$. We can see this is true for all values given in the table, we take this as a starting position on an inductive proof for general $k > 10$.

Thus at the k-th cycle, assume that there are $n_{h_d:k} = k$ copies of h_d, $n_{a:k} = 2^k - 1$ copies of a and $n_{a_d:k} = 2^{k-1} - k$ copies of a_d. Then in the next cycle:

- The number of h_d half-strands increases by 1, as the g makes a new copy and the previous copies are not destroyed, hence

$$n_{h_d:k+1} = n_{h_d:k} + 1 = k + 1.$$

- The number of a amplicons increases by the number of h_d and a_d products that were present on the previous cycle:

$$n_{a:k+1} = n_{a:k} + n_{h_d:k} + n_{a_d:k} = 2^{k-1} - 1 + k + 2^{k-1} - k = 2^k - 1$$

- The number of a_d amplicons increases by the number of a amplicons that were present on the previous cycle:

$$n_{a_d:k+1} = n_{a_d:k} + n_{a_d:k} = 2^{k-1} - k + 2^{k-1} - 1 = 2^k - (k + 1)$$

49

Hence the inductive hypothesis is proved. Similar calculations go through for the second table. From this we see that after $k + 1$ cycles the number of tagged amplicons is

$$2^k - 1 + 2^k - (k + 1) = 2^{k+1} - (k + 1) - 1,$$

which are the Eulerian numbers. Note also that the simple amplicon model would give 2^{k+1}. The above formulae correct the values in Table 4.1 of Butler (2011), who ignored the persistent presence of the original genomic strands and the half strands in the remaining cycles, assuming their contribution in subsequent cycles would be negligible and concluding that after $n > 2$ cycles there would be approximately 2^{n-2} amplicons.

6.3 The basic model: PGF formulation

The basic model can be formulated as a multivariate **PGF**, derived using vectorial generating functions. For this we can consider the **PGF**s of the two types of initial genomic strands separately.

We start with the g strand, which has the set of amplification sequences:

$$g \rightarrow g, h_d$$
$$h_d \rightarrow h_d, a$$
$$a \rightarrow a, a_d$$
$$a_d \rightarrow a_d, a$$

We introduce symbols t_g, t_{h_d} t_a and t_{a_d} to be used in the multivariate **PGF** for the number each type of strand. For a single strand of each type, each amplifies in a single cycle according to the **PGF**s

$$t_g \rightarrow (1 - p_g)t_g + p_g t_g t_{h_d}$$
$$t_{h_d} \rightarrow (1 - p_{h_d})t_{h_d} + p_{h_d} t_{h_d} t_a$$
$$t_a \rightarrow (1 - p_a)t_a + p_a t_a t_{a_d}$$
$$t_{a_d} \rightarrow (1 - p_{a_d})t_{a_d} + p_{a_d} t_{a_d} t_a$$

where $p_g, p_{h_d}, p_a, p_{a_d}$ are branching process probabilities for each of the types of strands.

Let $G_n(t_g, t_{h_d}, t_a, t_{a_d})$ denote the joint **PGF** arising from amplifying a single g strand for n cycles.

Let $H_{d;n}(t_{h_d}, t_a, t_{a_d})$ denote the joint **PGF** arising from amplifying a single h_d strand for n cycles.

Let $A_n(t_a, t_{a_d}))$ denote the joint **PGF** arising from amplifying a single a strand for n cycles.

Let $A_{d;n}(t_a, t_{a_d})$ denote the joint **PGF** arising from amplifying a single a_d strand for n cycles.

Then these **PGF**s obey the following recurrence relations, which follow the pattern of the single strand formulae above:

$$G_{n+1}(t_g, t_{h_d}, t_a, t_{a_d}) = (1 - p_g)G_n(t_g, t_{h_d}, t_a, t_{a_d}) + p_g G_n(t_g, t_{h_d}, t_a, t_{a_d})H_{d;n}(t_{h_d}, t_a, t_{a_d}),$$
$$H_{d;n+1}(t_{h_d}, t_a, t_{a_d}) = (1 - p_{h_d})H_{d;n}(t_{h_d}, t_a, t_{a_d}) + p_{h_d}H_{d;n}(t_{h_d}, t_a, t_{a_d})A_n(t_a, t_{a_d}),$$
$$A_{n+1}(t_a, t_{a_d}) = (1 - p_a)A_n(t_a, t_{a_d})) + p_a A_n(t_a, t_{a_d})A_{d;n}(t_a, t_{a_d}),$$
$$A_{d;n+1}(t_a, t_{a_d}) = (1 - p_{a_d})A_{d;n}(t_a, t_{a_d}) + p_{a_d}A_{d;n}(t_a, t_{a_d})A_n(t_a, t_{a_d}),$$

with initial conditions

$$G_0(t_g, t_{h_d}, t_a, t_{a_d}) = t_g$$
$$H_{d,0}(t_{h_d}, t_a, t_{a_d}) = t_{h_d}$$
$$A_d(t_a, t_{a_d}) = t_a$$
$$A_{d,0}(t_a, t_{a_d}) = t_{a_d}$$

It is the last two that give rise to the exponential growth of amplicons in the **PCR** process. Similar equations arise when starting from a genomic strand g_d, specifically:

$$G_{d;n+1}(t_{g_d}, t_h, t_a, t_{a_d}) = (1 - p_{g_d})G_{d;n}(t_{g_d}, t_h, t_a, t_{a_d}) + p_{g_d}G_{d;n}(t_{g_d}, t_h, t_a, t_{a_d})H_n(t_h, t_a, t_{a_d}),$$
$$H_{n+1}(t_h, (t_a, t_{a_d}) = (1 - p_h)H_n(t_h, t_a, t_{a_d}) + p_h H_n(t_h, t_a, t_{a_d})B_{d;n}(t_a, t_{a_d}),$$
$$B_{d;n+1}(t_a, t_{a_d}) = (1 - p_{a_d})B_{d;n}(t_a, t_{a_d}) + p_{a_d}B_n(t_a, t_{a_d})B_{d;n}(t_a, t_{a_d}),$$
$$B_{n+1}(t_a, t_{a_d}) = (1 - p_a)B_n(t_a, t_{a_d}) + p_a B_{d;n}(t_a, t_{a_d})B_n(t_a, t_{a_d}),$$

with initial conditions

$$G_{d;0}(t_{g_d}, t_h, t_a, t_{a_d}) = t_{g_d}$$
$$H_0(t_h, t_a, t_{a_d}) = t_h$$
$$B_0(t_a, t_{a_d}) = t_a$$
$$B_{d,0}(t_a, t_{a_d}) = t_{a_d}$$

where we introduce functions B and B_d in place of A and A_d as these are to be considered as iterating (amplifying) independently. The justification of the recurrence relations is similar to that given in Section 5.5 for the joint distribution of target and stutter amplicons in the amplicon model, and is omitted.

In general, this is a multivariate polynomial in six t-parameters, as well as depending on six branching probabilities. However, because the genomic strand itself does not duplicate, we see that G and G_d are proportional to t_g and t_{g_d} respectively, which is a simplification that effectively reduces the number of t parameters to four.

We are particularly interested in the final number of dye-tagged amplicons. This is the sum of their number arising from the g and g_d strands, and therefore (because of independence of the branching process amplifications) is the coefficient of t_{a_d} in the product of the **PGF**s of each strand:

$$F_n(t_g, t_{g_d}, t_h, t_{h_d}, t_a, t_{a_d}) = G_n(t_g, t_{h_d}, t_a, t_{a_d})G_{d;n}(t_{g_d}, t_h, t_a, t_{a_d}) \qquad (10)$$

in which we may set all of the t's except t_{a_d} to unity to obtain the marginal **PGF** for the tagged amplicons, that is:

$$F_n(1, 1, 1, 1, t_{a_d}) = G_n(1, 1, 1, t_{a_d})G_{d;n}(1, 1, 1, t_{a_d})$$

6.4 Moment analysis

Of interest also are the various moments, in particular the mean and variance, which may be found from the marginal **PGF** by differentiation with respect to t_{a_d} and then setting this to 1. Algebraic derivations maybe found in Appendix B, where it is shown, for example, that the mean number of tagged amplicons is given by

$$\frac{p_g p_{h_d}}{p_a p_{a_d}} \left(\sqrt{\frac{p_a}{p_{a_d}}} \frac{(1 + \sqrt{p_a p_{a_d}})^n - (1 - \sqrt{p_a p_{a_d}})^n}{2} - np_a \right) + \frac{p_{g_d} p_h}{p_a p_{a_d}} \left(\frac{(1 + \sqrt{p_a p_{a_d}})^n + (1 - \sqrt{p_a p_{a_d}})^n}{2} - 1 \right)$$

If $p_a = p_{a_d} = p$, this simplifies to:

$$\frac{p_g p_{h_d}}{p^2} \left(\frac{(1 + p)^n - (1 - p)^n}{2} - np \right) + \frac{p_{g_d} p_h}{p^2} \left(\frac{(1 + p)^n + (1 - p)^n}{2} - 1 \right)$$

and if in addition $p_g = p_{g_d} = p_h = p_{h_d} = p$ this reduces to

$$(1 + p)^n - np - 1.$$

52

When $p = 1$ this yields $2^n - n - 1$, the Eulerian numbers given earlier.

There are far too many parameters to explore the behaviour of the variance in detail here, however one special case could be of interest, that in which all the amplification parameters take the same value. We can compare the behaviour for the mean and variance to that of the amplicon model. We see the mean values will be close, viz $(1 + p)^n - np - 1$ compared to $(1 + p)^n$. Somewhat surprisingly, the variance of the genomic amplification model turns out to be almost exactly half that of the Gill amplification model for sufficient number of cycles (the ratio is 0.49997 with N=20 and p=0.7, and 0.50000 if we increase to n=24 cycles) and appears to asymptote to almost 0.5 as the number of cycles increases. Thus, although the exact formula for the variance is quite lengthy, for $n \geq 24$ cycles taking the variance formula from the simplified amplicon model, and dividing the result by 2, appears to give an excellent approximation to it.

6.5   Full distribution from vectorial PGF

The numerical derivation of the full distribution follows a similar pattern to the derivation for amplicon model with stutter. Using a 6-dimensional **DFT** one could, in principle, derive the full joint distribution for the six types of strand. However the number of g and g_d strands does not change in each cycle, thus a 4-dimensional **DFT** suffices (for amplification of a single genome). The number of each of the h and h_d strands increases by at most 1 in each cycle, with at most $n-1$ of each after n cycles. The numbers of a and a_d strands will have a maximum of $2^n - n - 1$, hence the size of the **DFT** required is approximately $n^2 2^{2n}$, too large for forensic applications with n between 27 and 34 cycles.

For M genomic strands pre-sampled binomially with probability ϕ, the joint **PGF** is given by

$$(1 - \phi + \phi F_n(t_g, t_{g_d}, t_h, t_{h_d}, t_a, t_{a_d}))^M \tag{11}$$

However, obtaining the marginal distribution of tagged amplicons can be found by setting $t_g = t_{g_d} = t_h = t_{h_d} = t_a = 1$, and using 1-dimensional **DFT**s of size at most 2^n. The algorithm is given in Algorithm 6.1, with an R implementation in Appendix E.2.3.

Algorithm 6.1 [MARGINAL TARGET AMPLICON DISTRIBUTION FOR THE GENOMIC MODEL]

- Set $N = M2^K$

- Initialize $G[]$,$G_D[]$,$H[]$, $H_D[]$ and $A[]$ to be an N dimensional arrays a such that all entries are zero except the first, eg, $G[0] = 1$.

- Initialize $A_D[]$ to be an N dimensional array such that all entries are zero except the second, $AD[1] = 1$.

- Find the **DFT** of all the arrays, for example, $\mathcal{G}[]$.

- Initialize $\mathcal{F}[]$ to be an N dimensional array.

- for each index g of $\mathcal{G}[]$

  - For K times do:
    * update $\mathcal{G}[g] := (1 - p_g)\mathcal{G}[g] + p_g\mathcal{G}[g]\mathcal{H}_\mathcal{D}[g]$
    * update $\mathcal{G}_\mathcal{D}[g] := (1 - p_{g_d})\mathcal{G}_\mathcal{D}[g] + p_{g_d}\mathcal{G}_\mathcal{D}[g]\mathcal{H}[g]$
    * update $\mathcal{H}[g] := (1 - p_h)\mathcal{H}[g] + p_h\mathcal{H}[g]\mathcal{A}_\mathcal{D}[g]$
    * update $\mathcal{H}_\mathcal{D}[g] := (1 - p_{h_d})\mathcal{H}_\mathcal{D}[g] + p_{h_d}\mathcal{H}_\mathcal{D}[g]\mathcal{A}[g]$
    * set $a = \mathcal{A}[g]$ and $a_d = \mathcal{A}_\mathcal{D}[g]$
    * update $\mathcal{A}[g] := (1 - p_a)a + p_a a a_d$
    * update $\mathcal{A}_\mathcal{D}[g] := (1 - p_{a_d})a_d + p_{a_d} a a_d$

  update $\mathcal{F}[g] := (1 - \phi + \phi\mathcal{G}[g]\mathcal{G}_\mathcal{D}[g])^M$

- Set $F[]$ equal to the inverse **DFT** of $\mathcal{F}[]$. □

Figure 15 shows the tagged amplicon distribution for the genomic strand model, with all amplification probabilities equal to $p = 0.9$, for $K = 14$ cycles ($M = 1$ and $\phi = 1$); in red is shown the corresponding amplicon model distribution We see that the genomic plot is somewhat smoother than the amplicon model, and more peaked as well, confirming visually the lower variance discussed above. The plot on the right shows the results on lowering $p \rightarrow 0.8$. The additional green curve shows a normal distribution with mean and variance matching the genomic model - we see the fit is appears to be quite good. However it is the vertical distances at each x value that are important for evaluating likelihoods) and in this regard the ratios of values are quite different from 1 in places. For example in the range [1000,5000] the ratio of the normal approximation to full distribution value ranges from 0.777 to 1.07. Multiplying many such ratios together for many observed peaks could lead cumulatively to a gross over-estimation or under-estimation of the likelihood, if there is a systematic bias.

Figure 15:
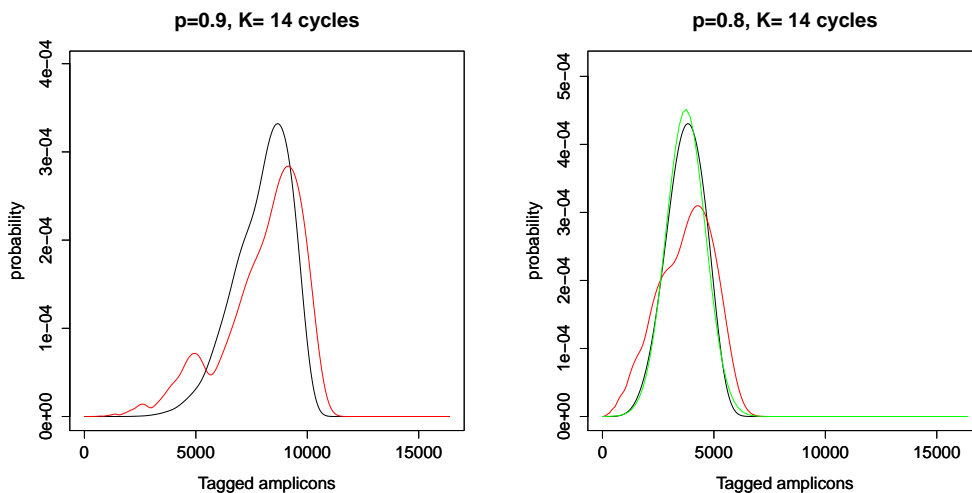
6.6 Including single step backward stutter

We now include stutter into the genomic model. For simplicity we do not consider
either forward stutter or double stutter, nor allow a stutter to stutter, at this stage.
The iterative equations for amplifying a *g*-strand without stutter is:

$$t_g \rightarrow t_g(1 - p_g) + p_g t_g t_{h_d}$$
$$t_{h_d} \rightarrow t_{h_d}(1 - p_{h_d}) + p_{h_d} t_{h_d} t_a$$
$$t_a \rightarrow t_a(1 - p_a) + p_a t_a t_{a_d}$$
$$t_{a_d} \rightarrow t_{a_d}(1 - p_{a_d}) + p_{a_d} t_{a_d} t_a$$

To include stutter we allow there to be stutter variants of h_d, *a* and a_d strands,
which we denote with an extra *s* suffix. We need extra *t*'s to corresponding to
each of these variants, and also additional amplification probabilities for the new
amplification possibilities. We could introduce many stutter probabilities as well,
but will keep for simplicity to a single conditional stutter probability. Our non-
stutter equations become extended to:

$$t_g \rightarrow t_g(1 - p_g) + p_g(1 - \xi)t_g t_{h_d} + p_g \xi t_g t_{h_{sd}}$$

$$t_{h_d} \rightarrow t_{h_d}(1 - p_{h_d}) + p_{h_d}(1 - \xi)t_{h_d} t_a + p_{h_d} \xi t_{h_d} t_{a_s}$$

$$t_{h_{sd}} \rightarrow t_{h_{sd}}(1 - p_{h_{sd}}) + p_{h_{sd}} t_{h_{sd}} t_{a_s}$$

$$t_a \rightarrow t_a(1 - p_a) + p_a(1 - \xi)t_a t_{a_d} + p_a \xi t_a t_{a_{sd}}$$

$$t_{a_d} \rightarrow t_{a_d}(1 - p_{a_d}) + p_{a_d}(1 - \xi)t_{a_d} t_a + p_{a_d} \xi t_{a_d} t_{a_s}$$

$$t_{a_s} \rightarrow t_{a_s}(1 - p_{a_s}) + p_{a_s} t_{a_s} t_{a_{sd}}$$

$$t_{a_{sd}} \rightarrow t_{a_{sd}}(1 - p_{a_{sd}}) + p_{a_{sd}} t_{a_{sd}} t_{a_s}$$

For the initial g_d strand we have to introduce the additional stutter variant h_s and symbols t_{g_d} and t_{h_s}. The g_d equations are thus:

$$t_{g_d} \rightarrow t_{g_d}(1 - p_{g_d}) + p_{g_d}(1 - \xi)t_{g_d} t_h + p_{g_d} \xi t_{g_d} t_{h_s}$$

$$t_h \rightarrow t_h(1 - p_h) + p_h(1 - \xi)t_h t_{a_d} + p_h \xi t_h t_{a_{sd}}$$

$$t_{h_s} \rightarrow t_{h_s}(1 - p_{h_s}) + p_{h_s} t_{h_s} t_{a_s}$$

$$t_a \rightarrow t_a(1 - p_a) + p_a(1 - \xi)t_a t_{a_d} + p_a \xi t_a t_{a_{sd}}$$

$$t_{a_d} \rightarrow t_{a_d}(1 - p_{a_d}) + p_{a_d}(1 - \xi)t_{a_d} t_a + p_{a_d} \xi t_{a_d} t_{a_s}$$

$$t_{a_s} \rightarrow t_{a_s}(1 - p_{a_s}) + p_{a_s} t_{a_s} t_{a_{sd}}$$

$$t_{a_{sd}} \rightarrow t_{a_{sd}}(1 - p_{a_{sd}}) + p_{a_{sd}} t_{a_{sd}} t_{a_s}$$

Hence we need to keep track of 10 t's corresponding to the 2 genomic strands, the 4 half strands and 4 amplicon strands. For the marginal stutter distribution we are interested in the tagged stutter amplicons, $t_{a_{sd}}$.

These single-strand equations can be 'lifted' to iterative equations for the **PGFs**, giving generalizations of Algorithm 6.1 that are omitted, for obtaining the marginal distributions of target and stutter amplicons. Figure 16 shows the marginal distribution of stutter amplicons for the genomic model, with the red curve showing the marginal from the amplicon model. We see that the genomic stutter distribution is narrower and more peaked, thus having a lower variance than the amplicon model. For the parameters in the plot, the means and variances are shown in Table 1. The means are approximately equal, whereas the variances are about a factor of 2 different. The derivation of moments is deferred to Appendix C. Figure 17 shows an example of a marginal stutter distribution with binomial pre-sampling of strands.

K= 16 M= 1 p= 0.85 xi= 0.03
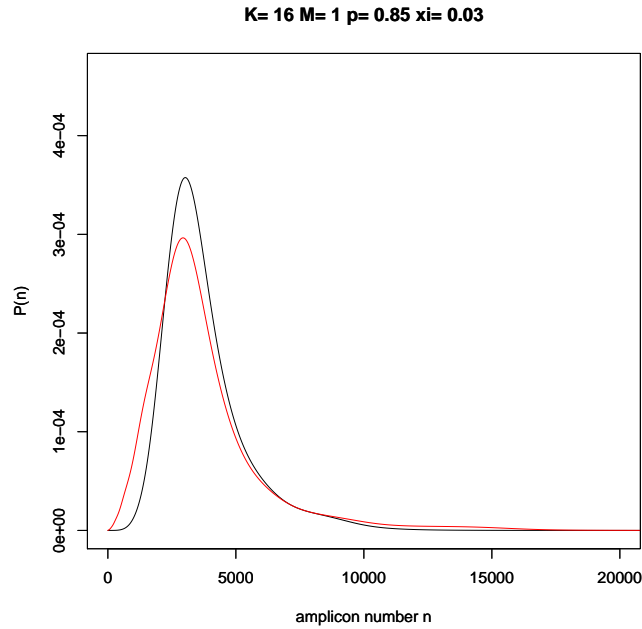
Figure 16: Marginal stutter distributions for the genomic (black) and amplicon model (red), with all amplifications probabilities equal to 0.85, and conditional stutter probability equal to 0.03, for a single strand pair amplified for 16 cycles.

Table 1: Means and variances of the amplicon and genomic model curves shown in Figure 16.

	mean	variance
Amplicon model	3749.002	5330275
Genomic model	3748.594	2664897
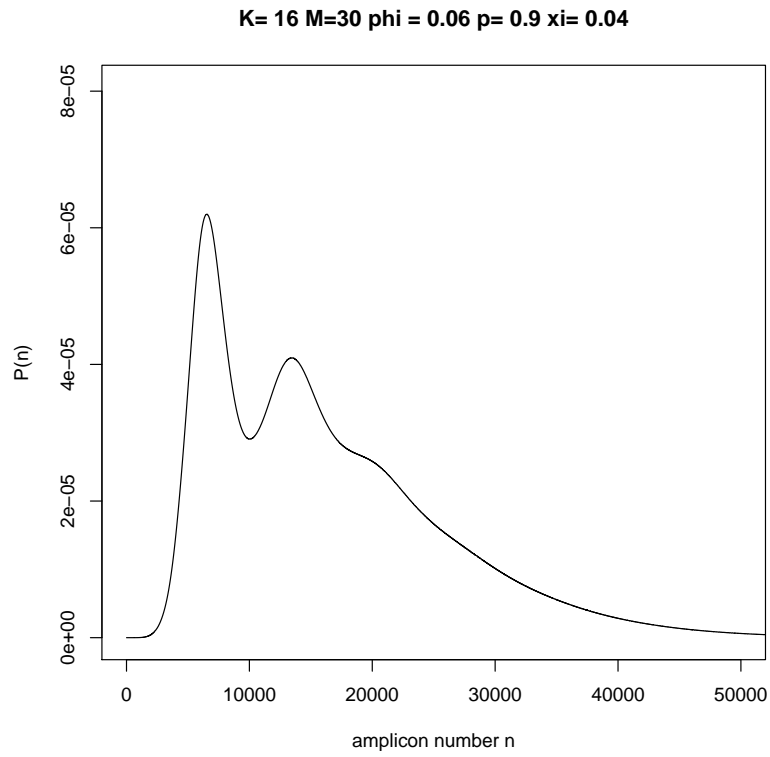
Figure 17: Marginal stutter distribution for the genomic model, with all amplifications probabilities $p = 0.9$, conditional stutter probability $\xi = 0.04$, $M = 30$ genome strands selected with probability $\phi = 0.06$ and amplified for $K = 16$ cycles. The complete dropout probability value $0.94^{30} = 0.1562556$ at $n = 0$ is not shown.

6.7 Extension to forward stutter and double stutter

The extension to include forward stutter and double back-stutter is straightforward, and follows the path of stutter. We need two extra h variables for the forward stutter and double stutter products, and 4 extra a variables, two for forward stutter and two for the double stutter. Thus we have 16 variables altogether.

Let the subscript f denotes forward stutter, and r double reverse stutter. Let ξ_r denote the conditional probability of double stutter in a cycle, and ξ_f that for forward stutter. Then the individual branching equations are given by:

$$t_g \rightarrow t_g(1 - p_g) + p_g(1 - \xi_r - \xi_s - \xi_f)t_g t_{h_d} + p_g \xi_r t_g t_{h_{rd}} + p_g \xi_s t_g t_{h_{sd}} + p_g \xi_f t_g t_{h_{fd}}$$

$$t_{g_d} \rightarrow t_{g_d}(1 - p_{g_d}) + p_{g_d}(1 - \xi_r - \xi_s - \xi_f)t_{g_d} t_h + p_{g_d} \xi_r t_{g_d} t_{h_r} + p_{g_d} \xi_s t_{g_d} t_{h_s} + p_{g_d} \xi_f t_{g_d} t_{h_f}$$

$$t_h \rightarrow t_h(1 - p_h) + p_h(1 - \xi_r - \xi_s - \xi_f)t_h t_{a_d} + p_h \xi_r t_h t_{a_{rd}} + p_h \xi_s t_h t_{a_{sd}} + p_h \xi_f t_h t_{a_{fd}}$$

$$t_{h_r} \rightarrow t_{h_r}(1 - p_{h_r}) + p_{h_r}(1 - \xi_f)t_{h_r} t_{a_{rd}} + p_{h_r} \xi_f t_{h_r} t_{a_{sd}}$$

$$t_{h_s} \rightarrow t_{h_s}(1 - p_{h_s}) + p_{h_s}(1 - \xi_s - \xi_f)t_{h_s} t_{a_{sd}} + p_{h_s} \xi_s t_{h_s} t_{a_{rd}} + p_{h_s} \xi_f t_{h_s} t_{a_d}$$

$$t_{h_f} \rightarrow t_{h_f}(1 - p_{h_f}) + p_{h_f}(1 - \xi_s)t_{h_f} t_{a_{fd}} + p_{h_f} \xi_s t_{h_f} t_{a_d}$$

$$t_{h_d} \rightarrow t_{h_d}(1 - p_{h_d}) + p_{h_d}(1 - \xi_r - \xi_s - \xi_f)t_{h_d} t_a + p_{h_d} \xi_r t_{h_d} t_{a_r} + p_{h_d} \xi_s t_{h_d} t_{a_s} + p_{h_d} \xi_f t_{h_d} t_{a_f}$$

$$t_{h_{rd}} \rightarrow t_{h_{rd}}(1 - p_{h_{rd}}) + p_{h_{rd}}(1 - \xi_f)t_{h_{rd}} t_{a_r} + p_{h_{rd}} \xi_f t_{h_{rd}} t_{a_s}$$

$$t_{h_{sd}} \rightarrow t_{h_{sd}}(1 - p_{h_{sd}}) + p_{h_{sd}}(1 - \xi_f)t_{h_{sd}} t_{a_s} + p_{h_{sd}} \xi_f t_{h_{sd}} t_a$$

$$t_{h_{fd}} \rightarrow t_{h_{fd}}(1 - p_{h_{fd}}) + p_{h_{fd}}(1 - \xi_s)t_{h_{fd}} t_{a_f} + p_{h_{fd}} \xi_s t_{h_{fd}} t_a$$

$$t_a \rightarrow t_a(1 - p_a) + p_a(1 - \xi_s - \xi_f)t_a t_{a_d} + p_a \xi_s t_a t_{a_{sd}} + p_a \xi_f t_a t_{a_{fd}}$$

$$t_{a_d} \rightarrow t_{a_d}(1 - p_{a_d}) + p_{a_d}(1 - \xi_s - \xi_f)t_{a_d} t_a + p_{a_d} \xi_s t_{a_d} t_{a_s} + p_{a_d} \xi_f t_{a_d} t_{a_f}$$

$$t_{a_s} \rightarrow t_{a_s}(1 - p_{a_s}) + p_{a_s}(1 - \xi_s - \xi_f)t_{a_s} t_{a_{sd}} + p_{a_s} \xi_s t_{a_s} t_{a_{rd}} + p_{a_s} \xi_f t_{a_s} t_{a_d}$$

$$t_{a_{sd}} \rightarrow t_{a_{sd}}(1 - p_{a_{sd}}) + p_{a_{sd}}(1 - \xi_s - \xi_f)t_{a_{sd}} t_{a_s} + p_{a_{sd}} \xi_s t_{a_{sd}} t_{a_r} + p_{a_{sd}} \xi_f t_{a_{sd}} t_a$$

$$t_{a_r} \rightarrow t_{a_r}(1 - p_{a_r}) + p_{a_r}(1 - \xi_f)t_{a_r} t_{a_{rd}} + p_{a_r} \xi_r t_{a_r} t_{a_{sd}}$$

$$t_{a_{rd}} \rightarrow t_{a_{rd}}(1 - p_{a_{rd}}) + p_{a_{rd}}(1 - \xi_f)t_{a_{rd}} t_{a_r} + p_{a_{rd}} \xi_f t_{a_{rd}} t_{a_s}$$

$$t_{a_f} \rightarrow t_{a_f}(1 - p_{a_f}) + p_{a_f}(1 - \xi_s)t_{a_f} t_{a_{fd}} + p_{a_f} \xi_s t_{a_f} t_{a_d}$$

$$t_{a_{fd}} \rightarrow t_{a_{fd}}(1 - p_{a_{fd}}) + p_{a_{fd}}(1 - \xi_s)t_{a_{fd}} t_{a_f} + p_{a_{fd}} \xi_s t_{a_{fd}} t_a$$

The corresponding recurrence relations for the multivariate **PGF** in these 18 variables is left to the reader.

With the introduction of forward and double stutter we have the possibility that over several cycles a stutter product may amplify by forward stuttering to make target amplicon, or could itself stutter to make a double stutter. Similarly

a forward stutter product from a target could amplify and stutter thus producing a target, or could double stutter and product a stutter. Likewise a double stutter product could amplify by forward stuttering and create a stutter product. This means that there is a cyclic dependency in the equations above, so care is required in their computer implementation.

Note that the above equations do not describe the possibility that a double-stutter strand could itself stutter or double stutter when amplified, or a forward stutter strand could itself forward stutter. These more general possibilities are accounted in Part III, in which we give a general modelling framework, and also include the additional artefacts of drop-in and background noise, and DNA degradation, that we have not dealt with so far. But first we look at some other mathematical computational aspects of the branching process.

7 Further Mathematical and computational aspects

In this section, further mathematical properties of the branching process as revealed by the probability generating functions are explored. Readers interested in forensic applications may wish to skip this part and go onto Part III.

7.1 Finding marginal distributions without a full DFT

We consider again the simple amplicon model, in which we start with a single amplicon with **PGF** recurrence relation

$$F_{k+1}(t) = (1 - p)F_k(t) + pF_k(t)^2 \tag{12}$$

and initial condition $F_0(t) = t$. If we let $N = 2^K$, then we can find the full distribution using the **DFT**, or alternatively, for a particular value n we can find the probability of exactly n amplicons via Cauchy's residue theorem

$$
\begin{aligned}
F[n] &= \frac{1}{2\pi i} \oint \frac{F_K(t)}{t^{n+1}} dt \\
&= \frac{1}{N} \sum_{j=0}^{N-1} F_K(e^{-i2\pi j/N}) e^{i2\pi jn/N}
\end{aligned}
\tag{13}
$$

To evaluate this sum, we have to evaluate each term $A_K(e^{-i2\pi j/N})$ for points located on the unit circle in the complex plane. This can be done the recurrence equation

(12). If one views (12) as a nonlinear discrete dynamical system, the we see that it has fixed points at $t = 0$ and $t = 1$. The fixed point at $t = 0$ is stable, whilst the fixed point at $t = 1$ is unstable: for real values of $t \in [0, 1)$, iterates of (12) converges to zero, whilst for real $t > 1$ iterates diverge to infinity. It turns out that, apart from the $j = 0$ term which corresponds to the stable point $t = 1$, the iteration scheme $t \rightarrow (1 - p)t + p * t^2$ on the unit circle forms a contraction mapping so that the $F_k(e^{-i2\pi j/N})$ iterates converge to the origin as $k \rightarrow \infty$. This is illustrated in Figure 18. (See also Stolovitzky and Cecchi (1996b).)
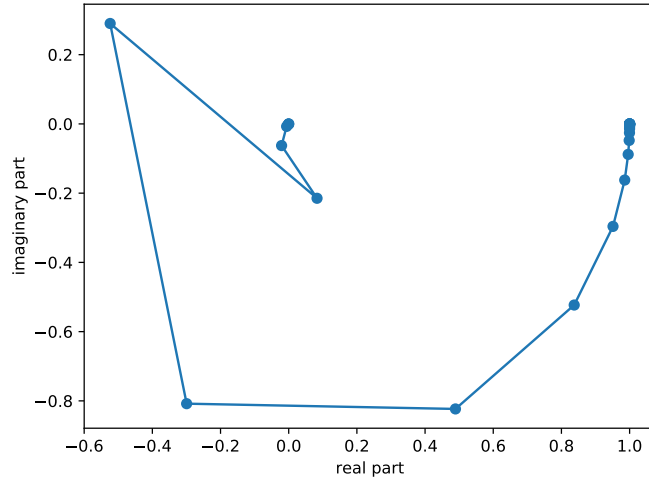
Figure 18: Convergence of iterates to 0 in the complex plane for the simple amplicon model, of $F_k(e^{-i2\pi j/N})$: $k = 0, 1, \ldots K$, for $j = 201$ in (13), for $p = 0.85$ and up to $K = 28$ iterations. The initial value is $F_0(e^{-i2\pi j/N}) = 0.9999999999890425 - i4.681337853637813 \times 10^{-6}$, and the the final iterate is at $F_{28}(e^{-i2\pi j/N}) = -2.084 \times 10^{-5} - i2.223 \times 10^{-5}$ in the complex plane.

Not only do the $F_k(e^{-i2\pi j/N})$ converge to the origin, they do so rapidly with increasing j. Hence, we may approximate (13) by a truncated series with a point symmetrically located around $j = 0$ (ensuring the sum total is real valued), thus:

$$F[n] \approx \frac{1}{N} \sum_{j=-L}^{L} F_K(e^{-i2\pi j/N})e^{i2\pi jn/N} \tag{14}$$

61

Figure 19 overlays the exact distribution obtained from a full **FFT** analysis, and the distribution for the truncated approximation of (14). The curves are visually indistinguishable.
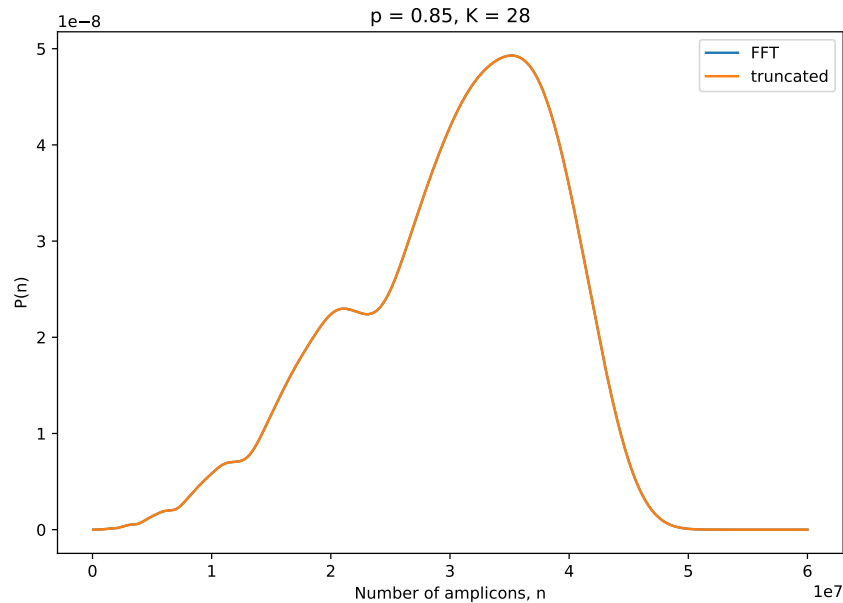
Figure 19: Distribution of the number of amplicons for the simple amplicon model, starting with a single amplicon, amplified for 28 cycles with amplification probability 0.85 per cycle. The figure shows plots of 1000 evenly spaced n values, generated using the Julia code in Appendix E.3.1 for the exact distribution calculated using the a **FFT** analysis, and using the truncation approximation of (14) with $L = 1024$. The exact **FFT** took several minutes to evaluate, and required approximately 10Gb of ram. In contrast, evaluating all 1000 points using the truncated approximation took around 0.25 seconds with minimal memory overhead. The two curves are visually indistinguishable.

Taking account of binomial pre-sampling with truncation requires a little care. The full series expansion, for M starting amplicons, is

$$\frac{1}{N}\sum_{j=0}^{N-1}(1-\phi+\phi F_K(e^{-i2\pi j/N}))^M e^{i2\pi jn/N}$$

To carry out the truncation, we set $F_K(e^{-i2\pi j/N})) = 0$ on the j terms on the circle further than $\pm L$ from the $j = 0$ term, to obtain

$$\frac{1}{N}\sum_{j=-L}^{L}(1-\phi+\phi F_K(e^{-i2\pi j/N}))^M e^{i2\pi jn/N} + \frac{1}{N}\sum_{j=-L*}^{L*}(1-\phi)^M e^{i2\pi jn/N}$$

where the second summation is over terms complementary to the first summation. We now use that $e^{i2\pi n/N}$ is an N-th root of unity, for which $\sum_{j=0}^{N-1} e^{i2\pi jn/N} = 0$, to obtain

$$\sum_{j=-L*}^{L*}(1-\phi)^M e^{i2\pi jn/N} = -\sum_{j=-L}^{L}(1-\phi)^M e^{i2\pi jn/N}$$

so that

$$P[n] \approx \frac{1}{N}\sum_{j=-L}^{L}\left((1-\phi+\phi F_K(e^{-i2\pi j/N})^M - (1-\phi)^M\right)e^{i2\pi jn/N} \qquad (15)$$

Drop-in can be handled in a similar manner, as can finding stutter marginal distribution values. Obtaining good convergence typically requires more terms than for (14). Details are left to the interested reader to investigate (or assign to a research student if available). Note that if the series is truncated prematurely it could lead to poor, and even negative, probabilities.

Bivariate distributions may also be found using similar truncated series. As pointed out in Appendix E.1.3, to do a full **FFT** analysis to obtain the bivariate distribution of a target and stutter amplicons numbers would require an impossible amount of computer memory and time. However, by writing the 2-D**FFT** function out as a double series and truncating to a smaller set of terms near the origin, efficient and accurate evaluation of individual bivariate probabilities may be carried out. Accuracy can be gauged by seeing how the values change with using an increasing number of terms in the double series. The details are left to the reader to fill in: Figure 20 shows two views of the bivariate distribution for a single starting amplicon, of the number of target and stutter amplicons, using summation limits of $L = \pm 10^{12}$ for each evaluated point (thus around $2^{26} \approx 67$ million terms altogether).
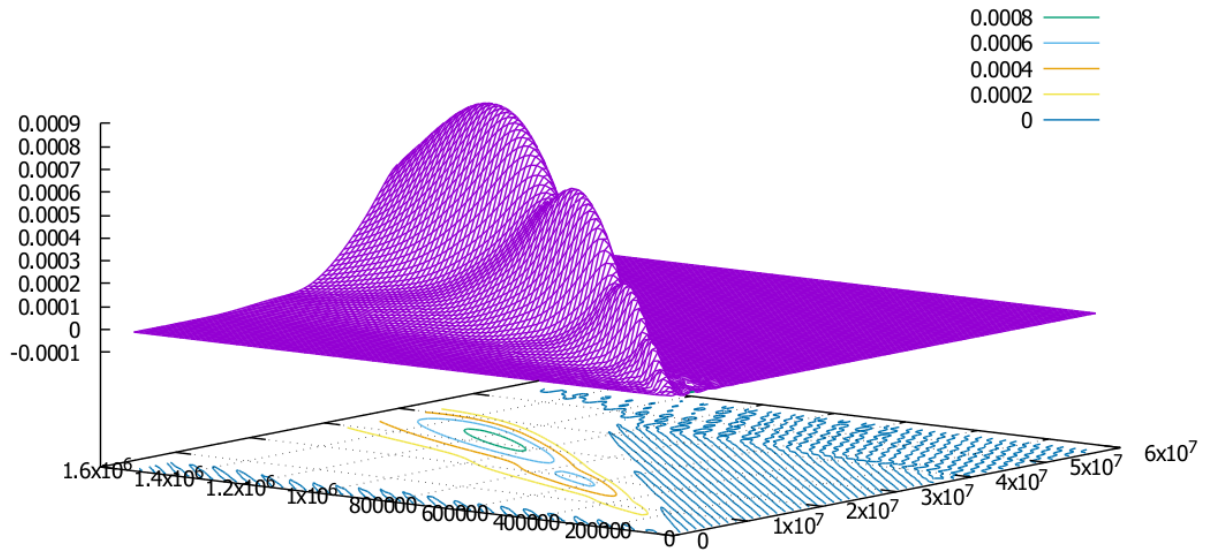
Figure 20: Bivariate distribution for target and stutter amplicons, starting from a single amplicon, for $K = 28$, $p = 0.85$ and $\xi = 0.004$. Note that the vertical scale (i.e., the probability values) have been scaled upwards by a factor of $598684 *$ $15822 = 9472378248$ so that the legend for the contour levels show non-zero values. The projected contour plot is similar to the plot in Figure 11. (The values 598684 and 15822 are the intervals in the target and stutter amplicon numbers for the grid of points used to generate the data-points in the plot. In each direction 96 values were used, thus 9126 evaluations in total.)

64

Part III
New Framework in detail

The previous sections have given some indication of the possible models that can be formulated, and how they may be analyzed using the mathematical tools of multivariate **PGF**s combined with **DFT**s. In this part in Section 8 we present a general framework of the process leading to an **EPG**, or set of **EPG**s in the case of replicate analyses. Specialization of this framework to a specific model is then presented in Section 9, and its performance is illustrated using simulated in Section 10 and publicly available real data in Section 11.

8   Modelling the EPG generation process

8.1   Contributor DNA

We assume that we have a sample of C DNA cells in a volume V. The DNA is assumed to come from I individuals, with the i-th individual denoted by K_i, who is a contributor of c_i cells to the sample. Thus $C = \sum_{i=1}^{I} c_i$. Let L denote the set of STR loci under investigation, and let A_l denote the set of alleles for a given locus $l \in L$. The total number of genomic strands of type $a_l \in A_l$ within the cells contributed by K_i depends on the genotype of the individual. Let n_{ia_l} denote the number of alleles of type $a_l \in A_l$ of individual K_i. The values that n_{ia_l} can take depends on the locus l. With a few exceptions, the possibilities are as follows.

- If l is autosomal, then $n_{ia_l} \in \{0, 1, 2\}$.

- if l is Amelogenin, then $n_{iX} \in \{1, 2\}$ and $n_{iY} \in \{0, 1\}$. If K_i is male then $n_{iX} = n_{iY} = 1$; otherwise K_i is female with $n_{iX} = 2$ and $n_{iY} = 0$.

- If l is a Y-linked locus, then either $n_{ia_l} \in \{0, 1, 2\}$ or $n_{ia_l} \in \{0, 1\}$, depending on the precise locus.

- if If l is an X-linked locus, then $n_{ia_l} \in \{0, 1\}$ if K_i is male, and $n_{ia_l} \in \{0, 1, 2\}$ if K_i is female.

Let g_{a_l} and $g_{a_l:d}$ denote the two complimentary strands for the genome of type $a_l \in A_L$. We use $t_{g_{a_l}}$ and $t_{g_{a_l:d}}$ for symbols in their generating functions. It is

not until the **PCR** process begins that the g_{a_l} and $g_{a_l:d}$ strands become separated. Prior to **PCR** they are combined, hence the **PGF** of the number of both of these genomic strands in the DNA sample of allele type a_l from K_i is $(t_{g_{a_l}} t_{g_{a_l:d}})^{n_{ia_l} c_i}$, and the multivariate **PGF** of all alleles in A_l from person K_i is

$$\prod_{a_l \in A_l} (t_{g_{a_l}} t_{g_{a_l:d}})^{n_{ia_l} c_i}. \tag{16}$$

If, for example, l is autosomal and K_i is homozygous with genotype (a_l, a_l) then the **PGF** is $(t_{g_{a_l}} t_{g_{a_l:d}})^{2c_i}$.

Using enzymes, DNA is extracted from the cells in the volume V. Let $\pi_{e:i,a_l}$ denote the extraction efficiency, that is, the probability that a genome segment containing the allele $a_l \in A_l$ from K_i is extracted in a state suitable for amplification. The efficiency $\pi_{e:i,a_l}$ will depend on the process of the DNA extraction, and also the allele via its length. The extraction process, as well as removing genomes from cells, breaks them up into small pieces. The location of the breakage points along a genome can be considered a Poisson process, so that the distance between breaks has an exponential distribution. If a break occurs in or between the flanking regions of a genomic strand pair, then it cannot be amplified, hence the dependence of $\pi_{e:i,a_l}$ on the allele.[4] The **PGF** for extraction of the (single) pair is thus

$$E_x(t_{g_{a_l}}, t_{g_{a_l:d}}) = 1 - \pi_{e:i,a_l} + \pi_{e:i,a_l} t_{g_{a_l}} t_{g_{a_l:d}}.$$

However, prior to extraction the DNA may be degraded by age, environmental or other factors. Such degradation could also be person specific (for example, depending on the cell type of the DNA from the person).

One form of degradation leads to a break in the genome-pair strand in or between the flanking regions. If we let λ denote the probability of there not being such a break, then the **PGF** for extraction, of amplify-able (single) genome pair, becomes

$$E_x(t_{g_{a_l}}, t_{g_{a_l:d}}) = 1 - \pi_{e:i,a_l} \lambda + \pi_{e:i,a_l} \lambda t_{g_{a_l}} t_{g_{a_l:d}}.$$

Alternatively degradation could lead to one of the complimentary strand pairs having a break and the other not, as illustrated in Figure 21. If we assume such breaks occur independently for each if the complimentary strands, then the joint **PGF** for extraction of the (single) genome pair strands becomes

$$Ex(t_{g_{a_l}}, t_{g_{a_l:d}}) = 1 - \pi_{e:i,a_l}(1 - (1-\lambda)(1-\lambda_d)) + \pi_{e:i,a_l}(1 - \lambda + \lambda t_{g_{a_l}})(1 - \lambda_d + \lambda_d t_{g_{a_l:d}}).$$

---

[4]With the Poisson process just described, i $\pi_{e:i,a_l}$ will decay exponentially at a rate proportional to the total base-pair size of the between and including the flanking regions. This is one possible mechanism of *preferential amplification* (Walsh et al., 1992).

where we allow for the possibility of different breakage probabilities, λ and λ_d, for the two strands (arising from their different, but complimentary, chemical base composition).
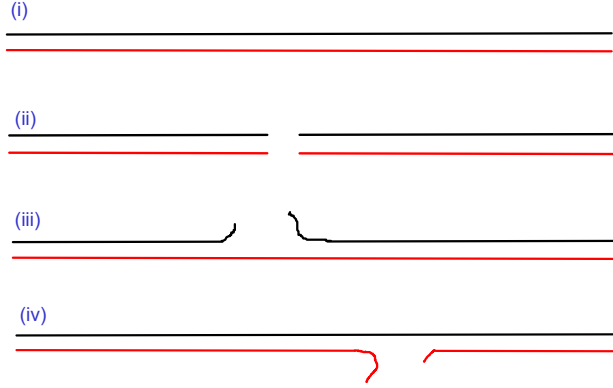
Figure 21: Genomic strand breakage possibilities for a degradation model. (i) An intact strand pair; (ii) a simultaneous breakage in both strands at a common point; (iii) breakage in one strand; (iv) breakage in the complementary strand.

A fraction π_f of the volume V is taken for amplification. Hence the joint **PGF** for successful extraction and selection of the genome strands from a single pair is

$$1 - \pi_f + \pi_f E_x(t_{g_{a_l}}, t_{g_{a_l:d}})$$

The total number of such strands from person K_i extracted and selected for amplification and are amplify-able therefore has the **PGF**

$$\left(1 - \pi_f + \pi_f E_x(t_{g_{a_l}}, t_{g_{a_l:d}})\right)^{n_{ia_l}c_i}. \tag{17a}$$

where $E_x(t_{g_{a_l}}, t_{g_{a_l:d}})$ depends on the breakage model chosen.

The full multivariate **PGF** for the contributors' strands from all loci under consideration ready for amplification is therefore

$$\prod_{l \in L} \prod_{a \in A_l} \prod_{i \in I} \left(1 - \pi_f + \pi_f E_x(t_{g_{a_l}}, t_{g_{a_l:d}})\right)^{n_{ia_l}c_i}. \tag{18}$$

8.2   Including Drop-in

In addition to the extracted alleles, there is a possibility that spurious *drop-in* alleles may get into the minitube in which the aliquot is ready for the **PCR** process.

67

We follow Puch-Solis (2014) and assume that such drop-in events occur by a Poisson process. Denote the drop-in rate for allele $a_l \in A_l$ by λ_{a_l}. Then the **PGF** for the total number of genome strand pairs that drop-in is given by

$$D_r(\, t_{g_{a_l}}, t_{g_{a_l:d}}) = \exp\left(\lambda_{a_l}(t_{g_{a_l}} t_{g_{a_l:d}} - 1)\right) \tag{19}$$

Drop-ins occur independently for each locus, and independently of the genotypes of the I individuals. Hence the **PGF** for the genomic strands from drop-in and contributors prior to amplification is

$$\prod_{l \in L} \prod_{a \in A_l} \prod_{i \in I} (1 - \pi_f + \pi_f E_x(t_{g_{a_l}}, t_{g_{a_l:d}}))^{n_{ia_l} c_i} D_r(\, t_{g_{a_l}}, t_{g_{a_l:d}}) \tag{20}$$

Within the genomic strand framework presented here, there is an alternative model for drop-in, in which amplicon-pair strands, rather than genomic-pair strands, fall into the minitube that the **PCR** is carried out in. One reason amplicons could drop-in is that there is a build-up over time of contaminating amplicons from the previous **PCR** analyses carried out in the forensic laboratory. This possibility is supported by the observation that there are lower levels of drop-in in samples amplified after a laboratory has been deep-cleaned, compared to just before a deep-cleaning has been carried out, and that as time goes on dropin-rates increase until the laboratory is cleaned again[5]

To model this alternative, we use a Poisson drop-in model for the number of amplicons that drop-in, given by the **PGF**

$$D_r(\, t_{a_{a_l}}, t_{a_{a_l:d}}) = \exp\left(\lambda_{a_l}(t_{a_{a_l}} t_{a_{a_l:d}} - 1)\right), \tag{21}$$

instead of the genomic strand drop-in model (19). Hence the **PGF** for the genomic strands and amplicons prior to amplification is now

$$\prod_{l \in L} \prod_{a \in A_l} \prod_{i \in I} (1 - \pi_f + \pi_f E_x(t_{g_{a_l}}, t_{g_{a_l:d}}))^{n_{ia_l} c_i} D_r(\, t_{a_{a_l}}, t_{a_{a_l:d}}). \tag{22}$$

One could even consider both Poisson processes occurring simultaneously so that we allow drop-in of both genomic strands and amplicon strands, leading to

$$\prod_{l \in L} \prod_{a \in A_l} \prod_{i \in I} (1 - \pi_f + \pi_f E_x(t_{g_{a_l}}, t_{g_{a_l:d}}))^{n_{ia_l} c_i} D_r(\, t_{g_{a_l}}, t_{g_{a_l:d}}) D_r(\, t_{a_{a_l}}, t_{a_{a_l:d}}). \tag{23}$$

in which we can allow a different drop-in rate λ_{a_l} for the two processes.

---

[5]Sue Pope, personal communication.

8.3 PCR amplification

During the **PCR** process we may generate strands of type $g_{a_l}, g_{a_l d}, h_{a_l}, h_{a_l d}, a_{a_l}$ and $a_{a_l d}$. For any of these strands to make a successful copy (or copy of some stutter type) a primer has to bind at the primer binding site. The probability of this happening will depend on various factors in how the **PCR** is carried out (e.g., the kit, temperature etc.). It could also depend on the type of strand considered. For example the g strands could be quite long and coil up to create a barrier preventing a primer from binding. It also depends on the binding energy of the primer to the strand, and each end of the flanking region generally has different base-pair composition, so we should expect the binding energies to be different. We thus introduce primer binding probabilities specific to each complementary-strand

$$p_{l,g}, p_{l,gd}, p_{l,h}, p_{l,hd}, p_{l,a} \text{ and } p_{l,ad}.$$

Binding a primer is a pre-requisite for a successful copy. However during the remainder of the duplication process a copying error could occur, leading to a stutter variant. The probability that this happens, and the resulting stutter artefact, will depend on the initial allele a_l and the resulting allele b_l. We thus introduce $\xi_{b_l|a_l}$ to denote the conditional probability that a strand of allele type a_l creates strand of allele type b_l given that some product is produced We have that for all $a_l \in A_l$,

$$\sum_{b_l \in A_l} \xi_{b_l|a_l} = 1$$

Note that we have the conditional probability for copying without stuttering, given some sort of copy if made, is

$$\xi_{a_l|a_l} = 1 - \sum_{b_l \in A_l: b_l \neq a_l} \xi_{b_l|a_l}.$$

We shall assume that these probabilities remain constant throughout all of the cycles of the **PCR** process, though this assumption could be relaxed.

The set of **PGF**s for single-strand single-cycle duplication is then given by

$$g_{a_l} : (1 - p_{l,g})t_{g_{a_l}} + p_{l,g} \sum_{b_l \in A_l} \xi_{b_l | a_l} t_{g_{a_l}} t_{h_{a_l d}} \tag{24a}$$

$$g_{a_l d} : (1 - p_{l,gd})t_{g_{a_l}} + p_{l,gd} \sum_{b_l \in A_l} \xi_{b_l | a_l} t_{g_{a_l d}} t_{h_{a_l}} \tag{24b}$$

$$h_{a_l} : (1 - p_{l,h})t_{h_{a_l}} + p_{l,h} \sum_{b_l \in A_l} \xi_{b_l | a_l} t_{h_{a_l}} t_{a_{a_l d}} \tag{24c}$$

$$h_{a_l d} : (1 - p_{l,hd})t_{h_{a_l d}} + p_{l,hd} \sum_{b_l \in A_l} \xi_{b_l | a_l} t_{h_{a_l d}} t_{a_{a_l}} \tag{24d}$$

$$a_{a_l} : (1 - p_{l,a})t_{a_{a_l}} + p_{l,a} \sum_{b_l \in A_l} \xi_{b_l | a_l} t_{a_{a_l}} t_{a_{a_l d}} \tag{24e}$$

$$a_{a_l d} : (1 - p_{l,ad})t_{a_{a_l d}} + p_{l,ad} \sum_{b_l \in A_l} \xi_{b_l | a_l} t_{a_{a_l d}} t_{a_{a_l}} \tag{24f}$$

These single strand **PGF**s are 'lifted' to the full vectorial **PGF** of the **PCR** process, as follows. Let $F_n(\mathbf{t}_l \,|\, s)$ denote the multivariate **PGF** for all the possible types of strands that are generated from a single strand of types

$$s \in \{g_{a_l}, g_{a_l d}, h_{a_l}, h_{a_l d}, a_{a_l}, a_{a_l d} : a_l \in A_l\}.$$

The $\mathbf{t}_l$ represents all the possible symbols for all the possible alleles and their strand types (there will be $6|A_l|$ such symbols). Then the recurrence relations for the **PCR** branching process have the form:

$$F_{n+1}(\mathbf{t}_l \,|\, g_{a_l}) = (1 - p_{l,g})F_n(\mathbf{t}_l \,|\, g_{a_l}) + p_{l,g} \sum_{b_l \in A_l} \xi_{b_l | a_l} F_n(\mathbf{t}_l \,|\, g_{a_l})F_n(\mathbf{t}_l \,|\, h_{a_l d}) \tag{25a}$$

$$F_{n+1}(\mathbf{t}_l \,|\, g_{a_l d}) = (1 - p_{l,gd})F_n(\mathbf{t}_l \,|\, g_{a_l d}) + p_{l,gd} \sum_{b_l \in A_l} \xi_{b_l | a_l} F_n(\mathbf{t}_l \,|\, g_{a_l d})F_n(\mathbf{t}\_l \,|\, h_{a_l}) \tag{25b}$$

$$F_{n+1}(\mathbf{t}_l \,|\, h_{a_l}) = (1 - p_{l,h})F_n(\mathbf{t}_l \,|\, h_{a_l}) + p_{l,h} \sum_{b_l \in A_l} \xi_{b_l | a_l} F_n(\mathbf{t}_l \,|\, h_{a_l})F_n(\mathbf{t}_l \,|\, a_{a_l d}) \tag{25c}$$

$$F_{n+1}(\mathbf{t}_l \,|\, h_{a_l d}) = (1 - p_{l,hd})F_n(\mathbf{t}_l \,|\, h_{a_l d}) + p_{l,hd} \sum_{b_l \in A_l} \xi_{b_l | a_l} F_n(\mathbf{t}_l \,|\, h_{a_l d})F_n(\mathbf{t}_l \,|\, h_{a_l}) \tag{25d}$$

$$F_{n+1}(\mathbf{t}_l \,|\, a_{a_l}) = (1 - p_{l,a})F_n(\mathbf{t}_l \,|\, a_{a_l}) + p_{l,a} \sum_{b_l \in A_l} \xi_{b_l | a_l} F_n(\mathbf{t}_l \,|\, a_{a_l})F_n(\mathbf{t}_l \,|\, a_{a_l d}) \tag{25e}$$

$$F_{n+1}(\mathbf{t}_l \,|\, a_{a_l d}) = (1 - p_{l,ad})F_n(\mathbf{t}_l \,|\, a_{a_l d}) + p_{l,ad} \sum_{b_l \in A_l} \xi_{b_l | a_l} F_n(\mathbf{t}_l \,|\, a_{a_l d})F_n(\mathbf{t}_l \,|\, a_{a_l}) \tag{25f}$$

with initial conditions

$$F_0(\mathbf{t}_l \mid g_{a_l}) = t_{g_{a_l}} \tag{26a}$$

$$F_0(\mathbf{t}_l \mid g_{a_l d}) = t_{g_{a_l d}} \tag{26b}$$

$$F_0(\mathbf{t}_l \mid h_{a_l}) = t_{h_{a_l}} \tag{26c}$$

$$F_0(\mathbf{t}_l \mid h_{a_l d}) = t_{h_{a_l d}} \tag{26d}$$

$$F_0(\mathbf{t}_l \mid a_{a_l}) = t_{a_{a_l}} \tag{26e}$$

$$F_0(\mathbf{t}_l \mid a_{a_l d}) = t_{a_{a_l d}} \tag{26f}$$

The joint **PGF** of all types of strand products after n cycles generated from a single initial pair strand $(g_{a_l}, g_{a_l d})$ is

$$F_n(\mathbf{t}_l \mid g_{a_l}) F_n(\mathbf{t}_l \mid g_{a_l d}) \tag{27}$$

8.4 The joint PGF after PCR

If using the genomic drop-in model (19), one now substitutes $t_{g_{a_l}} \to F_n(\mathbf{t}_l \mid g_{a_l})$ and $t_{g_{a_l d}} \to F_n(\mathbf{t}_l \mid g_{a_l d})$ into (20) to obtain the joint **PGF** of all types of **PCR** product:

$$\prod_{l \in L} \prod_{a \in A_l} \prod_{i \in I} (1 - \pi_f + \pi_f E_x(F_n(\mathbf{t}_l \mid g_{a_l}), F_n(\mathbf{t}_l \mid g_{a_l d})))^{n_{i a_l} c_i} D_r(F_n(\mathbf{t}_l \mid g_{a_l}) F_n(\mathbf{t}_l \mid g_{a_l d}))$$

$$\tag{28}$$

Alternatively, if using the amplicon drop-in model (21), one substitutes $t_{g_{a_l}} \to F_n(\mathbf{t}_l \mid g_{a_l})$ and $t_{g_{a_l d}} \to F_n(\mathbf{t}_l \mid g_{a_l d})$ into (22) together with the additional substitutions of $t_{a_{a_l}} \to F_n(\mathbf{t}_l \mid a_{a_l})$ and $t_{a_{a_l d}} \to F_n(\mathbf{t}_l \mid a_{a_l d})$:

$$\prod_{l \in L} \prod_{a \in A_l} \prod_{i \in I} (1 - \pi_f + \pi_f E_x(F_n(\mathbf{t}_l \mid g_{a_l}), F_n(\mathbf{t}_l \mid g_{a_l d})))^{n_{i a_l} c_i} D_r(F_n(\mathbf{t}_l \mid a_{a_l}) F_n(\mathbf{t}_l \mid a_{a_l d}))$$

$$\tag{29}$$

Depending on the drop-in model chosen, either (28) or (29) is the multivariate **PGF** for all the possible **PCR** products. For the capillary electrophoresis we require only the multivariate **PGF** for the tagged amplicons. This is obtained by setting all of the $\mathbf{t}_l$ components to 1 except for the symbols representing the tagged amplicons, that is, the set $\{t_{a_{a_l d}} : l \in L, a_l \in A_l\}$. Let $\mathbf{t}_{ld}$ denote $\mathbf{t}_l$ with this substitution made. Then (28) with this substitution becomes

$$\prod_{l \in L} \prod_{a \in A_l} \prod_{i \in I} (1 - \pi_f + \pi_f E_x(F_n(\mathbf{t}_l \mid g_{a_l}), F_n(\mathbf{t}_{ld} \mid g_{a_l d})))^{n_{i a_l} c_i} D_r(F_n(\mathbf{t}_{ld} \mid g_{a_l}) F_n(\mathbf{t}_l \mid g_{a_l d}))$$

$$\tag{30}$$

71

with a similar equation for substitution into (29). Hence, taking into account the two variations of $E_x(\cdot, \cdot)$ given earlier, we have four modelling possibilities.

8.5   RFU scaling and baseline noise

During the capillary electrophoresis phase, a thin tube is dipped into the amplified product and a high voltage is applied. This forces a fraction of the product into the tube where it is carried along by a voltage differential. At a specific point along the capillary tube a lasers excite the dyes on the tagged amplicons, and the amount that fluoresces is recorded as the RFU reading. The RFU value is proportional to the number of tagged amplicons.

There is, therefore, some scale factor which we denote by ρ, that relates the final number of tagged amplicons of each type to the RFU reading. The factor will depend upon the machinery, but may also be expected to be dye dependent with all the other factors constant. Thus if we consider a single locus l, a given peak height RFU value $r_{a_l} > 0$ will correspond to the range $[\rho(r_{a_l} - 1/2), \rho(r_{a_l} + 1/2)]$ of tagged amplicons of that allele, and conversely.

However this does not take account the baseline noise that is usually present. If we denote the discrete probability distribution of the baseline noise distribution by η_l for the range $[0, w]$, say, then we may form the **PGF** of the distribution as

$$\sum_{j=0}^{w} \eta_l[j] z^j$$

Given the locus, the noise distribution will be independent of the allele type (it may depend on the dye lane that the locus is in). Thus for each $a_l \in A_l$ we may form a "tagged-amplicon equivalent" noise distribution given by

$$\eta_{l,a_l} := \sum_{j=0}^{w} \eta_l[j] t_{a_{a_l d}}^{j\rho}$$

These **PGF**s may then be multiplied into (30) and the resulting multivariate **PGF** used for assessing peak height likelihoods for observed data.

Alternatively one could derive peak height distributions from (28) and convolute them with the baseline noise distributions, and use the convolved distribution to evaluate peak height likelihoods.

8.6 Multiple replicates from a sample

Sometimes more than one **PCR** amplification is carried out on a sample from which DNA has been extracted, each amplified sub-sample is called a *replicate*. This maybe modelled using a multinomial **PGF** as follows. Let there be R replicates, with π_{f_r} the fraction of the sample used for replicate r.

If we ignore breakage through degradation, then for a single genomic pair strand $g_{a_l}g_{a_ld}$ in the sample, the multivariate **PGF** for the number of strands (0 or 1) of the pair being in each replicate is

$$1 - \sum_{r=1}^{R} \pi_{f_r} + \sum_{r=1}^{R} \pi_{f_r} t_{g_{a_l}:r} t_{g_{a_ld}:r}$$

where we introduce new symbols to represent the specific replicate the pair get selected for, indicated by the additional ': r' subscripts. New symbols for half-strand and amplicons are also required to specify the replicate they belong to.

To take into account the extraction efficiency, we multiply each π_{f_r} by $\pi_{e:i,a_l}$:

$$\left(1 - \pi_{e:i,a_l} \sum_{r=1}^{R} \pi_{f_r}\right) + \pi_{e:i,a_l} \sum_{r=1}^{R} \pi_{f_r} t_{g_{a_l}:r} t_{d_{a_ld}:r} . \tag{31}$$

To take account of degradation breakage, replace $t_{g_{a_l}:r} t_{h_{a_ld}:r}$ by $E_x(t_{g_{a_l}:r}, t_{g_{a_ld}:r})$ in (31):

$$\left(1 - \pi_{e:i,a_l} \sum_{r=1}^{R} \pi_{f_r}\right) + \pi_{e:i,a_l} \sum_{r=1}^{R} \pi_{f_r} E_x(t_{g_{a_l}:r}, t_{g_{a_ld}:r}) . \tag{32}$$

so that for person K_i,

$$\left(\left(1 - \pi_{e:i,a_l} \sum_{r=1}^{R} \pi_{f_r}\right) + \pi_{e:i,a_l} \sum_{r=1}^{R} \pi_{f_r} E_x(t_{g_{a_l}:r}, t_{g_{a_ld}:r})\right)^{n_{ia_l} c_i} . \tag{33}$$

8.7 Untyped contributors

Equation (16) assumes that the genotypes of all contributors are known. For a contributor U_j whose genotype is not known, we replace (16), for autosomal loci, by the **PGF**

$$\left(\sum_{a_l \in A_l} p_{a_l} (t_{g_{a_l}} t_{g_{a_l:d}})^{c_j}\right)^2 \tag{34}$$

73

where p_{a_l} is the allele frequency of allele a_l in the locus l for the population that U_j comes from. For a set of J *unrelated* untyped individuals we have

$$\prod_{j=1}^{J}\left(\sum_{a_l \in A_l} p_{a_l} (t_{g_{a_l}} t_{g_{a_l:d}})^{c_j}\right)^2 . \tag{35}$$

This represents intact genomic pair strands in the sample prior to extraction and without degradation or splitting a fraction into $r \geq 1$ replicates. To take all these into consideration we replace the $t_{g_{a_l}} t_{g_{a_l:d}}$ product pairs thus:

$$\prod_{j=1}^{J}\left(\sum_{a_l \in A_l} p_{a_l} \left(\left(1 - \pi_{e:i,a_l} \sum_{r=1}^{R} \pi_{f_r}\right) + \pi_{e:i,a_l} \sum_{r=1}^{R} \pi_{f_r} E_x(t_{g_{a_l}:r}, t_{g_{a_l d}:r})\right)^{c_j}\right)^2 . \tag{36}$$

8.8 Another variation of the framework

Grisedale and van Daal (2014) proposed a method for improving the detection of alleles as described in the Method Summary of their paper:

> DNA template is first divided into two aliquots. One aliquot is used as template for a **PCR** using a primer mix containing all forward primers for loci targeted in the PowerPlex ESI 16 kit (Promega), while the other aliquot is amplified with all reverse primers. Amplification products are then pooled for use as template in a standard **PCR** with the STR kit primer mix. The forward and reverse primer reactions result in a linear amplification of the target sequences to boost the amount of template available for **PCR**, thus reducing the stochastic effects commonly seen with low template DNA analysis.

The framework presented so far does not apply to their experimental set-up; however it is readily adapted to it as follows. Assume that the DNA template is split into two equal aliquot parts for the first κ pre-cycles, and then put back together for n amplifications cycles. Consider a single genome-pair (g, g_d) (dropping the a_l indexing from earlier notation for simplicity) in the aliquot prior to splitting the sample. Let S and S_d denote the two split samples. If the sample is split into two equal volumes, then the (g, g_d) pair will be in S with probability 0.5, and S_d with probability 0.5. Suppose that the sample S has primers that bind to the g strand; then the number of h_d strand generated by the κ pre-cycles will be

binomially distributed as $\text{Bin}(\kappa, p_g)$ if the stand pair is in S This is because the g strand produces at most one h_d strand per cycle. Similarly the number of h strands generated in S_d in the κ pre-cycles will be binomially distributed as $\text{Bin}(\kappa, p_{g_d})$ if the strand pair is in S_d.

Hence when the two samples are re-combined for the main n **PCR** cycles that generate the amplicons, the **PGF** for the starting number of g, g_d, h and h_d strands will be

$$t_g t_{g_d} \frac{(1 + t_h)^\kappa + (1 + t_{h_d})^\kappa}{2}$$

One then replaces $t_g \to F_n(\mathbf{t}\,|\,t_g)$, and so on for the joint **PGF** after the n cycles of **PCR**. Other factors such as an unequal splitting of the DNA template, extraction efficiency, degradation, multiple replicates, number of cells and genotypes of contributors, and modification to the drop-in model, can be taken into account in a straightforward manner. For example, for the genomic drop-in model we make an adjustment from

$$D_r(\,t_g, t_{g_d}) = \exp\left(\lambda(t_g t_{g_d} - 1)\right)$$

to

$$D_r(\,t_g, t_{g_d}) = \exp\left(\lambda\left(t_g t_{g_d} \frac{(1 + t_h)^\kappa + (1 + t_{h_d})^\kappa}{2} - 1\right)\right).$$

9   A particular model realisation

In this section we present a model that specialises the framework given earlier, and which introduces approximations that make the model computationally tractable. A satisfying feature of this approach is that the mathematical nature of the model approximations are clearly specified, and they can be judged on their merits. The author has implemented the model in a computationally efficient and accurate system, and this implementation is used in the performance analysis of the model applied to real and simulated data presented below.

9.1   Model assumptions and approximations

In the model presented we shall assume that we have a single DNA sample from which a single replicate has been produced. First the sample is described, then the assumptions regarding the **PCR** process are given, and how the tagged amplicon number is interpreted as measurement in terms of **RFU** units. We shall

assume that the kit being used has autosomal loci, and perhaps also Amelogenin but no other sex-linked loci are among the loci of the kit. We also assume that all contributors are unrelated.

9.1.1 The sample

We shall assume that we have a mini-tube of volume V_s, that contains the extracted DNA of I contributors, in which the ith contributor has contributed c_i cells. The DNA has been extracted with an efficiency $\psi \in [0, 1]$, and may have degradation characterised by a parameter δ which has units of inverse length (measured in base pairs). The values of the cell amounts c_i and the degradation parameter are taken as unknown, and to be estimated from the **EPG**. The extraction efficiency is taken as known.

A very small amount of the sample in V_s is taken to quantify the concentration of DNA in V_s, and based on this a fraction fraction π_f of the volume V_s is taken is put into a mini-tube of volume V, to which is added primers etc.. **PCR** is carried out with this aliquot.

Note that quantification of DNA is usually carried out using qPCR, so that the amount of DNA estimated to be in V is the amplify-able amount of DNA. If the estimated amount of DNA in V is γ, then an estimate of the amount of DNA in the sample volume V_s is given by $\gamma_s = \gamma/(\psi \pi_f)$, if we ignore degradation.

We shall assume that degradation has the effect of breaking a pair strand in two or more pieces, according to a Poisson process. For a given locus $l \in L$, the total number of genomic pair strands of an allele $a_l \in A_L$, having total size in base-pairs between and including flanking regions denoted by b_l, that are in the aliquot volume V and are amplify-able is given by the binomial distribution, taken to be

$$\mathrm{Binom}\left(\sum_{i=1}^{I} n_{ia_l} c_i, \psi \pi_f \exp(-\delta b_l) \right).$$

We shall assume the genomic drop-in model, with a Poisson model for the number of drop-in genome strands with drop-rates for every allele assumed known. We ignore stutter products that may be generated during the **PCR** process by drop-in strands.

9.1.2 The PCR

We shall use the genomic model described earlier. We assume that all amplification probabilities, conditional and unconditional, are known for all allele and

76

loci.

We shall assume that in an amplification cycle, forward stutter, no-stutter, single reverse stutter and double reverse stutter products may be *directly* produced from a strand of type of the allele a_l. Note that we allow triple stutters arising indirectly via two amplification cycles. Some alleles might not form one or more of these stutter products, for example because they are at the low or high end of the allelic range of A_l; additionally Amelogenin is assumed not to form stutters.

We only allow stuttering for multiples of the base-pair repeat size of each locus. Thus while we include a stutter of $9.3 \to 8.3$, for TH01, we exclude the stutter possibility $9.3 \to 9$; this is purely for computational efficiency, to make the likelihood evaluation tractable.

9.1.3 Converting amplicon numbers to peak height RFUs

At the conclusion of the **PCR**, the volume V will have a large number of tagged amplicons for the various alleles in the amplification kit. A small number of these are drawn up electrostatically into the capillary-electrophoresis machine. We shall assume that the number of tagged amplicons of a specific allelic type drawn up is proportional to their number (the proportionality depends on other factors such as the voltage applied; see Butler (2011) pp.144-145), and that the **RFU** peak height is proportional to the number drawn up, and that the proportionality constant may depend upon the particular dye. Hence we introduce dye-lane proportionality factors so that the **RFU** peak height generated by the tagged amplicons is proportional to the total number in the volume V.

To this must be added a random value arising from the baseline noise. It is assumed that the prior baseline noise distribution is known, and may be dye-lane dependent.

9.1.4 Likelihood evaluation

In order to evaluate the likelihood function requires evaluation of the **PGF**s $F_n(\mathbf{t}_{ld} \mid g_{a_l})$ and $F_n(\mathbf{t}_{ld} \mid g_{a_{ld}})$, based on the assumed known amplification probabilities and binomial sampling rates and genome counts, for all the alleles. Let us write this as

$$\prod_{a_l \in A_L} F_n(\mathbf{t}_{ld} \mid g_{a_l}) = \prod_{a_l \in A_L} \prod_{b_l \in A_L} (1 - \phi_{b_l} + \phi_{b_l} G(t_{b,a_{ld}}))^{k_{b_l}}, \tag{37}$$

where $G(t_{b,a_{ld}})$ is the **PGF** of the joint distribution of all allelic products arising from a single genomic strand of type b_l, ϕ_{b_l} is the binomial sampling probability

77

for such alleles, of which there are k_{b_l} in the sample.

This is computationally intractable for two reasons. The first is in evaluating the individual **PGF**s $G(t_{b,a_{ld}})$. We therefore make the approximation in which each $G(t_{a_{ld}})$ factorizes as

$$G(t_{a_{ld}}) = G_{-2}(t_{a_{ld}})G_{-1}(t_{a_{ld}})G_0(t_{a_{ld}})G_{+1}(t_{a_{ld}}) = \prod_{j=-2}^{1} G_j(t_{a_{ld}}) \tag{38}$$

in which $G_{-2}(t_{a_{ld}})$ is the **PGF** of the number of tagged amplicons in double-stutter position, $G_{-1}(t_{a_{ld}})$ in stutter position, $G_0(t_{a_{ld}})$ copies of the target allele, and $G_{-1}(t_{a_{ld}})$ forward stutter.

Even with this approximation, the computations are still intractable, we therefor make the following further approximation:

$$\left(1 - \phi_{b_l} + \phi_{b_l} \prod_{j=-2}^{1} G_j(t_{a_{ld}})\right)^{k_{b_l}} \rightarrow \prod_{j=-2}^{1} \left(1 - \phi_{b_l} + \phi_{b_l} G_j(t_{a_{ld}})\right)^{k_{b_l}}. \tag{39}$$

Under these two approximations, the total likelihood, given the genotypes of contributors, will factorise into a product of functions, each of which depend on a single allele type. For a particular allele a, there will be up to four factors arising from alleles 2 repeats higher (which double stutter to make a, one repeat higher (which stutter to form a), alleles of the same type a, and alleles one repeat lower (which forward stutter to produce a product).

This needs to be multiplied by **PGF**s from each allele drop-in **PGF**, and combined with baseline noise distribution on each allele, to get the marginal peak-height distributions for each allele. Hence for each allele we have a product of univariate **PGF**s that can be convoluted using the **FFT** to find the marginal distribution on each allele, which can then be used directly to find the likelihoods on each allele given the peak height.

The peak height likelihood from all peaks is then found from these individual allele likelihoods by multiplication—given the genotypes of the contributors—and such products averaged using population genotype probabilities over the possible genotypes of the untyped contributors.

10   Model performance with simulated data

One of the useful features of the framework developed in this paper is that, because the model is an idealisation of the DNA extraction and amplification pro-

cess, not only can realistic simulated single source and mixtures **EPG**s be produced, the simulated data can be analysed by the model using the same parameters as used in simulating the data. The performance of the model can then be compared to the 'gold standard' simulated values. Additionally, one can tweak the parameters of the model so that they differ from those used to simulate the data, so that robustness of the model can be gauged. It is also possible to use unrealistic model parameters to isolate and analyse specific effects, for use with software validation and regression tests. All these can be used to judge the limitations of the model. Here we present a set of simulations of increasing complexity, beginning with unrealistic single contributor sample simulations. All the simulations use population Caucasian data from Butler et al. (2003). All allele frequencies in a locus were increased so that the minimum allele count of any was 5. (The total allele count was also increased to yield population probabilities that add to 1, so this is not quite the same as the $5/2N$ adjustment of (Bodner et al., 2016) which does not adjust the normalisation). An Fst value of 0.02 was used in all analyses. Following (Puch-Solis, 2014) we use a locus-wide drop-in rate of 0.021, with allele specific rates equal to this multiplied by the relative allele frequency in the *unadjusted* population counts. Contributor genotypes were taken from those in the dataset of contributors from the PROVEDIt Initiative (Alfonse et al., 2016, 2018), which we shall return to in Section 11 when we examine the model performance on experimental data.

All simulations are based on the Identifiler$^{\text{TM}}$ kit, in which we assume that all strand amplification probabilities are $p_g = p_{g_d} = p_h = p_{h_d} = p_a = p_{a_d} = 0.85$ for all loci.

10.1 Single contributor simulations

10.1.1 Simulations with no stutter and no noise

In this set of simulations we take all the conditional stutter probabilities ξ to be zero on all alleles and loci. With this assumption, we will have $G_{-2}(t_{a_{ld}}) = G_{-1}(t_{a_{ld}}) = G_{+1}(t_{a_{ld}}) = 1$, and (39) is no longer an approximation, with only the $j = 0$ terms surviving on both sides of the equation to give an equality. We are thus, in these simulations, testing the performance of the model under the approximation of (38).

We shall simulate data the genotype data of subject `RD14-0003-01` taken from the PROVEDIt dataset, and assume that the profile is known when estimating cell counts. We take as further idealisations that there is no drop-in (the drop-in rate

is zero), and that there is no baseline noise. We use a factor of 800,000 to scale post-**PCR** tagged-amplicon numbers to **RFU** values, and 28 cycles for the **PCR** amplification.

We use maximum likelihood to estimate the cell counts of the contributor, a value known at the time of simulation. We can thus examine the predictive accuracy and variability of the cell count estimates.

In the first set of simulations, we shall take the degradation parameter to be zero, and shall assume this value when estimating the cell counts. We compare the predictions made using the model based on the **FFT** analysis and normal, lognormal and gamma distribution models based on matching the means and variances of the marginal distribution. We take the binomial sampling probability ϕ to be the same for all loci and alleles, and see how the models behave as we vary the number of cells, and the values of ϕ. We include in the simulations the unrealistic value $\phi = 1$, so that (38) is exact, and we can compare the (now exact) **FFT** model to the moment approximation models.

The following table shows maximized log-likelihoods and estimated cells counts from 10 simulations, with 500 cells, $\phi = 1$, and an analytic threshold of 1 **RFU** in all simulations; we see that the estimates are very close to the true value of 500 cells used to generate the simulations. We also see that the log-likelihood maxima are all of a similar value.

Normal		Logormal		Gamma		**FFT**	
$\widehat{LL}_{max}$	cells	$\widehat{LL}_{max}$	cells	$\widehat{LL}_{max}$	cells	$\widehat{LL}_{max}$	cells
-171.356	499	-171.341	499	-171.345	499	-171.367	499
-168.651	499	-168.658	499	-168.655	499	-168.648	499
-170.734	500	-170.757	500	-170.749	500	-170.719	500
-169.804	499	-169.802	499	-169.802	499	-169.806	499
-171.148	500	-171.176	500	-171.166	500	-171.129	500
-173.965	500	-174.017	500	-173.999	500	-173.931	500
-173.689	498	-173.770	498	-173.743	498	-173.635	498
-170.764	499	-170.665	499	-170.697	499	-170.830	499
-172.017	500	-172.036	500	-172.029	500	-172.008	500
-172.890	499	-172.851	499	-172.863	499	-172.919	499

Reducing the initial number of cells to 10 , we obtain the following table from 10 simulations, in which every model estimated the actual number of cells used. Again the log-likelihood values are very similar in each simulation across the models.

Normal		Logormal		Gamma		**FFT**	
$\widehat{LL}_{max}$	cells	$\widehat{LL}_{max}$	cells	$\widehat{LL}_{max}$	cells	$\widehat{LL}_{max}$	cells
-110.371	10	-110.321	10	-110.322	10	-110.468	10
-106.731	10	-106.708	10	-106.716	10	-106.746	10
-116.895	10	-116.288	10	-116.455	10	-117.502	10
-105.7	10	-105.645	10	-105.663	10	-105.767	10
-107.805	10	-107.955	10	-107.896	10	-107.753	10
-111.267	10	-111.747	10	-111.564	10	-111.012	10
-112.118	10	-113.147	10	-112.767	10	-111.622	10
-110.533	10	-111.237	10	-110.984	10	-110.134	10
-106.879	10	-106.954	10	-106.926	10	-106.842	10
-119.358	10	-120.664	10	-120.166	10	-118.811	10

We now reduce the ϕ value to 0.7. For 500 cells, we obtain the following estimates:

Normal		Logormal		Gamma		**FFT**	
$\widehat{LL}_{max}$	cells	$\widehat{LL}_{max}$	cells	$\widehat{LL}_{max}$	cells	$\widehat{LL}_{max}$	cells
-200.822	495	-200.725	495	-200.749	495	-200.853	495
-193.161	502	-193.307	502	-193.256	502	-193.13	502
-203.948	500	-204.114	500	-204.047	500	-203.927	500
-192.587	504	-192.632	504	-192.616	504	-192.576	504
-191.827	498	-192.032	498	-191.962	498	-191.773	497
-194.707	500	-195.243	500	-195.057	500	-194.598	499
-195.202	498	-195.243	498	-195.227	498	-195.194	498
-195.921	496	-195.927	496	-195.921	496	-195.924	496
-195.392	498	-195.356	498	-195.365	498	-195.4	498
-192.545	498	-192.6	498	-192.58	498	-192.532	498

and for 10 cells

Normal		Logormal		Gamma		**FFT**	
$\widehat{LL}_{max}$	cells	$\widehat{LL}_{max}$	cells	$\widehat{LL}_{max}$	cells	$\widehat{LL}_{max}$	cells
-139.783	11	-147.468	10	-143.755	11	-139.270	11
-137.910	10	-142.610	10	-140.283	10	-137.284	10
-142.794	10	-146.055	9	-144.733	9	-142.067	10
-133.883	9	-134.231	10	-134.058	10	-133.530	9
-140.499	10	-142.933	10	-141.646	10	-140.285	10
-130.732	10	-129.973	10	-130.279	10	-131.016	10
-133.887	10	-133.595	10	-133.623	10	-134.086	10
-135.397	9	-133.938	9	-134.267	9	-136.617	9
-139.761	10	-141.720	10	-140.478	10	-140.018	10
-142.768	10	-147.142	9	-145.116	9	-142.328	10

Again the estimates are good for all models, and similar log-likelihoods are obtained. Reducing ϕ to 0.07, we obtain for 500 cells

Normal		Logormal		Gamma		**FFT**	
$\widehat{LL}_{max}$	cells	$\widehat{LL}_{max}$	cells	$\widehat{LL}_{max}$	cells	$\widehat{LL}_{max}$	cells
-177.336	495	-177.035	495	-177.027	495	-177.141	495
-175.239	477	-174.969	479	-175.003	479	-175.107	478
-176.421	497	-176.359	498	-176.295	498	-176.324	497
-171.300	460	-171.109	466	-171.179	464	-171.251	462
-176.719	537	-178.073	538	-177.447	538	-176.984	538
-184.978	501	-187.879	489	-186.498	494	-185.504	498
-177.330	523	-178.051	524	-177.673	524	-177.434	523
-183.672	510	-185.782	501	-184.699	504	-183.973	507
-171.51	523	-171.445	532	-171.511	529	-171.532	526
-176.99	516	-175.459	518	-175.868	517	-176.388	516

and for 10 cells

Normal		Logormal		Gamma		**FFT**	
$\widehat{LL}_{max}$	cells	$\widehat{LL}_{max}$	cells	$\widehat{LL}_{max}$	cells	$\widehat{LL}_{max}$	cells
-90.0015	12	-112.940	4	-96.5969	6	-74.8928	10
-90.1253	13	-112.852	4	-96.6292	7	-77.1458	11
-78.6269	8	-96.6019	4	-83.227	5	-63.8753	8
-88.6604	12	-108.518	4	-93.0871	7	-73.4382	10
-80.5898	11	-93.9211	3	-80.5046	4	-66.668	9
-86.3204	9	-107.53	5	-93.3741	7	-81.5557	9
-69.2068	8	-80.6773	2	-68.6397	3	-52.4727	7
-77.0180	9	-92.9245	3	-79.659	5	-61.3999	8
-81.5496	8	-108.38	4	-92.4763	6	-74.1947	9
-91.0582	11	-106.786	4	-92.8809	6	-78.1598	10

We see that variability in the cell estimates is increasing, and that for the 500-cell simulations the log-likelihoods are close amongst the four models in each simulation. However for the 10-cell simulations we see that the **FFT** based model has higher maximized likelihoods in all the simulations, indicating a better overall fit to the simulated peak heights. We can also see that the lognormal and gamma models appear to be underestimating the true cell-count value, whilst the normal and **FFT** models are less biased in their estimates, but the normal model having a greater variability. The following boxplot of cell counts estimated for 10 cells, and $\phi = 0.07$, is based on 200 simulations, and confirms the small sample behaviour in the table above:
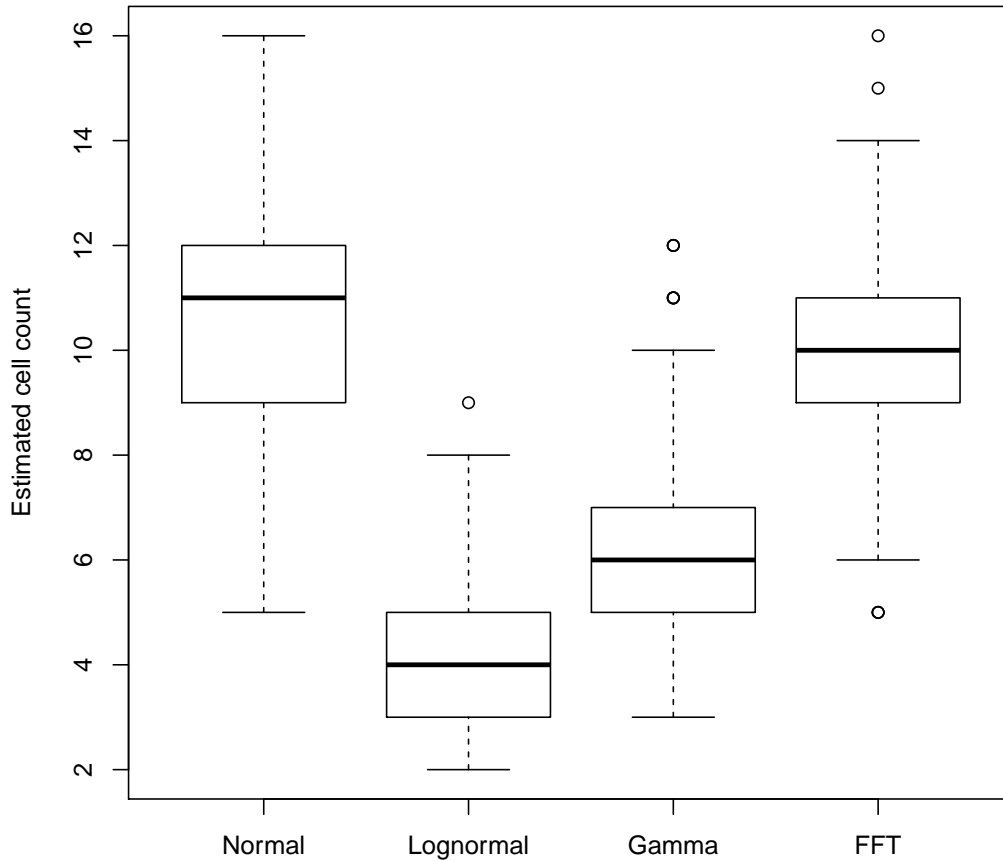
10.1.2 Simulations with stutter but no noise

We now include stutter products in the simulations. For all simulations we set the conditional probability of stutter on each allele to be 0.004, and for forward and double stutter conditional probabilities are all set to 0.001. We do not include background noise, but we set the analytic threshold to be 30 **RFU**.

For $\phi = 1$ and 500 cells, we obtain the following estimates from 10 simulations. We see that all models give similar cell count estimates and log likelihoods. However we see that there is much more variation amongst the maximized likeli-

hoods between the four models in each simulation.

Normal		Logormal		Gamma		FFT	
$\widehat{LL}_{max}$	cells	$\widehat{LL}_{max}$	cells	$\widehat{LL}_{max}$	cells	$\widehat{LL}_{max}$	cells
-398.925	500	-397.548	500	-397.95	500	-400.347	501
-401.835	500	-400.62	500	-400.966	500	-400.65	500
-390.493	501	-389.57	501	-389.845	501	-396.683	502
-401.541	500	-401.002	500	-401.14	500	-403.778	500
-399.756	500	-399.765	500	-399.731	500	-401.508	500
-390.409	499	-390.135	499	-390.196	499	-397.262	500
-403.813	500	-402.911	500	-403.161	500	-400.463	501
-394.292	499	-393.968	499	-394.046	499	-399.208	500
-393.24	498	-392.758	498	-392.896	498	-396.412	499
-392.309	500	-392.337	500	-392.311	500	-401.011	500

Reducing the number of cells to 200 we obtain the following table. We see that all models are making accurate estimates of the numbers of cells, but we also see that the **FFT** model likelihoods are, with one simulation exception, lower than the moment based models.

Normal		Logormal		Gamma		FFT	
$\widehat{LL}_{max}$	cells	$\widehat{LL}_{max}$	cells	$\widehat{LL}_{max}$	cells	$\widehat{LL}_{max}$	cells
-344.81	200	-343.656	200	-344.009	200	-354.253	200
-349.42	199	-346.64	199	-347.456	199	-353.245	200
-350.053	199	-348.586	199	-348.993	199	-354.592	199
-365.401	200	-364.874	200	-364.998	200	-372.019	200
-343.929	200	-342.793	200	-343.114	200	-351.199	200
-369.769	200	-366.598	200	-367.482	200	-366.688	200
-342.514	200	-341.61	200	-341.877	200	-350.469	200
-335.855	201	-335.204	201	-335.411	201	-347.73	201
-344.183	200	-343.186	200	-343.482	200	-349.88	200
-358.427	199	-357.657	199	-357.856	199	-363.16	200

Reducing the number of cells down to 100 we obtain the following table. Cell estimates are again good for all models, but we see that divergence between the **FFT** log-likelihood values and the moment models is becoming more pronounced.

Normal		Logormal		Gamma		**FFT**	
$\widehat{LL}_{max}$	cells	$\widehat{LL}_{max}$	cells	$\widehat{LL}_{max}$	cells	$\widehat{LL}_{max}$	cells
-233.411	100	-233.38	100	-233.384	100	-240.193	100
-236.636	101	-235.228	101	-235.645	101	-235.647	101
-237.502	100	-236.287	100	-236.657	100	-240.525	100
-234.364	99	-234.535	99	-234.442	99	-236.879	99
-223.076	100	-223.137	100	-223.106	100	-229.342	100
-228.312	101	-227.795	101	-227.945	101	-231.916	101
-230.257	99	-229.443	99	-229.69	99	-232.93	99
-228.276	100	-227.977	100	-228.071	100	-234.852	100
-224.315	100	-223.785	100	-223.957	100	-231.222	100
-221.219	100	-221.08	100	-221.128	100	-229.573	100

Reducing the number of cells down to 10 we obtain the following table, in which all models correctly estimate the number of cells in each simulations, but the divergence between the **FFT** log-likelihood values and the moment models is still apparent.

Normal		Logormal		Gamma		**FFT**	
$\widehat{LL}_{max}$	cells	$\widehat{LL}_{max}$	cells	$\widehat{LL}_{max}$	cells	$\widehat{LL}_{max}$	cells
-108.134	10	-108.002	10	-108.038	10	-115.534	10
-111.576	10	-111.361	10	-111.413	10	-119.017	10
-110.092	10	-110.252	10	-110.185	10	-117.129	10
-111.932	10	-111.352	10	-111.528	10	-119.666	10
-110.431	10	-111.194	10	-110.915	10	-117.359	10
-107.527	10	-108.362	10	-108.054	10	-114.481	10
-106.965	10	-106.724	10	-106.799	10	-114.368	10
-113.55	10	-113.298	10	-113.352	10	-121.412	10
-109.083	10	-108.913	10	-108.956	10	-116.539	10
-116.432	10	-117.402	10	-117.013	10	-123.514	10

We now set $\phi = 0.2$. For 500 cells, we obtain the following table, in which we are now seeing the effects of the pre-sampling variability in the wider range of cell estimates in all models, which are giving similar estimates.

Normal		Logormal		Gamma		**FFT**	
$\widehat{LL}_{max}$	cells	$\widehat{LL}_{max}$	cells	$\widehat{LL}_{max}$	cells	$\widehat{LL}_{max}$	cells
-279.819	496	-280.204	497	-280.053	497	-284.162	498
-313.331	497	-307.348	493	-308.797	494	-302.683	495
-279.83	496	-279.6	498	-279.678	497	-283.113	498
-279.828	504	-279.664	506	-279.717	505	-283.564	506
-288.832	496	-288.937	496	-288.811	496	-290.632	497
-302.379	497	-298.563	495	-299.36	495	-297.065	496
-286.874	504	-287.079	504	-286.944	504	-289.078	505
-286.703	507	-286.583	507	-286.567	507	-289.549	509
-301.076	502	-301.912	500	-301.295	500	-299.415	500
-292.959	500	-293.018	499	-292.885	500	-294.815	501

Reducing the number of cells to 200, and keeping $\phi = 0.2$ we obtain

Normal		Logormal		Gamma		**FFT**	
$\widehat{LL}_{max}$	cells	$\widehat{LL}_{max}$	cells	$\widehat{LL}_{max}$	cells	$\widehat{LL}_{max}$	cells
-227.224	199	-228.354	199	-227.737	199	-228.009	198
-237.356	196	-233.14	195	-234.183	195	-233.538	195
-229.561	205	-231.812	206	-230.937	206	-232.314	207
-233.089	196	-237.701	193	-235.661	194	-234.839	195
-223.573	197	-222.67	199	-222.915	198	-224.836	198
-233.505	205	-233.881	205	-233.493	205	-234.295	205
-232.002	198	-230.505	197	-230.724	197	-231.164	196
-225.549	195	-225.824	196	-225.692	195	-227.969	196
-216.563	192	-218.336	194	-217.713	193	-219.421	193
-220.548	199	-221.047	200	-220.84	199	-222.54	200

Reducing the number of cells to 100, and keeping $\phi = 0.2$ we obtain similar behaviour,

Normal		Logormal		Gamma		FFT	
$\widehat{LL}_{max}$	cells	$\widehat{LL}_{max}$	cells	$\widehat{LL}_{max}$	cells	$\widehat{LL}_{max}$	cells
-161.866	91	-163.224	92	-162.538	92	-162.197	91
-174.273	102	-174.564	99	-174.032	100	-173.428	100
-164.162	99	-163.554	100	-163.703	100	-164.374	99
-166.503	100	-168.923	100	-167.691	101	-167.244	100
-165.579	96	-165.367	96	-165.226	96	-165.526	96
-161.76	99	-161.274	101	-161.398	100	-161.841	100
-169.946	106	-171.175	105	-170.44	105	-170.32	106
-164.081	98	-164.207	99	-164.096	99	-164.48	98
-165.631	98	-167.698	97	-166.658	98	-166.109	98
-174.81	103	-173.074	101	-173.319	102	-174.481	102

However as we go below 40 cells the behaviours of the **FFT** and moment based models start to change. For 40 cells we obtain the following table, in which all the models are in broad agreement:

Normal		Logormal		Gamma		FFT	
$\widehat{LL}_{max}$	cells	$\widehat{LL}_{max}$	cells	$\widehat{LL}_{max}$	cells	$\widehat{LL}_{max}$	cells
-147.227	38	-151.059	38	-149.056	39	-147.405	39
-149.565	44	-149.253	44	-149.071	44	-148.65	46
-144.248	39	-145.536	40	-145.022	40	-144.202	41
-149.696	40	-159.711	38	-154.874	39	-150.288	41
-148.827	41	-148.863	41	-148.599	41	-148.133	42
-149.489	41	-149.389	41	-149.102	41	-148.598	42
-151.896	41	-153.712	40	-152.28	40	-150.926	41
-142.965	33	-143.202	35	-142.985	35	-143.77	37
-145.254	36	-149.028	36	-146.878	36	-145.521	37
-153.346	37	-149.71	35	-150	36	-151.28	37

However the further reduction to 35 cells produces the following table in which we start to see the **FFT** model overestimating the number of cells in a biased manner, although the likelihoods of the four models are in broad agreement.

Normal		Logormal		Gamma		**FFT**	
$\widehat{LL}_{max}$	cells	$\widehat{LL}_{max}$	cells	$\widehat{LL}_{max}$	cells	$\widehat{LL}_{max}$	cells
-144.129	36	-148.72	36	-146.337	37	-144.584	37
-146.785	36	-149.664	36	-147.998	37	-146.792	37
-150.221	33	-151.583	32	-149.991	33	-151.201	37
-142.658	34	-143.072	36	-142.915	36	-143.154	37
-152.339	33	-153.707	30	-152.106	31	-153.466	35
-147.424	37	-144.977	38	-145.683	38	-146.49	39
-152.856	36	-156.567	34	-154.021	35	-152.478	37
-152.798	33	-154.999	28	-152.755	30	-155.032	35
-146.274	34	-150.299	34	-148.062	34	-147.571	37
-144.768	36	-145.235	37	-144.882	37	-144.767	37

Reducing the number of cells to 30 yields divergence in the likelihood estimates too, as in the following table:

Normal		Logormal		Gamma		**FFT**	
$\widehat{LL}_{max}$	cells	$\widehat{LL}_{max}$	cells	$\widehat{LL}_{max}$	cells	$\widehat{LL}_{max}$	cells
-140.094	28	-142.829	29	-141.302	29	-145.536	34
-140.487	29	-143.953	29	-142.178	29	-146.174	34
-137.771	27	-138.535	29	-138.321	28	-145.971	33
-142.205	30	-145.612	28	-143.452	29	-146.512	34
-141.715	30	-146.407	29	-143.991	30	-146.539	34
-147.524	30	-146.787	29	-146.315	29	-151.487	34
-145.765	30	-146.033	30	-145.324	30	-149.674	34
-139.777	30	-143.263	30	-141.447	30	-144.618	34
-146.34	32	-153.725	28	-149.89	29	-150.328	35
-148.841	31	-147.083	30	-146.882	31	-150.594	35

Reducing the number of cells to 10 we obtain a stark difference between the **FFT** and moment based models, as shown in the following table:

Normal		Logormal		Gamma		**FFT**	
$\widehat{LL}_{max}$	cells	$\widehat{LL}_{max}$	cells	$\widehat{LL}_{max}$	cells	$\widehat{LL}_{max}$	cells
-73.3783	10	-76.5299	10	-75.1702	10	-138.845	23
-69.2668	10	-69.0933	10	-68.4735	10	-129.504	23
-66.276	10	-63.7138	10	-64.0525	10	-130.571	23
-83.0595	11	-84.5144	13	-84.3105	12	-138.676	24
-67.5142	9	-68.668	10	-68.2279	9	-137.273	3
-81.0544	12	-81.9969	12	-81.2933	12	-132.806	24
-80.4326	11	-79.8365	11	-79.5108	11	-137.78	23
-66.6831	9	-67.4642	11	-67.4318	10	-130.458	23
-76.19	11	-78.2126	11	-77.0102	11	-135.338	23
-65.9317	9	-65.3378	10	-65.1538	10	-130.649	23

It appears that the moment based models are giving close to unbiased estimates for the number of cells, whereas the **FFT** model is giving quite biased estimates. The problem with the **FFT** model can be traced to factorisation approximation of (39). Recall that this is a double approximation here: one in which the joint **PGF** is replaced with a factorised product, given in (38), and the second factorisation approximation made in going to (39). Now consider an allele having k genomes. The probability that it completely drops out will be $(1 - \phi)^k$. However, if the allele completely drops out then it cannot produce any stutter products, hence the joint probability of dropout for that allele and its stutter products will be $(1 - \phi)^k$. However the factorisation approximation (39) means that the factor $(1 - \phi)^k$ is counted for the allele and each of it stutter product, hence will give a total joint probability of dropout of $(1 - \phi)^{4k}$. For large ϕ and k, both $(1 - \phi)^k$ and $(1 - \phi)^{4k}$ will be very close to zero, and so the factorisation approximation will be good, but if k and/or ϕ are small, then the terms will have a large effect on the likelihood calculations, and their differences will also grow. It appears from the results in the tables above that the transition point where the approximation starts becoming bad is when the number of cells is around 35-40: with $\phi = 0.2$ this corresponds to around 7-8 amplify-able cells, approximately 45-50pg by weight, of DNA subject to **PCR**.

It is curious that the moment models appear to give approximately unbiased estimates for the number of cells. If we compare to the 10-cell, $\phi = 1$ table on page 83, in which the lognormal and gamma models gave underestimates for the number of cells, it appears that the factorisation approximation has had a correcting effect on these models. The normal model appears to have less variability in its log-likelihood values when compared to to the lognormal and gamma models.

Now $\phi = 0.2$ is a high value for forensic samples. Recall that ϕ is the product of the extraction efficiency and the fraction of extracted DNA that is taken for **PCR** amplification. A more typical extraction efficiency value would be around 0.2, and similarly the fraction of aliquot taken for amplification would also be around 0.2, so that ϕ values of around $\phi = 0.04$ would be more realistic for forensic casework Gill et al. (2005). Hence, if the transition for the **FFT** model happens when expected number of amplify-able cells is around 7-8, this corresponds to around 200 cells in the sample.

The following table shows estimated cell counts and log-likelihoods for 200 cells and $\phi = 0.04$, corresponding to around 8 cells of DNA. We see that all the models are quite comparable in their estimates of cell counts and their likelihoods values.

Normal		Logormal		Gamma		FFT	
$\widehat{LL}_{max}$	cells	$\widehat{LL}_{max}$	cells	$\widehat{LL}_{max}$	cells	$\widehat{LL}_{max}$	cells
-153.806	218	-158.376	212	-155.638	217	-154.016	222
-158.168	213	-160.208	199	-158.317	206	-157.783	208
-156.432	212	-158.452	204	-156.755	208	-156.127	208
-154.188	195	-155.784	189	-154.183	193	-153.931	195
-153.257	201	-152.824	199	-152.443	201	-152.747	202
-145.644	177	-143.678	190	-144.625	187	-146.097	190
-157.511	206	-157.945	190	-156.17	196	-155.666	202
-149.454	197	-149.449	203	-149.159	202	-148.911	202
-146.514	183	-152.516	182	-149.646	185	-148.237	192
-156.928	227	-157.76	220	-156.721	224	-155.927	224

The following boxplots for estimated cell counts and log-likelihoods, based on 200 simulations confirms this:
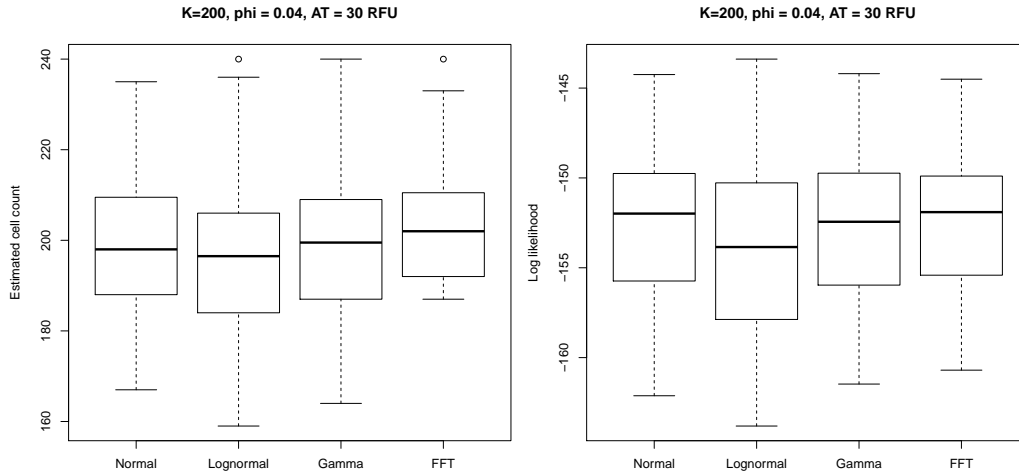
However, reducing the number of cells to 150 we obtain the following table

Normal		Logormal		Gamma		**FFT**	
$\widehat{LL}_{max}$	cells	$\widehat{LL}_{max}$	cells	$\widehat{LL}_{max}$	cells	$\widehat{LL}_{max}$	cells
-144.025	136	-142.352	143	-142.807	142	-151.579	170
-137.712	141	-144.199	131	-140.921	136	-146.336	170
-140.71	141	-142.032	147	-141.36	147	-147.833	173
-150.072	171	-151.597	164	-150.225	167	-151.937	188
-145.085	138	-142.67	143	-143.295	143	-151.939	171
-140.398	135	-142.12	134	-140.728	136	-148.936	168
-144.896	146	-146.134	145	-144.956	147	-151.04	175
-142.788	140	-145.464	127	-143.368	133	-151.46	169
-137.54	131	-141.125	134	-139.346	135	-147.239	167
-148.65	156	-146.808	158	-147.003	158	-151.945	181

and these corresponding plots based on 200 simulations:

K=150, phi = 0.04, AT = 30 RFU
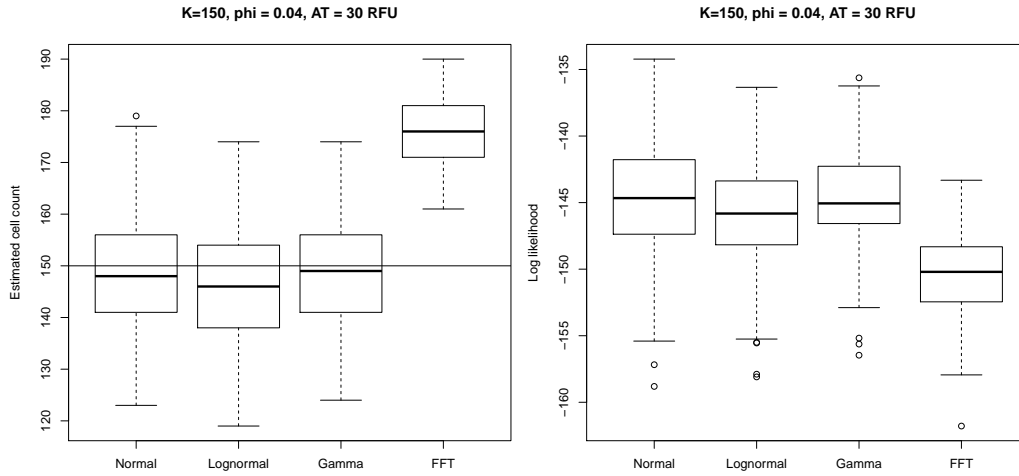
Reducing the number of cells to just 30, (so giving an average of just 1.2 cells worth of DNA for **PCR**) we obtain the following:

Normal		Logormal		Gamma		**FFT**	
$\widehat{LL}_{max}$	cells	$\widehat{LL}_{max}$	cells	$\widehat{LL}_{max}$	cells	$\widehat{LL}_{max}$	cells
-26.6781	26	-26.6658	27	-26.226	24	-51.4625	4
-31.7871	30	-31.8301	32	-31.5047	29	-64.4055	6
-29.1594	27	-29.4184	33	-29.4628	29	-61.8782	5
-35.5867	28	-37.4363	39	-37.6121	34	-72.5157	6
-25.1085	25	-24.6105	28	-24.5907	24	-51.6145	4
-20.4599	24	-20.3479	25	-20.191	22	-44.142	4
-27.5168	25	-28.6467	30	-28.5487	26	-53.8391	4
-35.9236	31	-36.4142	35	-36.2378	32	-74.6161	7
-17.6097	21	-17.9368	25	-18.0696	21	-38.5006	3
-38.5072	33	-37.1138	34	-36.9363	31	-75.1298	7

and these corresponding plots:

93

K=30, phi = 0.04, AT = 30 RFU
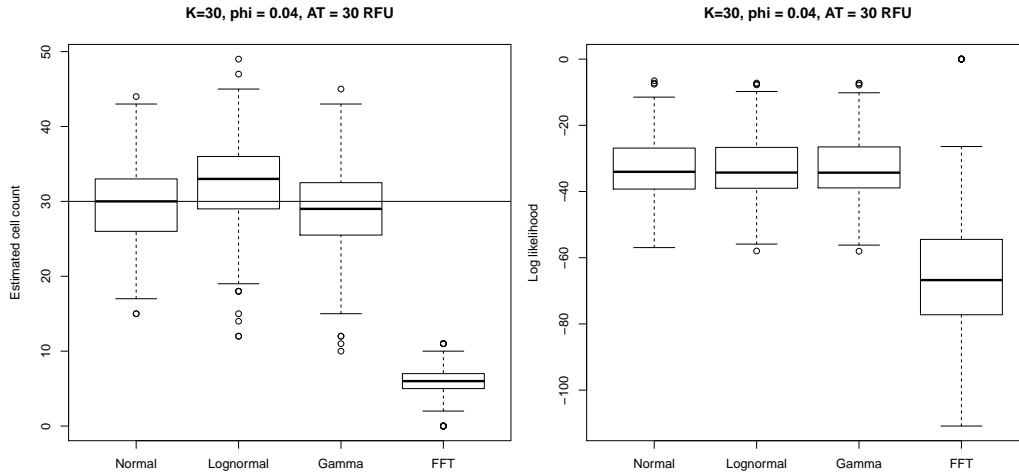
However, if we look at the simulated data for these latter simulations, we find that they have complete drop-out on most of the markers, and just one peak on each of the other markers. For such samples it is not necessary to include double and forward stutters in the model. If we remove these model components, so that we include only the target and single back-stutter allele distributions, we obtain the following fits for the models (using the same simulated data).

Normal		Logormal		Gamma		**FFT**	
$\widehat{LL}_{max}$	cells	$\widehat{LL}_{max}$	cells	$\widehat{LL}_{max}$	cells	$\widehat{LL}_{max}$	cells
-15.3989	21	-14.676	18	-14.4406	16	-20.3993	11
-26.7267	26	-26.7212	27	-26.2684	24	-32.4348	25
-31.7885	30	-31.8266	32	-31.4997	29	-37.5075	31
-29.1259	28	-29.3837	33	-29.4362	29	-35.7485	31
-35.5782	28	-37.4145	39	-37.5979	34	-42.0806	33
-25.0822	25	-24.588	28	-24.5746	24	-31.628	26
-20.4623	24	-20.3585	25	-20.1993	22	-27.3342	23
-27.4902	25	-28.6197	30	-28.5286	26	-33.9025	25
-35.9469	31	-36.4683	35	-36.2816	32	-41.3409	35
-17.6271	21	-17.9428	25	-18.0737	21	-24.178	19

We see that the **FFT** estimate are now much better. The lower log-likelihoods are explained by the inclusion of modelling stutters. However the few observed peaks heights in the simulations are within the range 30-100, so that any stutter peaks would not be observed with the threshold 30. So, if we also remove the

94

modelling of stutter, then we obtain the following fits, in which we see that the log-likelihoods of all four models are now comparable.

Normal		Logormal		Gamma		**FFT**	
$\widehat{LL}_{max}$	cells	$\widehat{LL}_{max}$	cells	$\widehat{LL}_{max}$	cells	$\widehat{LL}_{max}$	cells
-15.366	21	-14.6613	18	-14.4301	16	-14.3498	15
-26.6653	27	-26.6806	27	-26.2362	24	-26.1813	22
-31.7059	30	-31.7632	32	-31.4469	29	-31.785	27
-29.2184	28	-29.4225	33	-29.4644	29	-30.134	27
-35.5742	29	-37.4283	39	-37.6174	34	-36.6476	29
-25.388	26	-24.8448	28	-24.7658	24	-25.9578	23
-20.4145	24	-20.3252	25	-20.1738	22	-21.0171	21
-27.437	25	-28.5662	30	-28.4889	26	-27.6955	23
-35.856	32	-36.3818	36	-36.2137	32	-36.0407	31
-17.5942	21	-17.9095	25	-18.0512	21	-17.7821	19

10.1.3   Simulations with degradation, but no baseline noise

In the simulations above, we have simulated samples with a degradation parameter equal to zero, and have used that value in estimating the cell counts. We now consider simulations in which the degradation parameter is non zero, and is estimated from the data along with the cell counts.

Our first simulation set will have $\phi = 0.04$, and degradation parameter $\delta = 0.01$. This means that for an allele of size l in base-pairs, that its binomial selection probability if $\phi \exp(-\delta l)$. So an an allele of size 100 will have a selection probability of around 0.0147, whilst a longer allele of length 400 will have a selection probability of around 0.0007.

We take the initial number of cells to be 1000. Including all possible forms of stutter in fitting the model we obtain the following estimates from 10 simulations (the degradation for only the FFT model is shown);

Normal		Logormal		Gamma		FFT		$\hat{\delta}_{FFT}$
$\widehat{LL}_{max}$	cells	$\widehat{LL}_{max}$	cells	$\widehat{LL}_{max}$	cells	$\widehat{LL}_{max}$	cells	
-119.379	1055	-120.355	1003	-119.455	1029	-147.95	1172	0.00995539
-110.236	1002	-111.833	1038	-111.143	1030	-140.249	1146	0.0100925
-118.145	1218	-116.529	1127	-115.724	1154	-147.429	1320	0.0111535
-123.923	1033	-123.257	1113	-123.683	1092	-149.485	1172	0.00954747
-113.382	1020	-111.865	1012	-111.872	1017	-142.634	1147	0.0101153
-128.499	1108	-127.712	1028	-126.872	1059	-153.195	1204	0.00958187
-133.743	1002	-133.587	954	-132.82	965	-161.607	1098	0.00973301
-116.822	1038	-117.803	1036	-116.58	1037	-146.971	1165	0.0103188
-124.35	1025	-122.464	1058	-122.859	1049	-149.219	1145	0.0093805
-117.821	1082	-114.408	1066	-114.787	1066	-148.147	1207	0.0108218

Give the quite high level of degradation we would not expect to see double or forward stutters, even amongst the smaller alleles. So removing these from the model, but retaining the stutter model, we obtain (for the same simulated data) much better concordance between the **FFT** model and the moment-based models.

Normal		Logormal		Gamma		FFT		$\hat{\delta}_{FFT}$
$\widehat{LL}_{max}$	cells	$\widehat{LL}_{max}$	cells	$\widehat{LL}_{max}$	cells	$\widehat{LL}_{max}$	cells	
-119.262	1057	-120.176	1007	-119.301	1033	-120.526	1058	0.00995539
-110.268	1004	-111.917	1040	-111.211	1032	-111.825	1027	0.0100925
-118.006	1220	-116.363	1132	-115.572	1159	-117.445	1190	0.0111535
-123.927	1035	-123.266	1116	-123.691	1095	-124.538	1070	0.00954747
-113.252	1023	-111.715	1016	-111.741	1021	-113.954	1027	0.0101153
-128.584	1111	-127.824	1030	-126.974	1061	-128.595	1094	0.00958187
-133.737	1005	-133.594	957	-132.831	968	-133.919	984	0.00973301
-116.784	1040	-117.731	1039	-116.525	1040	-117.751	1046	0.0103188
-124.403	1028	-122.545	1060	-122.924	1052	-124.78	1043	0.0093805
-117.763	1084	-114.387	1069	-114.757	1070	-117.423	1076	0.0108218

The following plot shows the peak height data used in the last simulation of the previous table. We see that there is complete allelic drop-out on the loci CSF1PO and D18S51.
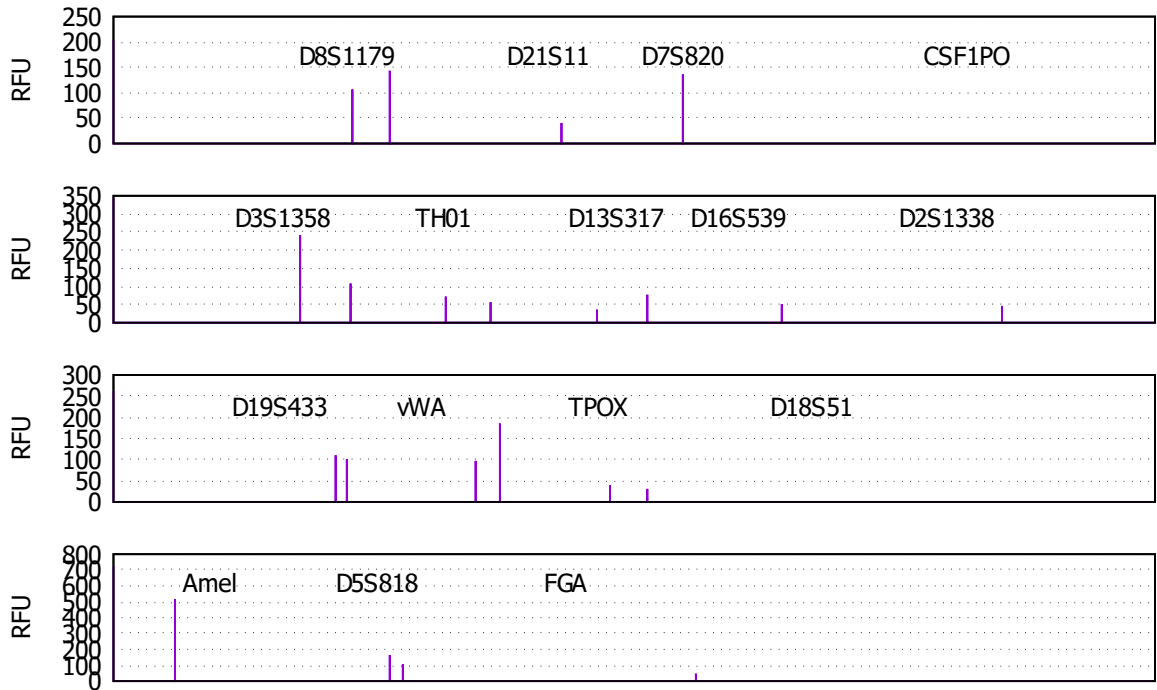
The following plot shows the peak height probability distribution obtained from the **FFT** model, for allele 25 of the locus FGA, in which the distribution is conditional on the values all of the other peak heights and the profile of the contributor. The smaller vertical line at $(30, 0)$ locates the analytic threshold, the larger vertical line locates the observed peak. The complete dropout probability value point at $(0, 0.0569)$, is off the scale of the plot. The plot suggests that, most likely, either 3 or 4 intact genomic strands were randomly selected for the simulated **PCR** amplification.
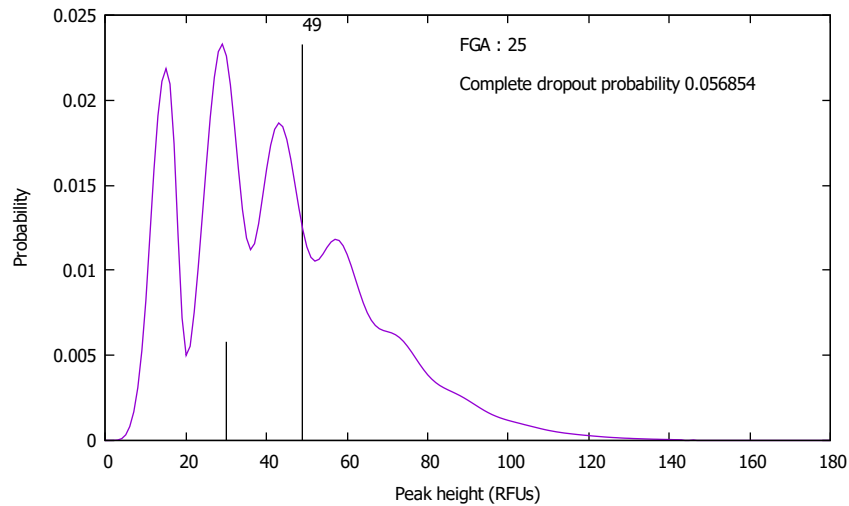
Summary for single contributor simulations

For moderate to large numbers of cells, all three moment models and the **FFT** based model yield comparable estimates for estimated cell counts and maximized log-likelihood values. However when the expected number of cells drops below 8 or so, the **FFT** model exhibits bias in overestimating the number of cells, and produces more extreme (lower) likelihoods. Overall the lognormal and gamma models appear to give the better estimates. However, for such low amounts it seems sensible to simplify the model by omitting the forward and double backward stutter model components; doing so it appears that the **FFT** model is concordant with the moment based models.

10.2   Two person simulations

We now look at a few two-person simulations, concentrating on low-template scenarios with various relative initial amounts of DNA.

10.2.1   Two person mixtures

In the first simulation we have no degradation, that is $\delta = 0$, set $\phi = 0.04$, and we simulate from contributors RD14-0003-01 ($C_1 = 200$ cells) and RD14-0003-2 ($C_2 = 200$ cells). With $\phi = 0.04$ this corresponds to an average of 16 amplify-able cells worth of DNA, around $150pg$. Using all four stutter distributions, we obtain

this set of simulated fits, assuming that both contributor profiles are known. All models are giving similar maximized likelihood and cell estimates.

Normal			Logormal			Gamma			FFT		
$\widehat{LL}_{max}$	$\hat{C}_1$	$\hat{C}_2$	$\widehat{LL}_{max}$	$\hat{C}_1$	$\hat{C}_2$	$\widehat{LL}_{max}$	$\hat{C}_1$	$\hat{C}_2$	$\widehat{LL}_{max}$	$\hat{C}_1$	$\hat{C}_2$
-242.429	193	194	-241.955	200	201	-242.155	198	200	-242.31	200	200
-244.799	202	196	-241.404	210	198	-242.383	208	198	-243.576	208	200
-248.631	184	181	-248.005	182	180	-247.48	184	181	-249.832	201	196
-246.318	175	207	-244.447	187	206	-244.682	182	206	-246.326	194	206
-249.793	207	224	-247.785	207	226	-247.889	208	226	-248.492	208	224
-240.07	180	214	-239.761	185	225	-239.775	185	222	-240.727	190	222
-253.473	204	212	-251.879	200	209	-251.465	203	210	-251.749	204	213
-252.464	197	207	-251.199	192	206	-250.913	194	208	-251.412	195	208
-246.45	198	214	-252.804	210	197	-249.38	206	205	-247.265	205	206
-245.234	191	209	-243.718	200	209	-243.995	198	210	-244.59	200	212

Repeating the simulation but with $C_1 = 50$ and $C_2 = 200$ cells, (a 1:4 mixture), we see that the three moment models are in broad agreement, but that the FFT model is diverging in both the cell estimates for RD14-0003-01 and the maximized likelihoods, which are much lower than the moment models in comparison.

Normal			Logormal			Gamma			FFT		
$\widehat{LL}_{max}$	$\hat{C}_1$	$\hat{C}_2$	$\widehat{LL}_{max}$	$\hat{C}_1$	$\hat{C}_2$	$\widehat{LL}_{max}$	$\hat{C}_1$	$\hat{C}_2$	$\widehat{LL}_{max}$	$\hat{C}_1$	$\hat{C}_2$
-181.783	41	239	-180.183	40	237	-179.908	39	238	-215.229	9	251
-193.674	50	193	-192.84	47	193	-191.837	46	195	-239.032	16	204
-186.171	42	209	-190.008	51	212	-188.724	47	213	-232.002	13	224
-193.501	50	199	-190.686	54	200	-191.185	52	200	-234.826	111	189
-188.659	48	200	-191.771	46	204	-189.964	47	204	-235.36	15	204
-201.354	56	202	-200.354	60	196	-199.818	57	200	-240.015	115	192
-172.509	34	201	-173.196	41	215	-173.62	38	212	-205.595	9	208
-177.388	41	189	-176.959	42	196	-176.441	40	195	-213.534	11	204
-190.686	44	201	-194.281	48	188	-191.67	45	195	-233.393	13	204
-194.286	52	196	-200.514	54	192	-197.259	53	195	-237.177	112	187

However if we take out the double and forward stutter models, we see that balance is restored:

Normal			Logormal			Gamma			**FFT**		
$\widehat{LL}_{max}$	$\hat{C}_1$	$\hat{C}_2$	$\widehat{LL}_{max}$	$\hat{C}_1$	$\hat{C}_2$	$\widehat{LL}_{max}$	$\hat{C}_1$	$\hat{C}_2$	$\widehat{LL}_{max}$	$\hat{C}_1$	$\hat{C}_2$
-181.742	42	240	-180.308	42	238	-179.996	41	239	-183.262	45	237
-193.528	51	194	-192.87	49	193	-191.85	47	195	-195.064	52	193
-186.354	43	209	-190.206	52	213	-188.941	49	213	-191.354	50	212
-193.559	51	199	-190.807	55	201	-191.313	53	201	-194.136	55	200
-188.622	49	201	-191.907	48	204	-190.039	48	204	-191.171	53	201
-201.419	57	203	-200.684	61	196	-200.109	59	200	-202.325	60	202
-172.836	35	202	-173.856	43	215	-174.24	40	212	-176.951	39	207
-177.56	42	189	-177.187	44	196	-176.674	41	196	-179.332	44	192
-190.541	44	202	-194.199	49	189	-191.58	46	196	-192.827	49	199
-194.748	53	196	-200.858	56	192	-197.676	55	195	-197.303	57	196

We now look at the data from the final simulation. We refit the set of models under three more scenarios, making the following four scenarios, in which the K1K2 scenario is that use in the previous table.

K1K2 scenario RD14-0003-01 genotype is treated as known, and RD14-0003-02 genotype is treated as known

U1K2 scenario RD14-0003-01 genotype is treated as unknown, and RD14-0003-02 genotype is treated as known

K1U2 scenario RD14-0003-01 genotype is treated as known, and RD14-0003-02 genotype is treated as unknown

U1U2 scenario RD14-0003-01 genotype is treated as unknown, and RD14-0003-02 genotype is treated as unknown

The genotypes of the individuals, and the observed peaks using the analytic threshold of 30 RFUs, are shown in Table 2, and the simulated **EPG** is plotted in Figure 22. From Table 2 we can see that a number of alleles have dropped out, and that for some loci there is complete drop-out of the low-donor contributor.

The results of fitting each of the models to each of the four scenarios is shown in Table 3. We see that for each, the models give similar results, even with the considerable allelic drop-out that is taking place. Note also that the table may be used to find for prosecution to defence likelihood ratios. Suppose that the prosecution case is that RD14-0003-01 is a contributor, and the defence hypothesis

Table 2: Genotypes and peaks heights in a two person simulation, with RD14-0003-01 having 50 cells, and RD14-0003-02 200 cells.

| Locus	RD14-0003-01	RD14-0003-02	Allele/height	Allele/height	Allele/height	Allele/height
Amelogenin	X / X	X / Y	X 199	Y 88		
CSF1PO	11 / 12	7 / 8	7 147	8 148	11 55	
D13S317	8 / 12	11 / 11	8 53	11 160	12 46	
D16S539	12 / 13	11 / 13	11 123	12 34	13 114	
D18S51	13 / 15	17 / 17	15 31	17 251		
D19S433	14 / 15	13 / 14	13 77	14 154	15 54	
D21S11	29 / 31	29 / 31	29 118	31 96		
D2S1338	20 / 22	21 / 21	20 61	21 219	22 66	
D3S1358	14 / 18	15 / 16	15 161	16 149		
D5S818	11 / 12	11 / 12	11 89	12 240		
D7S820	9 / 9	8 / 10	8 145	9 33	10 93	
D8S1179	12 / 15	13 / 13	13 198			
FGA	20 / 25	24 / 28	20 33	24 163	25 60	28 103
TH01	6 / 9.3	6 / 9	6 188	9 125		
TPOX	8 / 11	9 / 9	9 178			
vWA	17 / 19	15 / 17	17 185			
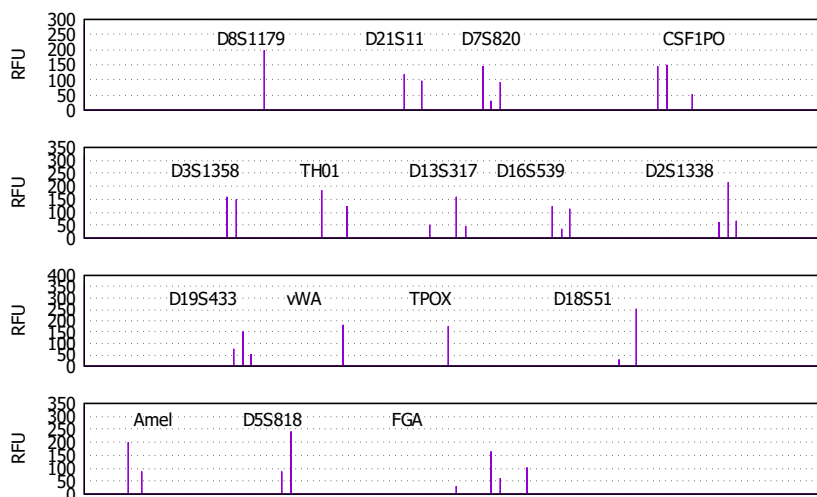
Figure 22: Simulated **EPG** for the 1:4 mixture of two persons of Table 2.

Table 3: Fitting each of the four scenarios to each of the four models.

Scenario	Normal			Logormal			Gamma			FFT		
	$\widehat{LL}_{max}$	$\hat{C}_1$	$\hat{C}_2$	$\widehat{LL}_{max}$	$\hat{C}_1$	$\hat{C}_2$	$\widehat{LL}_{max}$	$\hat{C}_1$	$\hat{C}_2$	$\widehat{LL}_{max}$	$\hat{C}_1$	$\hat{C}_2$
K1K2	-194.748	53	196	-200.858	56	192	-197.676	55	195	-197.303	57	196
U1K2	-209.557	57	189	-215.185	67	185	-212.8	62	189	-212.005	63	191
K1U2	-237.658	55	193	–239.057	55	200	-238.359	54	199	-239.642	58	198
U1U2	-250.112	54	192	-250.986	58	195	-250.658	55	196	-251.555	59	195

Table 4: Various log-likelihood ratios for possible prosecution vs defence hypothesis concerning the presence of one of the individuals, for each of the four models: values given are log-likelihood ratios expressed in Bans.

Hypotheses	Normal	Lognormal	Gamma	FFT
K1K2 vs U1K2	6.43	6.22	6.57	6.38
K1U2 vs U1U2	5.41	5.18	5.34	5.17
K1K2 vs K1U2	18.64	16.59	17.67	18.39
U1K2 vs U1U2	17.61	15.55	16.44	17.18

that `RD14-0003-01` is not. Then the log-likelihood ratio in favour of the prosecution hypothesis will be $(-194.748 - (-209.557))/\log(10) = 6.43$ Bans. Table 4 shows various combinations of log-likelihood ratios. Notice that the values are higher for the last two rows, which are hypotheses concerning the presence of the major contributor, than equivalents hypothesis comparisons in the first two rows concerning the presence of the minor contributor. This is to anticipated. What is perhaps surprising are the quite high values in the first two rows, concerning the presence of the minor contributor, given the very low template DNA from the minor contributor.

11 Application to sample data

This section describes the performance of the model above to the publicly available DNA dataset from the PROVEDIt Initiative (Alfonse et al., 2016, 2018). This is a very large dataset of laboratory controlled single source and mixed DNA samples, with amplifications carried out for the Identifiler Plus[TM], PowerPlex16H[TM] and Globalfiler[TM] kits. From it we shall use the sets of samples for the Identifiler

Plus^{TM} kit that were amplified for 28 cycles. We shall use the processed data in the EXCEL files available from the PROVEDIt Initiative website, rather than the raw fsa files that are also available. The EXCEL files contain allele calls (including O/L designations) in Genemapper output format, in which an analytic threshold has been set to 1 **RFU**. Although these files contain artefacts such as split-peaks and dye-blobs, and the PROVEDIt Initiative provides an EXCEL spreadsheet to help remove these, they have been left in so that the data can be processed in batch automatically. Hence our analyses presented here are using quite noisy data.

11.1   Calibration of model parameters to the data

The samples from the PROVEDIt Initiative were prepared from the dilution of high-density extracted DNA. Hence a Poisson model for the amount of DNA would be appropriate. However, we use a binomial model as presented so far, as this is more appropriate for real life samples.[6] We assume an extraction efficiency of $\psi = 0.3$, a sample volume of $25\mu L$ of which $10\mu L$ is used in the amplification, hence $\pi_f = 0.06$. We also used a drop-in rate per locus of 0.021.

To estimate the noise distribution, the peak heights of all *off-ladder* (O/L) designated alleles in the high DNA single source samples were extracted and treated as empirical distributions for each lane - each lane distribution is based on over 40,000 values. A cut-off of 100 **RFU**s was used for the noise distribution. Figure 23 shows the noise distributions for each of the four dyes, omitting the long tail up to 100 **RFU**s.

To form the **EPG** data files, we retained for each sample all of the alleles that were called, that is, those that were given an allele designation that was not given as O/L.

Amplification probabilities were assigned as follows. It is assumed that all strand probabilities in any given locus are the same, that is $p_g = p_{g_d} = p_h = p_{h_d} = p_a = p_{a_d} = p$. From the high-template DNA single source, non-degraded, samples, in each sample the peak heights of called alleles were added together. These total peak height values were scaled by the estimated amount of initial DNA in each sample (this information is provided in the name of each sample). The mean peak heights of every locus in the kit was then found. It was found that TPOX had the largest mean value. This locus was - somewhat arbitrarily - assigned an amplification probability of 0.85 for all types of strand. Using the

---

[6]Essentially we are approximating Poisson distributions by binomial distributions, usually the approximation is the other way around.

Peak height noise distributions
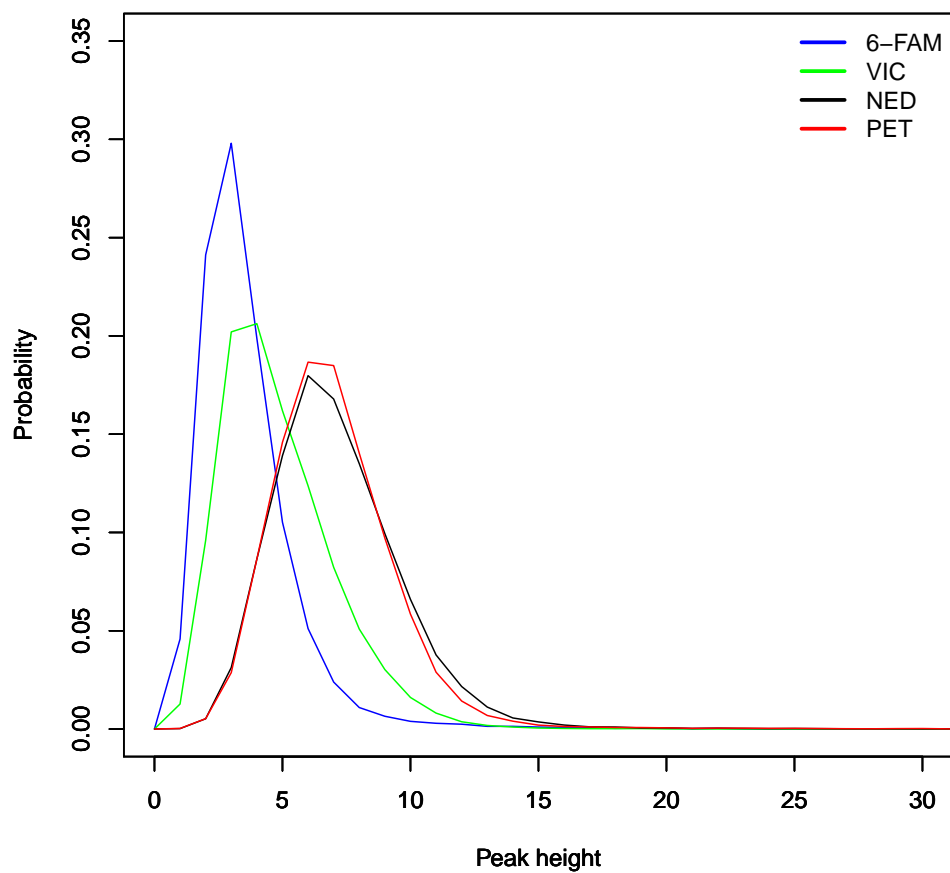
Figure 23: Empirical noise distributions for each dye lane for analyzing the PROVEDIt Initiative data for the Identifiler-Plus^{TM} kit. The long tails going out to 100 **RFU**s is omitted.

fact that the number of cycles was 28, and that the mean number of amplicons from a single strand is approximately $(1 + p)^{28}$, amplification probabilities for the other loci were found so that their mean values scaled correctly according to their empirical mean when compared to the mean peak height of TPOX.

Conditional stutter probabilities were either assigned values of 0.001 for forward and double stutter and 0.004 for single stutter, except for the loci in the allelic ladder of the kit where mean stutter ratios were available from the manufacturer's literature, (Scientific, 2012) in which case somewhat crude estimates were obtained from the plots of stutter ratio versus allele lengths to obtain stutter probabilities that matched in mean; forward and double stutter probabilities for the alleles were obtained from these by division by 4.

A scale factor of two million was used for all lanes to convert the number of tagged amplicons to an **RFU** equivalent value.

We shall focus on the samples that were amplified for 5 seconds, and for these use an analytic threshold of 15 **RFU**s.

With all of these parameters set, and using the laboratory estimated amount in each sample, maximum likelihood estimation was used to estimate the degradation and initial cell counts of each hypothesised contributor.

11.2   Analysis of a two person sample

From the two-person data the author extracted the profiles of 189 samples. These two person mixtures were treated as 3 person mixtures in analysis. The profiles are discussed here, and in later sections use the naming convention of the PROVEDIt Initiative datasets.

Sample E02_RD14-0003-42_43-1_9-M2S10-0.15IP-Q1.0_001.5sec

This two sample mixture was prepared in 1 ratio of 1:9, and subject to 10 seconds of sonification to simulate degradation. The target amount of DNA was 0.15ng. With our use of $\phi = 0.06$, this corresponds to approximately $150/0.06 = 2500pg$ of DNA initially, that is around 378 cells in total, with around 22 cells worth in the amplified sample. This is a highly degraded very low template sample, we therefore omit the double and forward stutter components when fitting the models: the **EPG** plot is shown in Figure 24;

We first analyse this sample under the hypothesis that both of the actual contributors are contributors, and an additional untyped contributor is assumed to be present as well. Maximized likelihoods and estimated cell amounts are shown in Table 5. The degradation is estimated on a discretized scale, and in this case all four models have estimated the same degradation value.
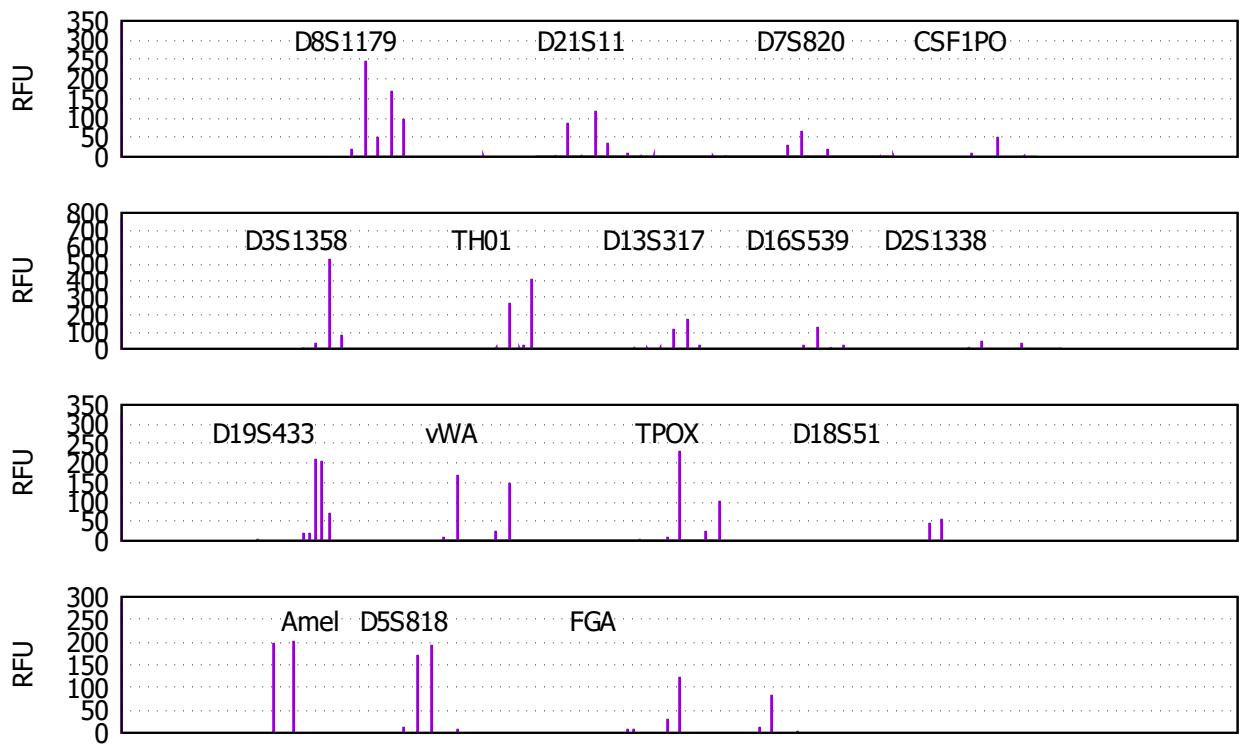
Figure 24: Schematic **EPG** plot for the E02_RD14-0003-42_43-1_9-M2S10-0.15IP-Q1.0_001.5sec sample.

Table 5: Maximum likelihood estimates for the `E02_RD14-0003-42_43-1_9-M2S10-0.15IP-Q1.0_001.5sec` sample.

Model	$\widehat{LL}_{max}$	$\hat{C}_1$	$\hat{C}_2$	$\hat{C}_3$	$\hat{\delta}$
Normal	-236.85	72	343	0	0.00504874
Lognormal	-240.971	64	337	0	0.00504874
Gamma	-237.857	67	343	0	0.00504874
FFT	-235.605	71	347	0	0.00504874

Of particular note is that all models have estimated the cell amount for the extra untyped contributor to be 0 - which is in agreement with the manner of the preparation of the two-person mixture. The forensic science literature contain much discussion concerning how to estimate the number of contributors to a mixture(see for example (Haned et al., 2011; Lauritzen and Mortera, 2002; Egeland et al., 2003; Swaminathan et al., 2015)). In the models presented here the maximum likelihood estimates can return 0 for cell counts, because the cell amounts beign estimated are discrete integers. This is in marked contrast to other continuous peak height models that model contributor amounts or relative amounts by continuous variables, for which the nesting of models by adding extra hypothesised contributors will lead to increasing maximized likelihoods. (Cowell et al., 2015)

(Graversen and Lauritzen, 2015; Cowell et al., 2015) introduced various statistically based diagnostics to check how well a model fits the profile data. One such diagnostic is a QQ-plot in which for each allelic peak h_a in the set $\mathcal{H}$ of peaks observed above the threshold T the quantities $P(H < h_a | H > T, h_b \in \mathcal{H}, b \neq a)$ are calculated. If the models is 'true', then these values should follow a uniform distribution, so that a plot of these sorted values should follow a straight line when plotted against the quantiles of the uniform distribution. Figure 25 shows the QQ-plot for the **FFT** model, which is the model with the highest likelihood in Table 5: we see that the fit is very good.

As an example of the predictive distribution of a peak, we take the allele 13 of locus D13S317. For that locus, three peaks were observed above the threshold of 15 **RFU**s: allele 11 with a peak height of 117, allele 12 with a height of 177 and allele 13 with a height of 27. Contributor `RD14-0003-42` has genotype (12/13) on locus D13S317, and `RD14-0003-43` has genotype (11/12). Thus the 13 peak can arise from the minor contributor `RD14-0003-42` (recall that we are not including forward stutter in this analysis) or drop-in. From the **FFT** estimates in Table 5,
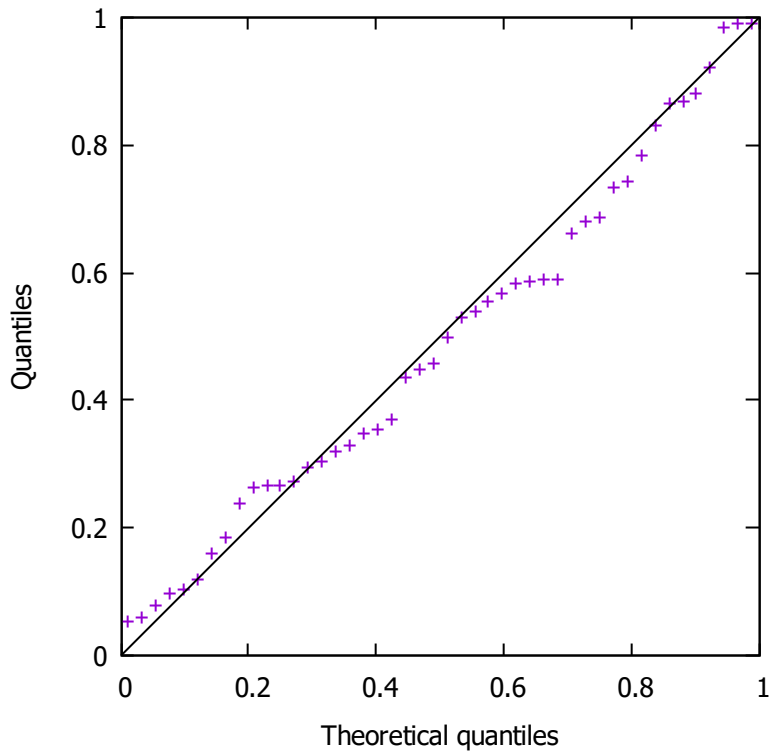
Figure 25: QQ-plot for the **FFT** model for the E02_RD14-0003-42_43-1_9-M2S10-0.15IP-Q1.0_001.5sec sample.

Table 6: Maximum likelihood estimates for the `E02_RD14-0003-42_43-1_9-M2S10-0.15IP-Q1.0_001.5sec` sample assuming 3 untyped contributors.

Model	$\widehat{LL}_{max}$	$\hat{C}_1$	$\hat{C}_2$	$\hat{C}_3$	$\hat{\delta}$
Normal	-297.752	90	370	9	0.00567983
Lognormal	-297.842	79	388	0	0.00567983
Gamma	-297.56	78	391	0	0.00567983
FFT	-298.815	71	347	0	0.00567983

there are an estimated 71 initial genomic strands of this allele type, sampled intact with probability 0.06 for amplification, hence an estimated mean of around 4.26 amplify-able strands . Figure 26 shows the predictive distribution for this allele conditional on the observed peak heights and estimated cell amounts. The first peak on the left is the baseline-noise distribution for VIC lane (compare it to Figure 23). The plot is giving a clear signal that just one amply-able strand of this allele was in the aliquot minitube when the **PCR** was carried out. For comparison, the distribution obtained from using the Gamma model is also shown in Figure 26.

Table 6 shows estimates for each model analyzed under the assumption that the mixture is of three untyped persons. The gamma model has the highest likelihood, and now the normal model is giving a non-zero cell count estimate for all three persons. Distribution plots for allele 13 of locus D13S317 are given in Figure 27.
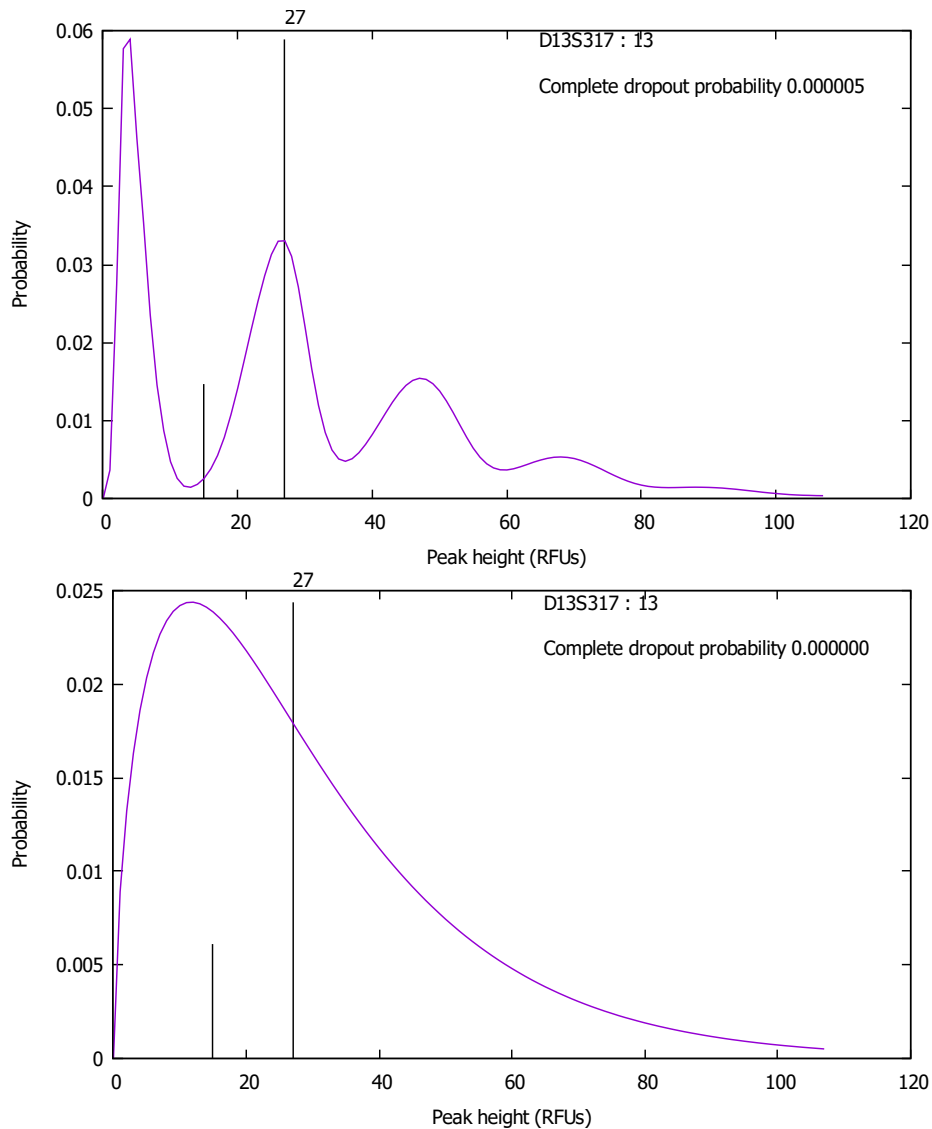
Figure 26: Predictive distributions for allele 13 of locus D13S317, for the `E02_RD14-0003-42_43-1_9-M2S10-0.15IP-Q1.0_001.5sec` sample assuming the genotypes of the true contributors and a third untyped contributor. Top plot, the **FFT** model, bottom plot the (moment matching) Gamma model. The first vertical line at 15 RFUs is the location of the analytic threshold, the second at 27 RFUs is the observed peak height.

110
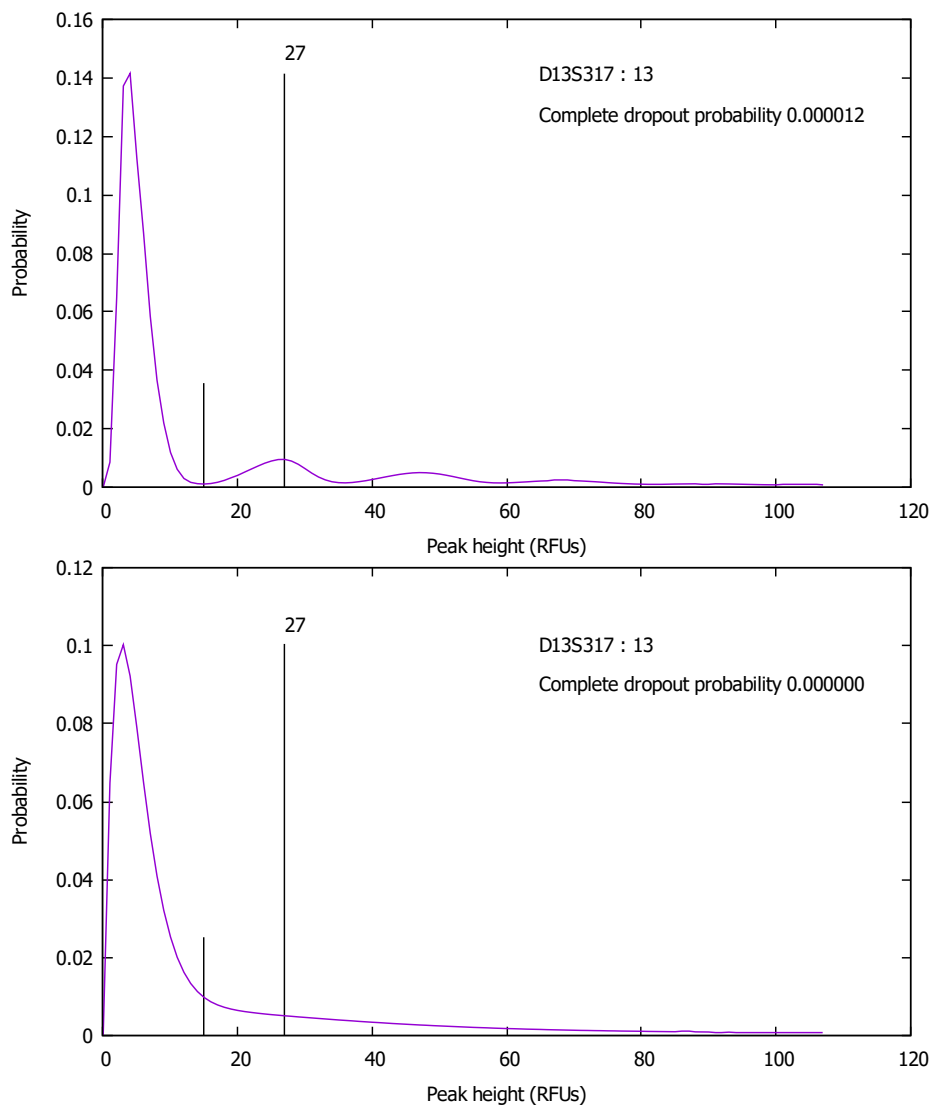
Figure 27: Predictive distributions for allele 13 of locus D13S317, for the E02_RD14-0003-42_43-1_9-M2S10-0.15IP-Q1.0_001.5sec sample assuming three contributors of unknown genotype. Top plot, the **FFT** model, bottom plot the (moment matching) Gamma model.

11.3 Analysis of a three person sample

The sample `A06_RD14-0003-47_48_49-1_9_9-M2c-0.589IP-Q1.1_001.5sec` has contributor amounts in the proportions of 1:9:9, with a medium level of degradation cause by rDNase I enzyme added to the extract. Analyzing as a four person mixture, assuming as knowns the genotypes of the three contributors and one extra untyped individual, and ignoring forward and double stutter, we obtain the estimates in Table 7. The **FFT** model correctly estimate zero cells for the untyped contributor, and the **FFT** model gives the highest likelihood. The estimated mixture proportions are in line with the experimentally prepared ratios for all four models. The QQ-plot for the **FFT** model is shown in Figure 28.

Table 7: Maximum likelihood estimates for the `A06_RD14-0003-47_48_49-1_9_9-M2c-0.589IP-Q1.1_001.5sec` sample assuming the genotypes of the three contributors, plus a fourth of unknown genotype.

| Model	$\widehat{LL}_{max}$	$\hat{C}_1$	$\hat{C}_2$	$\hat{C}_3$	$\hat{C}_4$	$\hat{\delta}$
Normal	-384.74148962	73	687	718	2	0.00490963394042
Lognormal	-386.801221118	67	693	682	2	0.00490963394042
Gamma	-384.573053649	68	693	695	2	0.00490963394042
FFT	-382.407751392	62	622	639	0	0.00490963394042
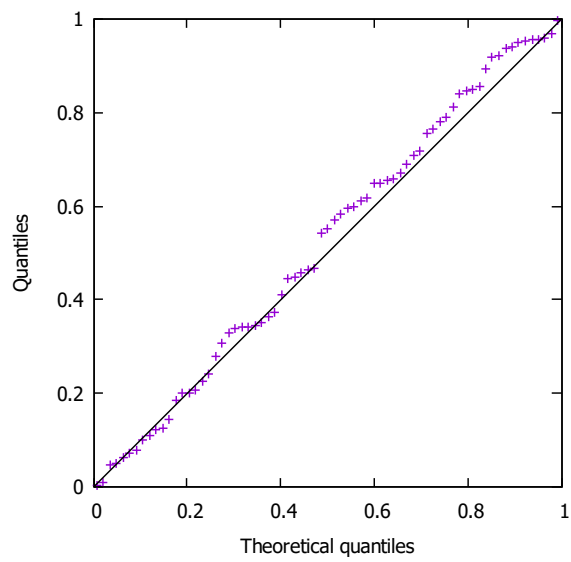
Figure 28: QQ-plot for the **FFT** model for the
`A06_RD14-0003-47_48_49-1_9_9-M2c-0.589IP-Q1.1_001.5sec` sample,
with stutter but no double or forward stutter.

Table 8: Maximum likelihood estimates for the `A06_RD14-0003-47_48_49-1_9_9-M2c-0.589IP-Q1.1_001.5sec` sample assuming the genotypes of the three contributors, plus a fourth of unknown genotype, with estimation include stutter, double stutter and forward stutter distributions.

Model	$\widehat{LL}_{max}$	$\hat{C}_1$	$\hat{C}_2$	$\hat{C}_3$	$\hat{C}_4$	$\hat{\delta}$
Normal	-395.225614561	59	591	615	0	0.00436411905815
Lognormal	-401.337705571	45	587	584	4	0.00436411905815
Gamma	-394.142509492	53	595	604	3	0.00436411905815
FFT	-411.894302982	17	599	625	0	0.00436411905815

If we include forward and double stutter in the models, we obtain the estimates obtained in Table 8. We see that the **FFT** model has become out-of-line with the other models in having a much lower likelihood, and much lower estimates for the number of cells from the minor contributor. The normal model is now the one having the highest likelihood: QQ-plots for the Normal and **FFT** model are shown in Figure 29.
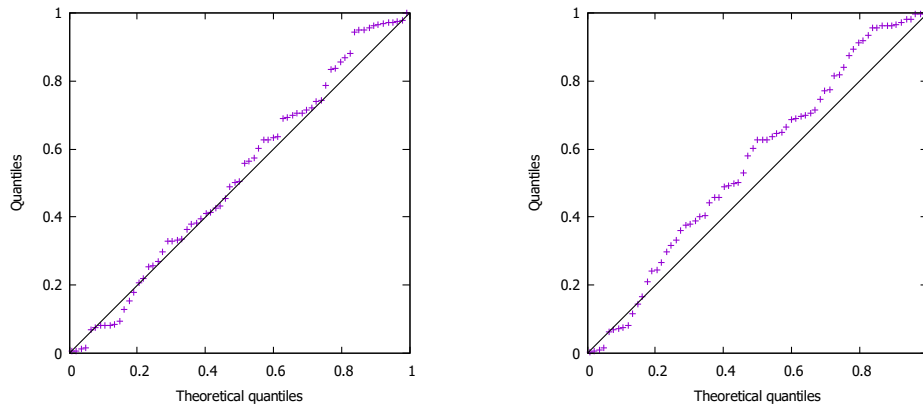

Figure 29: QQ-plots the`A06_RD14-0003-47_48_49-1_9_9-M2c-0.589IP-Q1.1_001.5sec` sample, when forward and double stutter are included. The Normal model (left), and the **FFT** model ((right).

12 A modification of the FFT model to correct for correlations

We have seen that in some cases we can improve the **FFT** model by removing the forward and double back-stutters; however this will not be appropriate for all cases. Here we introduce an adjustment to the **FFT** model that puts back some of the correlation that was discarded in the factorization approximations of (38) and (39); we denote the new model by **mFFT**.

Recall that the point of making those approximations was purely to make the computations tractable, by enabling the peak height likelihood to factorize into a product of convolutions of univariate probability distributions of individual alleles. However, as pointed out earlier, a side effect of this approximation is that the complete dropout probability for an allele is included as a factor multiple times in the likelihood. The modification here aims to reduce such multiple factors.

For any given allele a, there will up to 6 distributions to convolve in finding its peak height likelihood contribution:

1. The base-line noise distribution

2. The drop-in distribution

3. The peak height distribution arising from genomes of type a

4. The peak height distribution arising from stutter from genomes of type one repeat larger than a

5. The peak height distribution arising from double stutter from genomes of type two repeats larger than a

6. The peak height distribution arising from forward stutter from genomes of type one repeat smaller than a

In the new approximation we always retain the first three distributions. Now consider the contribution from say stutter from one repeat higher. Suppose that no peak above threshold is observed at the one-repeat higher position. This means that any genomic material of allelic type one-repeat higher than a has dropped out. In this case, we can therefore omit the marginal stutter peak height distribution in the convolution as it is extremely likely that any stutter product would be too low to be observed. However, given that stutter peaks are typically around 5-15% of the target peak producing the stutter, this means that even if a peak is

115

observed at one-repeat higher than a, but is below a small multiple of the analytic threshold then we can assume that any stutter contribution it makes to the allele a will not be seen. A similar argument applies also to the double stutter and forward stutter distributions—more so as these tend to have smaller stutter ratios than single stutter peaks.

Hence the modification is as follows. In evaluating the peak height likelihood for an allele a, when forming the marginal peak height distribution:

- Always include the base-line noise distribution.

- Always include the drop-in distribution.

- Always include the peak height distribution arising from genomes of type a.

- Only include the peak height distribution arising from stutter from genomes of type one repeat larger than a if there is a peak above three times the threshold at that position.

- Only include the peak height distribution arising from double stutter from genomes of type two repeats larger than a if there is a peak above three times the threshold at that position.

- Only include the peak height distribution arising from forward stutter from genomes of type one repeat smaller than a if there is a peak above three times the threshold at that position.

- Convolve all of the included distributions to obtain the marginal peak height distribution to use for finding the likelihood for the peak of the allele a.

A factor different to three for the multiple of the analytic threshold could be used—further research is required to find the best factor to use.

12.1 Revisiting the two person simulation of Section 10.2.1

The following table shows the model fits obtained using the **mFFT** model for the simulation with $C_1 = 50$ cells and $C_2 = 200$, which should be compared to the second table in Section 10.2.1: we see that the **mFFT** model is now much more in line with the other models both in its maximum likelihood values and the cell estimates of the two contributors.

Normal			Logormal			Gamma			mFFT		
$\widehat{LL}_{max}$	$\hat{C}_1$	$\hat{C}_2$	$\widehat{LL}_{max}$	$\hat{C}_1$	$\hat{C}_2$	$\widehat{LL}_{max}$	$\hat{C}_1$	$\hat{C}_2$	$\widehat{LL}_{max}$	$\hat{C}_1$	$\hat{C}_2$
-181.783	41	239	-180.183	40	237	-179.908	39	238	-180.334	38	237
-193.674	50	193	-192.84	47	193	-191.837	46	195	-191.74	47	199
-186.171	42	209	-190.008	51	212	-188.724	47	213	-188.69	44	215
-193.501	50	199	-190.686	54	200	-191.185	52	200	-193.364	52	202
-188.659	48	200	-191.771	46	204	-189.964	47	204	-188.564	47	204
-201.354	56	202	-200.354	60	196	-199.818	57	200	-205.226	61	202
-172.509	34	201	-173.196	41	215	-173.62	38	212	-172.733	34	210
-177.388	41	189	-176.959	42	196	-176.441	40	195	-176.003	39	195
-190.686	44	201	-194.281	48	188	-191.67	45	195	-190.566	44	200
-194.286	52	196	-200.514	54	192	-197.259	53	195	-195.177	51	199

12.2 Revisiting the three person mixture of Section 11.3 from the PROVEDit Initiative

Re-analyzing `A06_RD14-0003-47_48_49-1_9_9-M2c-0.589IP-Q1.1_001.5sec`, with both forward and double stutter included using the **mFFT** model, we obtain a maximized log-likelihood of -405.944809925, and estimated cell counts of $\hat{C}_1 = 31$, $\hat{C}_2 = 596$, $\hat{C}_3 = 617$ and $\hat{C}_4 = 0$, less extreme than the estimates in Table 8. The corresponding QQ-plot is little changed from Figure 29 and is omitted.

12.3 Another 2-person mixture from the PROVEDit datatset

In all the examples seen so far, we have seen broad agreement between the various models. We now look at an example from PROVEDit datatset in which the models give quite different model fits. The dataset we shall look at is `C04_RD14-0003-42_43-1_9-M1U105-0.54IP-Q0.6_003.5sec`. This is a two-person mixture of 540pg total DNA template in the ratio of 1:9 from the two contributors. The U105 indicates that the sample was subject to 105 minutes exposure to ultra-violet radiation (to degrade the sample) before **PCR**. Table 9 shows the peak heights of the sample, above the analytic threshold of 15 **RFU**s, and the profiles of the two contributors. A plot of the **EPG** is shown in Figure 30.

We shall analyse this mixture under the assumption of two contributors. If we assume the true genotypes of the contributors, and include forward and double

Table 9: Peaks heights and the genotypes of constributors RD14-0003-42 RD14-0003-43 .

Locus	RD14-0003-42	RD14-0003-43	Allele/height	Allele/height	Allele/height	Allele/height	Allele/height	Allele/height	Allele/height
Amelogenin	X/X	X/Y	X/1686	Y/1049					
CSF1PO	10/12	10/12	9/33	10/848	10.2/17	11/53	12/867		
D13S317	12/13	11/12	10/67	11/1269	12/1125	13/79			
D16S539	9/12	10/10	9/297	10/2682	11/22	12/183			
D18S51	17/18	18/19	15/15	16/18	17/130	18/834	19/633		
D19S433	14/14.2	13.2/14	12/18	12.2/92	13/88	13.2/1250	14/1295	14.2/141	
D21S11	30/31.2	27/29	26/29	27/616	28/61	29/786	30/122	31.2/100	
D2S1338	22/23	19/22	18/92	19/1148	21/127	22/1230	23/109		
D3S1358	15/16	15/15	13/20	14/252	15/3613	16/266			
D5S818	12/13	11/12	10/49	11/848	12/989	13/124			
D7S820	11/11	8/9	8/523	9/426	11/138				
D8S1179	12/14	11/13	10/44	11/858	12/207	13/1309	14/204		
FGA	20/21	21/28	20/134	21/617	27/40	28/557	31.2/23	35/19	36/23
TH01	9/9.3	8/9.3	7/90	8/1508	8.3/22	9/230	9.3/1896		
TPOX	8/10	8/11	7/23	8/1234	10/141	11/880			
vWA	16/17	13/17	12/37	13/1123	16/215	17/932			
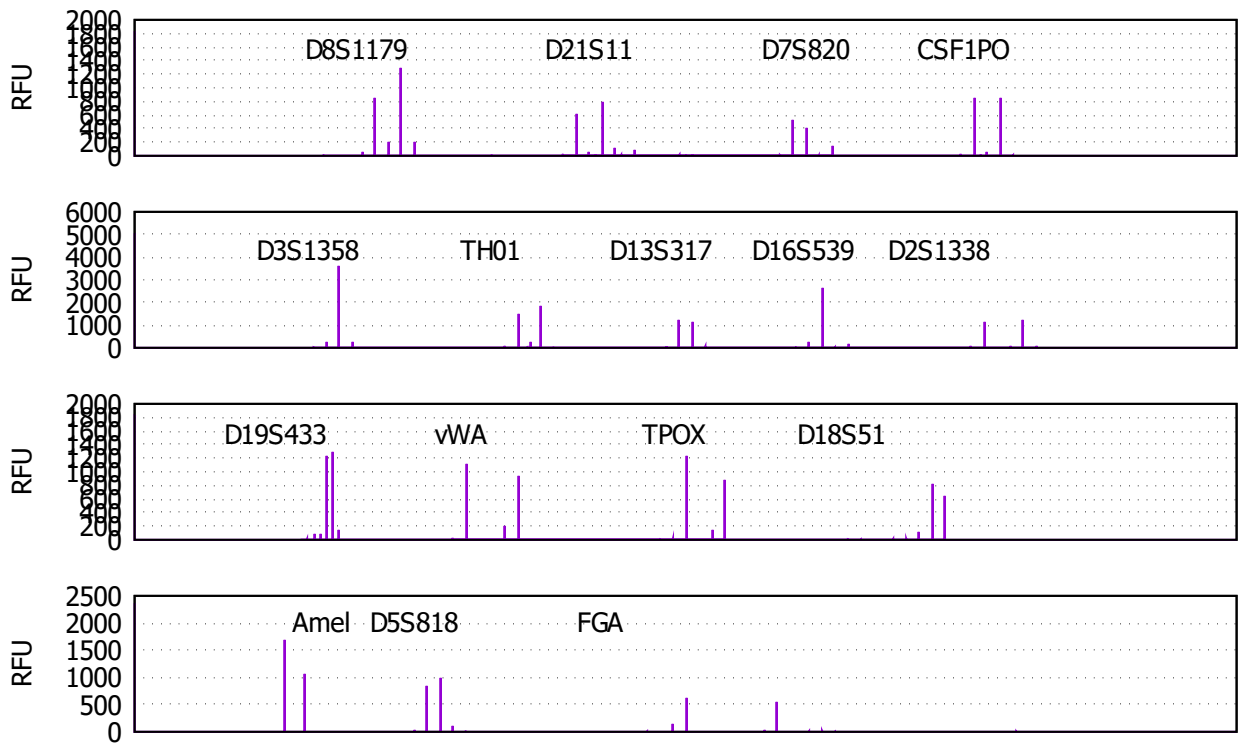
Figure 30: **EPG** plot for the `C04_RD14-0003-42_43-1_9-M1U105-0.54IP-Q0.6_003.5sec` sample.

Table 10: Fitting each of the four scenarios to each of the four models.

Scenario	Normal			Logormal			Gamma			mFFT		
	$\widehat{LL}_{max}$	$\hat{C}_1$	$\hat{C}_2$	$\widehat{LL}_{max}$	$\hat{C}_1$	$\hat{C}_2$	$\widehat{LL}_{max}$	$\hat{C}_1$	$\hat{C}_2$	$\widehat{LL}_{max}$	$\hat{C}_1$	$\hat{C}_2$
42-43	-651.92	154	1267	-528.83	162	1108	-543.31	161	1158	-502.20	158	1158
U1-43	-599.47	138	1233	-549.52	142	1094	-553.55	136	1145	-534.37	140	1161
42-U2	-700.63	154	1267	-577.53	162	1108	-592.01	161	1158	-550.90	158	1158
U1-U2	-648.809	138	1223	-598.54	143	1094	-602.67	136	1145	-583.39	141	1161

stutter, then obtain a maximized log-likelihood of -756.241357805 using the normal model. Omitting the forward and double stutter, the maximized log-likelihood increases significantly to -651.9280003. Hence in all analyses we shall include only stutter, and omit both forward and double stutter model components.

Table 10 shows the results of fitting models to four possible two-contributor scenarios. The first line of the table is the scenario in which we assume as known the profiles of the (true) contributors RD14-0003-42 and RD14-0003-43. In the second line we replace RD14-0003-42 with an untyped contributor labelled U1. In the third line we replace RD14-0003-43 with an untyped contributor labelled U2. In the last line we treat both contributors as having unknown genotypes.

We see that cell estimates are broadly in line for all models except the normal model, which has higher major contributor estimates, and in agreement with the 1:9 preparation ratio of the sample. There is quite a lot of variation between the models in their log-likelihood estimates for each scenario, with the **mFFT** model outperforming the moment based models, by a considerable margin. The log-likelihood estimates are also out of line with the other models, in that for the second and fourth scenarios in which the RD14-0003-42 has been replaced by an unknown person, the likelihoods are lower than the scenario in which both contributor genotype are assumed known, indicating evidence against RD14-0003-42 being a contributor.

Table 11 shows various log-likelihood ratios (expressed in bans) obtained by comparing pairs of scenarios from Table 10. We see that all models are giving similar log-likelihood ratios in favour of the major contributor, compared to the maximum of 24.71 Bans (the inverse log profile probability of RD14-0003-43), and the **mFFT** model gives much larger values in favour of the minor contributor compared to the other models, with the normal model suggesting very strong evidence *against* RD14-0003-42 being a contributor (the inverse log profile probability of RD14-0003-42 is 20.22 Bans).

Table 11: Various scenario log-likelihood ratios expressed in Bans.

Hypotheses	Normal	Lognormal	Gamma	**mFFT**
42-43 vs U1-43	-22.78	8.99	4.45	13.97
42-U2 vs U1-U2	-22.51	9.12	4.63	14.11
42-43 vs 42-U2	21.15	21.15	21.15	21.15
U1-43 vs U1-U2	21.43	21.29	21.33	21.29

Figure 31 shows the QQ-plots for each of the models under the scenario in which both contributors are known.
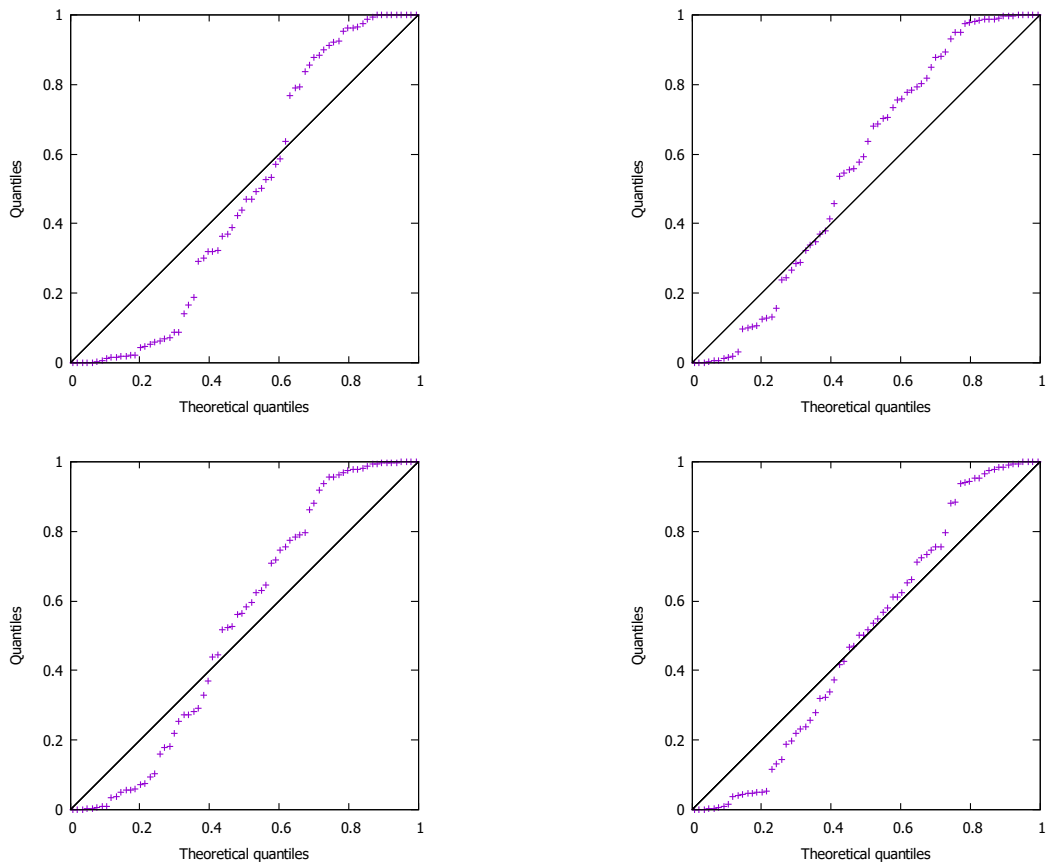
Figure 31: Top-left: normal model; top-right: lognormal model; bottom left: Gamma model; bottom right: **mFFT** model.

If we add a third un-profiled contributor, then all the models give similar results. Here are the values under the scenario of the two known contributors and a third untyped contributor.

Model	$\widehat{LL}_{max}$	$\hat{C}_1$	$\hat{C}_2$	$\hat{C}_3$
Normal	-489.24	153	1204	16
Lognormal	-500.16	153	1081	26
Gamma	-496.16	153	1121	27
mFFT	-491.83	152	1140	17

If we add another untyped contributor, so that we analyse the sample assuming

the profiles of the two (true) contributors and two untyped contributors, we obtain the following estimates in which the **mFFT** model gives an estimate of no cells to the second untyped contributor, unlike the moment based models:

Model	$\widehat{LL}_{max}$	$\hat{C}_1$	$\hat{C}_2$	$\hat{C}_3$	$\hat{C}_4$
Normal	-487.71	150	1202	14	8
Lognormal	-500.04	151	1085	17	13
Gamma	-495.48	150	1126	15	15
mFFT	-491.83	152	1140	17	0

13 Summary and outlook

In this paper, a framework for modelling single source and multiple donor forensic DNA samples has been elaborated for STR loci, based on an idealisation of the steps for forming an **EPG** from an initial DNA sample. It was shown that multivariate probability generating functions provide a succinct and efficient mathematical representation of the steps in the process, and that their evaluation can be carried out efficiently using **FFT**. Factorization approximations to make the mathematical models tractable were shown to introduce some biases for low template samples, but these biases can be largely removed by a modification, the **mFFT** model, which reintroduces, in a principled manner, some of the correlation lost by factorization approximations without affecting computational efficiency.

The examples treated in this paper have assumed that contributors are unrelated individuals. The framework may be extended to include relatedness of individuals, which might require that linkage between some loci would need to be taken into account.

An issue not explored in this paper is the robustness of the performance of the models to mis-specifications of model parameters. This could be readily explored via simulations in which, for example, data is simulated using one set of amplification, stutter and selection probabilities, and the simulated data is then fitted assuming different probabilities. Given the reaonably good performance of the model on the experimental data from the PROVEDit initiative, for which reasonable values were assumed for the parameters but without any detailed knowledge of what the true experimental values were, one could anticipate that the model will prove to be reasonably robust to such parameter mis-specifications.

The current paper has focussed on **EPG**s obtained by capillary electrophoresis, however it may not limited to this. Recently, Bleka et al. (2017) showed that by substituting read coverages for peak heights, autosomal SNP mixtures analyzed using massively parallel sequencing can be interpreted by the open source software Euroformix (Bleka et al., 2016), originally developed for **STR**s. By making the same substitution, that is, by replacing the **RFU** scale factors by 'read factors', the framework developed in this paper is also applicable to such SNP mixtures. Moreover, because SNPs are biallelic and do not stutter, the factorization approximations are no longer required.

Finally, other branching processes outside of the forensic applications focussed on in this paper can be treated by the methods introduced in this paper.

Appendices

A Derivation of moments for amplicon model

Let N denote the number of target amplicons, and M the number of stutter amplicons, arising from the amplification of a single target amplicon. We have that

$$\mathbb{E}N\,|\,n = \frac{\partial F_n(t, s)}{\partial t}\Big|_{t=1, s=1}$$

$$\mathbb{E}N(N-1)\,|\,n = \frac{\partial^2 F_n(t, s)}{\partial t^2}\Big|_{t=1, s=1}$$

$$\mathbb{E}M\,|\,n = \frac{\partial F_n(t, s)}{\partial s}\Big|_{t=1, s=1}$$

$$\mathbb{E}N(N-1)\,|\,n = \frac{\partial^2 F_n(t, s)}{\partial s^2}\Big|_{t=1, s=1}$$

$$\mathbb{E}NM\,|\,n = \frac{\partial^2 F_n(t, s)}{\partial s \partial t}\Big|_{t=1, s=1}$$

from which the variance $\mathbb{V}N$ and $\mathbb{V}M$ may be found, and hence the correlation $\mathrm{Cor}(N, M)$. We take each in turn.

$\mathbb{E}N\,|\,n$:

Using the chain rule for differentiating, we have

$$\frac{\partial F_n(t, s)}{\partial t} = (1-p)\frac{\partial F_{n-1}(t, s)}{\partial t} + 2p(1-\xi)F_{n-1}(t, s)\frac{\partial F_{n-1}(t, s)}{\partial t} + p\xi\frac{\partial F_{n-1}(t, s)}{\partial t}G_{n-1}(s)$$

We now substitute $t = 1$ and $s = 1$, use the property that $F_n(1, 1) = 1$ for all n, to obtain a linear difference equation that can be solved:

$$\begin{aligned}
\mathbb{E}N\,|\,n &= (1 - p)(\mathbb{E}N\,|\,n - 1) + 2p(1 - \xi)(\mathbb{E}N\,|\,n - 1) + p\xi(\mathbb{E}N\,|\,n - 1) \\
&= (1 + p(1 - \xi))(\mathbb{E}N\,|\,n - 1) \\
&= (1 + p(1 - \xi))^n(\mathbb{E}N\,|\,0) \\
&= (1 + p(1 - \xi))^n
\end{aligned}$$

This could have been anticipated: a main peak allele is amplified with probability $p(1 - \xi)$, hence starting with one allele and doing n amplifications, the mean number is as shown, $(1 + p(1 - \xi))^n$.

$\mathbb{E}N(N - 1) \mid n$ **and** $\mathbb{V}N \mid n$:

These could also be written down directly based on the previous result, however we go through the formal steps.

$$\mathbb{E}N(N - 1) \mid n = \frac{\partial^2 F_n(t, s)}{\partial t^2}\Big|_{t=1, s=1}$$

$$\frac{\partial^2 F_n(t, s)}{\partial t^2} = (1 - p)\frac{\partial^2 F_{n-1}(t, s)}{\partial t^2} + 2p(1 - \xi)F_{n-1}(t, s)\frac{\partial^2 F_{n-1}(t, s)}{\partial t^2} +$$

$$2p(1 - \xi)\left(\frac{\partial F_{n-1}(t, s)}{\partial t}\right)^2 + p\xi\frac{\partial^2 F_{n-1}(t, s)}{\partial t^2}G_{n-1}(s)$$

$$\mathbb{E}N(N - 1) \mid n = (1 + p(1 - \xi))(\mathbb{E}N(N - 1) \mid n - 1) + 2p(1 - \xi)(\mathbb{E}N \mid n - 1)^2$$

$$\mathbb{E}N^2 \mid n = (1 + p(1 - \xi))(\mathbb{E}N^2 \mid n - 1) + 2p(1 - \xi)(\mathbb{E}N \mid n - 1)^2$$

$$= (1 + p(1 - \xi))(\mathbb{E}N^2 \mid n - 1) + 2(p(1 - \xi))(1 + p(1 - \xi))^{2n-2}$$

$$= (1 + p(1 - \xi))^n(\mathbb{E}N^2 \mid 0) + 2(p(1 - \xi))\sum_{j=1}^{n}(1 + p(1 - \xi))^{2j-2}(1 + p(1 - \xi))^{n-j}$$

$$= (1 + p(1 - \xi))^n + 2(p(1 - \xi))\sum_{j=0}^{n-1}(1 + p(1 - \xi))^{2j}(1 + p(1 - \xi))^{n-1-j}$$

$$= (1 + p(1 - \xi))^n + 2(p(1 - \xi))(1 + p(1 - \xi))^{n-1}\sum_{j=0}^{n-1}(1 + p(1 - \xi))^{j}$$

$$= (1 + p(1 - \xi))^n + 2(p(1 - \xi))(1 + p(1 - \xi))^{n-1}\frac{(1 + p(1 - \xi))^n - 1}{(1 + p(1 - \xi)) - 1}$$

$$= (1 + p(1 - \xi))^n\left[1 + 2\frac{(1 + p(1 - \xi))^n - 1}{1 + p(1 - \xi)}\right]$$

$$= (1 + p(1 - \xi))^{n-1}\left[2(1 + p(1 - \xi))^n + p(1 - \xi) - 1\right]$$

Hence the variance is

$$\mathbb{V}N \,|\, n = (\mathbb{E}N^2 \,|\, n) - (\mathbb{E}N \,|\, n)^2$$

$$= (1 + p(1 - \xi))^n \left[1 + 2\frac{(1 + p(1 - \xi))^n - 1}{1 + p(1 - \xi)} \right] - (1 + p(1 - \xi))^{2n}$$

$$= (1 + p(1 - \xi))^n \left[1 + 2\frac{(1 + p(1 - \xi))^n - 1}{1 + p(1 - \xi)} - (1 + p(1 - \xi))^n \right]$$

$$= \frac{1 - p(1 - \xi)}{1 + p(1 - \xi)}(1 + p(1 - \xi))^n \left[(1 + p(1 - \xi))^n - 1 \right]$$

We also have

$$\mathbb{E}N(N - 1) \,|\, n = (\mathbb{V}N \,|\, n) + (\mathbb{E}N \,|\, n)^2 - (\mathbb{E}N \,|\, n)$$

$$= \frac{1 - p(1 - \xi)}{1 + p(1 - \xi)}(1 + p(1 - \xi))^n \left[(1 + p(1 - \xi))^n - 1 \right] + (1 + p(1 - \xi))^{2n} - (1 + p(1 - \xi))^n$$

$$= 2(1 + p(1 - \xi))^{n-1}((1 + p(1 - \xi))^n - 1)$$

$\mathbb{E}M \,|\, n$:

This follows a similar pattern to the above for N:

$$\mathbb{E}M \,|\, n = \frac{\partial F_n(t, s)}{\partial s}\Big|_{t=1, s=1}$$

$$\frac{\partial F_n(t, s)}{\partial s} = (1 - p)\frac{\partial F_{n-1}(t, s)}{\partial s} + 2p(1 - \xi)F_{n-1}(t, s)\frac{\partial F_{n-1}(t, s)}{\partial s}$$

$$+ p\xi\frac{\partial F_{n-1}(t, s)}{\partial s}G_{n-1}(s) + p\xi F_{n-1}(t, s)\frac{\partial G_{n-1}(s)}{\partial s}$$

Hence

$$\mathbb{E}M \,|\, n = (1 + p(1 - \xi))(\mathbb{E}M \,|\, n - 1) + p\xi\frac{\partial G_{n-1}(s)}{\partial s}\Big|_{s=1}$$

Now

$$G_n(s) = (1 - p)G_{n-1}(s) + pG_{n-1}^2(s),$$

127

which is the recursion relation for the generating function of a single allele amplifying with probability p in the branching process, hence

$$\mathbb{E}M \mid n = (1 + p(1 - \xi))(\mathbb{E}M \mid n - 1) + p\xi(1 + p)^{n-1}$$

Now we start with no stutter amplicons, hence $\mathbb{E}M \mid 0 = 0$. Thus

$$
\begin{aligned}
\mathbb{E}M \mid n &= (1 + p(1 - \xi))(\mathbb{E}M \mid n - 1) + p\xi(1 + p)^{n-1} \\
&= (1 + p(1 - \xi))^2(\mathbb{E}M \mid n - 2) + (1 + p(1 - \xi))p\xi(1 + p)^{n-2} + p\xi(1 + p)^{n-1} \\
&= \vdots \\
&= (1 + p(1 - \xi))^n(\mathbb{E}M \mid 0) + p\xi \sum_{j=0}^{n-1} (1 + p(1 - \xi))^j (1 + p)^{n-j-1}
\end{aligned}
$$

We now use $\mathbb{E}M \mid 0 = 0$, $1 + p - (1 + p(1 - \xi) = p\xi$, and the relation

$$a^{n-1} + a^{n-2}b + a^{n-3}b^2 + \cdots ab^{n-2} + b^{n-1} = \frac{a^n - b^n}{a - b}$$

to deduce that

$$\mathbb{E}M \mid n = p\xi \frac{(1 + p)^n - (1 + p(1 - \xi))^n}{(1 + p) - (1 + p(1 - \xi))} = (1 + p)^n - (1 + p(1 - \xi))^n$$

When $\xi = 0$ this vanishes as it should. Note also that $\mathbb{E}[N + M \mid n] = (1 + p)^n$ which is also as expected– it is as if the stutter and the main target cannot be distinguished apart. We also have

$$\frac{\mathbb{E}M \mid n}{\mathbb{E}N + M \mid n} = 1 - \left(1 - \frac{p\xi}{1 + p}\right)^n$$

which $\to 1$ and $n \to \infty$ for $\xi > 0$. Hence ultimately the stutter allele peak will dominate the original allele peak with enough cycles, a result found by Weusten and Herbergs (2012).

$\mathbb{E}M(M-1)\,|\,n$ **and** $\mathbb{V}M\,|\,n$

Denote $F_{n;s}(t,s) = \partial F_n(t,s)/\partial s$, and $F_{n;ss}$ the second derivative.
Hence

$$\mathbb{E}M(M-1)\,|\,n = F_{n;ss}\big|_{t=1,s=1}$$

$$F_{n;ss} = (1-p)F_{n-1;ss} + 2p(1-\xi)F_{n-1}F_{n-1;ss} + 2p(1-\xi)F_{n-1;s}^2$$
$$+ p\xi F_{n-1;ss}G_{n-1} + 2p\xi F_{n-1;s}G_{n-1;s} + p\xi F_{n-1}G_{n-1;ss}$$

$$\mathbb{E}M(M-1)\,|\,n = (1 + p(1-\xi))(\mathbb{E}M(M-1)\,|\,n-1)+$$

$$\left(2p(1-\xi)F_{n-1;s}^2 + 2p\xi F_{n-1;s}G_{n-1;s} + p\xi F_{n-1}G_{n-1;ss}\right)\Bigg|_{s=t=1}$$

$$= (1 + p(1-\xi))(\mathbb{E}M(M-1)\,|\,n-1)+$$

$$2p(1-\xi)\left((1+p)^{n-1} - (1+p(1-\xi))^{n-1}\right)^2 +$$

$$2p\xi\left((1+p)^{n-1} - (1+p(1-\xi))^{n-1}\right)(1+p)^{n-1}+$$

$$2p\xi(1+p)^{n-2}[(1+p)^{n-1} - 1]$$

But we have that $\mathbb{E}M\,|\,n = (1 + p(1-\xi))(\mathbb{E}M\,|\,n-1) + p\xi(1+p)^{n-1}$, hence adding this to both sides we obtain

$$\mathbb{E}M^2\,|\,n = (1 + p(1-\xi))(\mathbb{E}M\,|\,n-1)$$

$$+ 2p(1-\xi)\left((1+p)^{n-1} - (1+p(1-\xi))^{n-1}\right)^2 +$$

$$2p\xi\left((1+p)^{n-1} - (1+p(1-\xi))^{n-1}\right)(1+p)^{n-1}+$$

$$p\xi(1+p)^{n-2}[2(1+p)^{n-1} + p - 1]$$

Expanding this out we have

$$\mathbb{E}M^2\,|\,n = (1 + p(1-\xi))(\mathbb{E}M^2\,|\,n-1)$$

$$+ 2p(1-\xi)\left((1+p)^{2(n-1)} - 2(1+p)^{n-1}(1+p(1-\xi))^{n-1} + (1+p(1-\xi))^{2(n-1)}\right)$$

$$+ 2p\xi\left((1+p)^{2(n-1)} - (1+p)^{n-1}(1+p(1-\xi))^{n-1}\right)$$

$$+ \frac{p\xi}{1+p}\left(2(1+p)^{2(n-1)} - (1-p)(1+p)^{n-1}\right)$$

Collecting together similar terms, this reduces to

$$\mathbb{E}M^2 \,|\, n = (1 + p(1 - \xi))(\mathbb{E}M^2 \,|\, n - 1)$$
$$+ \left(2p + \frac{2p\xi}{1 + p}\right)(1 + p)^{2(n-1)}$$
$$- (4p(1 - \xi) + 2p\xi)\,(1 + p)^{n-1}(1 + p(1 - \xi))^{n-1}$$
$$+ 2p(1 - \xi)(1 + p(1 - \xi))^{2(n-1)}$$
$$- \frac{p(1 - p)\xi}{1 + p}(1 + p)^{n-1}$$

We may now solve this linear difference equation, noting that the terms on the right are each of the form a^{n-1} or $a^{2(n-1)}$, making the particular solution terms of the form $(a^n - b^n)/(a - b)$ or $(a^{2n} - b^n)/(a^2 - b)$, where in each case $b = 1 + p(1 - \xi)$. We also use that $(\mathbb{E}M^2 \,|\, 0) = 0$. We obtain

$$\mathbb{E}M^2 \,|\, n = \left(2p + \frac{2p\xi}{1 + p}\right)\frac{(1 + p)^{2n} - (1 + p(1 - \xi))^n}{(1 + p)^2 - (1 + p(1 - \xi))}$$
$$- (4p(1 - \xi) + 2p\xi)\,(1 + p(1 - \xi))^{n-1}\frac{(1 + p)^n - 1}{1 + p - 1}$$
$$+ 2p(1 - \xi)(1 + p(1 - \xi))^{n-1}\frac{(1 + p(1 - \xi))^n - 1}{(1 + p(1 - \xi)) - 1}$$
$$- \frac{p(1 - p)\xi}{1 + p}\frac{(1 + p)^n - (1 + p(1 - \xi))^n}{(1 + p) - (1 + p(1 - \xi))}$$

Now

$$(1 + p) - 1 = p$$
$$(1 + p(1 - \xi)) - 1 = p(1 - \xi)$$
$$(1 + p) - (1 + p(1 - \xi)) = p\xi$$
$$(1 + p)^2 - (1 + p(1 - \xi)) = 1 + 2p + p^2 - 1 - p + p\xi = p(1 + p + \xi)$$

130

Hence simplifying further we obtain

$$\mathbb{E}M^2 \,|\, n = 2\frac{(1+p)^{2n} - (1 + p(1-\xi))^n}{1+p}$$
$$- (4 - 2\xi)(1 + p(1-\xi))^{n-1}((1+p)^n - 1)$$
$$+ 2(1 + p(1-\xi))^{n-1}((1 + p(1-\xi))^n - 1)$$
$$- \frac{(1-p)}{1+p}((1+p)^n - (1 + p(1-\xi))^n)$$

Now we had previously that

$$\mathbb{E}M \,|\, n = (1+p)^n - (1 + p(1-\xi))^n$$

Squaring this and subtracting from $EM^2 \,|\, n$ gives the desired variance $\mathbb{V}M \,|\, n$. However there does not appear to be a nice simple reduction in the result, so this is omitted.

For large n we may drop the terms in $(1 + p(1-\xi))^n$ and lower, and we have approximately

$$\mathbb{E}M^2 \,| \approx 2n(1+p)^{2n-1} - (4 - 2\xi)(1 + p(1-\xi))^{n-1}(1+p)^{n-1} + 2(1 + p(1-\xi))^{2(n-1)}$$

$\mathbb{E}NM\,|\,n$**:**

$$\mathbb{E}NM\,|\,n = \frac{\partial^2 F_n(t,s)}{\partial s \partial t}\Big|_{t=1,s=1}$$

$$\frac{\partial^2 F_n(t,s)}{\partial s \partial t} = (1-p)\frac{\partial^2 F_{n-1}(t,s)}{\partial s \partial t} + 2p(1-\xi)F_{n-1}(t,s)\frac{\partial^2 F_{n-1}(t,s)}{\partial s \partial t} + p\xi\frac{\partial^2 F_{n-1}(t,s)}{\partial s \partial t}G_{n-1}(s)$$

$$+ 2p(1-\xi)\frac{\partial F_{n-1}(t,s)}{\partial s}\frac{\partial F_{n-1}(t,s)}{\partial t}$$

$$+ p\xi\frac{\partial F_{n-1}(t,s)}{\partial t}\frac{\partial G_{n-1}(s)}{\partial s}$$

$$\mathbb{E}NM\,|\,n = (1+p(1-\xi))(\mathbb{E}NM\,|\,n-1) + 2p(1-\xi)(\mathbb{E}N\,|\,n-1)(\mathbb{E}M\,|\,n-1) + p\xi(\mathbb{E}N\,|\,n-1)(1+p)^{n-1}$$

$$= (1+p(1-\xi))(\mathbb{E}NM\,|\,n-1) + 2p(1-\xi)(1+p(1-\xi))^{n-1}[(1+p)^{n-1} - (1+p(1-\xi))^{n-1}]$$

$$+ p\xi(1+p(1-\xi))^{n-1}(1+p)^{n-1}$$

$$= (1+p(1-\xi))(\mathbb{E}NM\,|\,n-1) + p(2-\xi)(1+p(1-\xi))^{n-1}(1+p)^{n-1}$$

$$- 2p(1-\xi)(1+p(1-\xi))^{n-1}(1+p(1-\xi))^{n-1}$$

Using $\mathbb{E}NM\,|\,0 = 0$, the solution may be written as

$$\mathbb{E}NM\,|\,n = (2-\xi)p(1+p(1-\xi))^{n-1}((1+p)^n - 1)/(1+p-1)$$

$$- 2p(1-\xi)(1+p(1-\xi))^{n-1}\frac{(1+p(1-\xi))^n - 1}{(1+p(1-\xi)-1)}$$

$$= (2-\xi)(1+p(1-\xi))^{n-1}((1+p)^n - 1) - 2(1+p(1-\xi))^{n-1}((1+p(1-\xi))^n - 1)$$

$$= (1+p(1-\xi))^{n-1}((2-\xi)(1+p)^n - 1) - 2((1+p(1-\xi))^n - 1)$$

$$= (1+p(1-\xi))^{n-1}(\xi(1-(1+p)^n) + 2((1+p)^n - (1+p(1-\xi))^n))$$

$\mathrm{Cov}(M,N)$

The covariance $\mathrm{Cov}(M,N)$ is given by

$$\mathrm{Cov}(M,N) = \mathbb{E}NM\,|\,n - (\mathbb{E}N\,|\,n)(\mathbb{E}M\,|\,n)$$

$$= (1+p(1-\xi))^{n-1}(\xi(1-(1+p)^n) + 2((1+p)^n - (1+p(1-\xi))^n))$$

$$- ((1+p)^n - (1+p(1-\xi))^n))(1+p(1-\xi))^n$$

$$= (1+p(1-\xi))^{n-1}((1-p(1-\xi))((1+p)^n - (1+p(1-\xi))^n) - \xi((1+p)^n - 1))$$

from which the correlation may be found, by an appropriate scaling using the variances given earlier.

Binomial sampling

The generating function for Binomial sampling with n trials and success probability q is

$$(1 - q + qt)^n$$

Let $F(t, s)$ denote the joint **PGF** for main T and stutter S peaks for k cycles based on an initial single allele. Let $\mathbb{E}N$ denote the mean number of main alleles $\mathbb{E}S$ the mean number of stutter allele, and similarly for the variance $\mathbb{V}N$ and $\mathbb{V}S$. Then for an initial set of n alleles sampled with probability p the joint **PGF** is given by

$$Q(t, s) = (1 - q + qF(t, s))^n$$

With abuse of notation, let $\mathbb{E}t$ denote the mean number of main alleles for this **PGF**, etc., so that $\mathbb{E}t = \partial Q/\partial t|_{t=s=1}$, etc.

Thus

$$\frac{\partial Q(t, s)}{\partial t} = nq(1 - q + qF(t, s))^{n-1}\frac{\partial F(t, s)}{\partial t}$$

from which it follows that

$$\mathbb{E}t = nq\mathbb{E}N$$

Similarly

$$\frac{\partial Q(t, s)}{\partial s} = nq(1 - q + qF(t, s))^{n-1}\frac{\partial F(t, s)}{\partial s}$$

from which it follows that

$$\mathbb{E}s = nq\mathbb{E}S$$

Taking the second derivatives, we have

$$\frac{\partial^2 Q(t,s)}{\partial t^2} = n(n-1)q^2(1-q+qF(t,s))^{n-2}\left(\frac{\partial F(t,s)}{\partial t}\right)^2 + nq(1-q+qF(t,s))^{n-1}\frac{\partial^2 F(t,s)}{\partial t^2}$$

$$\mathbb{E}t(t-1) = n(n-1)q^2(\mathbb{E}N)^2 + nq(\mathbb{E}N(N-1))$$

$$\mathbb{V}t = n(n-1)q^2(\mathbb{E}N)^2 + nq(\mathbb{E}N(N-1)) + (nq\mathbb{E}N) - (nq\mathbb{E}N)^2$$

$$= nq(\mathbb{V}N + (1-q)(\mathbb{E}N)^2)$$

and similarly
$$\mathbb{V}s = nq(\mathbb{V}S + (1-q)(\mathbb{E}S)^2)$$

Finally

$$\frac{\partial^2 Q(t,s)}{\partial t \partial s} = nq(1-q+qF(t,s))^{n-1}\frac{\partial F(t,s)}{\partial t}\frac{\partial F(t,s)}{\partial s} + n(n-1)q^2(1-q+qF(t,s))^{n-2}\frac{\partial^2 F(t,s)}{\partial t \partial s}$$

$$\mathbb{E}ts = n(n-1)q^2(\mathbb{E}N\mathbb{E}S) + nq(\mathbb{E}NS)$$

$$\mathrm{Cov}(t,s) = n(n-1)q^2(\mathbb{E}N\mathbb{E}S) + nq(\mathbb{E}NS) - (nq\mathbb{E}N)(nq\mathbb{E}S)$$

$$= nq(\mathbb{E}NS - q(\mathbb{E}N)(\mathbb{E}S))$$

$$= nq(\mathrm{Cov}(N,S) + (1-q)(\mathbb{E}N)(\mathbb{E}S))$$

Hence

$$\mathrm{Cor}(t,s) = \frac{nq(\mathrm{Cov}(N,S) + (1-q)(\mathbb{E}N)(\mathbb{E}S))}{\sqrt{nq(\mathbb{V}N + (1-q)(\mathbb{E}N)^2)}\sqrt{nq(\mathbb{V}S + (1-q)(\mathbb{E}S)^2)}}$$

$$= \frac{\mathrm{Cov}(N,S) + (1-q)(\mathbb{E}N)(\mathbb{E}S))}{\sqrt{(\mathbb{V}N + (1-q)(\mathbb{E}N)^2)}\sqrt{(\mathbb{V}S + (1-q)(\mathbb{E}S)^2)}}$$

Poisson sampling

Suppose that the number of alleles to be sampled has a Poison distribution of mean λ. The using the **PGF** for a Poisson distribution, $\exp(\lambda(t-1))$, we proceed in a similar manner as for the Binomial sampling, using the joint **PGF**

$$Q(t,s) = \exp(\lambda(F(t,s) - 1))$$

$$\frac{\partial Q(t, s)}{\partial t} = \lambda \frac{\partial F(t, s)}{\partial t} Q(t, s)$$

$$\mathbb{E}t = \lambda \mathbb{E}N$$

$$\frac{\partial Q(t, s)}{\partial s} = \lambda \frac{\partial F(t, s)}{\partial s} Q(t, s)$$

$$\mathbb{E}s = \lambda \mathbb{E}S$$

$$\frac{\partial^2 Q(t, s)}{\partial t^2} = \lambda^2 \left(\frac{\partial F(t, s)}{\partial t} \right)^2 Q(t, s) + \lambda \frac{\partial^2 F(t, s)}{\partial t^2} Q(t, s)$$

$$Et(t - 1) = \lambda^2 (\mathbb{E}N)^2 + \lambda(\mathbb{E}N(N - 1))$$

$$\frac{\partial^2 Q(t, s)}{\partial s^2} = \lambda^2 \left(\frac{\partial F(t, s)}{\partial s} \right)^2 Q(t, s) + \lambda \frac{\partial^2 F(t, s)}{\partial s^2} Q(t, s)$$

$$Es(s - 1) = \lambda^2 (\mathbb{E}S)^2 + \lambda(\mathbb{E}S(S - 1))$$

$$\frac{\partial^2 Q(t, s)}{\partial t \partial s} = \lambda^2 \frac{\partial F(t, s)}{\partial t} \frac{\partial F(t, s)}{\partial s} Q(t, s) + \lambda \frac{\partial^2 F(t, s)}{\partial t \partial s} Q(t, s)$$

$$\mathbb{E}ts = \lambda(\mathbb{E}NS) + \lambda^2 (\mathbb{E}N)(\mathbb{E}S)$$

from which it follows that

$$\text{Cov}(t, s) = \lambda(\mathbb{E}NS) + \lambda^2 (\mathbb{E}N)(\mathbb{E}S) - \lambda^2 (\mathbb{E}N)(\mathbb{E}S)$$

$$= \lambda(\mathbb{E}NS)$$

$$\mathbb{V}t = \lambda^2 (\mathbb{E}N)^2 + \lambda(\mathbb{E}N(N - 1)) + \lambda(\mathbb{E}N) - (\lambda \mathbb{E}N)^2$$

$$= \lambda(\mathbb{E}N^2)$$

$$\mathbb{V}s = \lambda(\mathbb{E}S^2) \text{ similarly,}$$

$$\text{Cor}(t, s) = \frac{\lambda(\mathbb{E}NS)}{\sqrt{\lambda(\mathbb{E}N^2)} \sqrt{\lambda(\mathbb{E}S^2)}}$$

$$= \frac{\mathbb{E}NS}{\sqrt{(\mathbb{E}N^2)(\mathbb{E}S^2)}}$$

which does not depend on λ. In fact this result is the limiting result of taking $q \to 0$ in the earlier Binomial sampling.

B Derivation of moments for genomic model, no stutters

B.1 Moments of tagged amplicons

For convenience let $t = t_{a_d}$, and let D denote the derivative with respect to t. The marginal **PGF** for the tagged amplicons is given by the sum of such amplicons arising from the g and g_d strand: we obtain this by multiplying the **PGF**s.

$$F(t) = G_n(1, 1, 1, t)G_{d;n}(1, 1, t, 1),$$

from which

$$DF(t) = [DG_n(1, 1, 1, t)]G_{d;n}(1, 1, t, 1) + G_n(1, 1, 1, t)[DG_{d;n}(1, 1, t, 1)]$$

hence the mean number of tagged amplicons is given by the sum of two terms:

$$EN_{a_d} = [DG_n(1, 1, 1, t)]_{t=1} + [DG_{d;n}(1, 1, t, 1)]_{t=1}$$

where we use $G(1, 1, 1,) = G_d(1, 1, 1, 1) = 1$. We may find each term on the right hand side separately. Using the recurrence relation for the joint **PGFs** of each genomic type, we may derive recurrence relations for each of these two terms, which turn out to be coupled linear equations that can be solved either by hand or computer algebra. We consider each separately:

B.1.1 *DG*

We may substitute 1 for every component, except t_{a_d} which we set to t, in the joint **PGF** recurrence relations. Assume this is done. Then differentiating with respect to t and substituting $t = 1$ we obtain the following recurrence relations:

$$
\begin{aligned}
DG_{n+1} &= (1 - p_g)DG_n + p_g(DG_n + DH_{d;n}) \\
&= DG_n + p_g DH_{d;n} \\
DH_{d;n+1} &= (1 - p_{h_d})DH_{d;n} + p_{h_d}(DH_{d;n} + DA_n) \\
&= DH_{d;n} + p_{h_d}DA_n \\
DA_{n+1} &= (1 - p_a)DA_n + p_a(DA_n + DA_{d;n}) \\
&= DA_n + p_a DA_{d;n} \\
DA_{d;n+1} &= (1 - p_{a_d})DA_{d;n} + p_{a_d}(DA_{d;n} + DA_n) \\
&= DA_{d;n} + p_{a_d}DA_n
\end{aligned}
$$

with initial conditions $DG_0 = DH_{d;0} = DA_0 = 0$ and $DA_{d;0} = 1$.

Now consider the last two coupled equations:

$$DA_{n+1} = DA_n + p_a DA_{d;n}$$

$$DA_{d;n+1} = DA_{d;n} + p_{a_d} DA_n$$

We may write this in matrix form

$$\begin{pmatrix} DA_{n+1} \\ DA_{d;n+1} \end{pmatrix} = \begin{pmatrix} 1 & p_a \\ p_{a_d} & 1 \end{pmatrix} \begin{pmatrix} DA_n \\ DA_{d;n} \end{pmatrix}$$

from which we clearly obtain

$$\begin{pmatrix} DA_n \\ DA_{d;n} \end{pmatrix} = \begin{pmatrix} 1 & p_a \\ p_{a_d} & 1 \end{pmatrix}^n \begin{pmatrix} 0 \\ 1 \end{pmatrix}$$

and hence

$$DA_n = \begin{pmatrix} 1 & 0 \end{pmatrix} \begin{pmatrix} 1 & p_a \\ p_{a_d} & 1 \end{pmatrix}^n \begin{pmatrix} 0 \\ 1 \end{pmatrix}.$$

Let us denote the square matrix (not raised to the power n) by P:

$$P = \begin{pmatrix} 1 & p_a \\ p_{a_d} & 1 \end{pmatrix}.$$

Then

$$DA_n = \begin{pmatrix} 1 & 0 \end{pmatrix} P^n \begin{pmatrix} 0 \\ 1 \end{pmatrix}$$

and from the earlier recurrence for DH_d;

$$DH_{d;n+1} = DH_{d;n} + p_{h_d} DA_n$$

we obtain

$$DH_{d;n} = p_{h_d} \sum_{j=0}^{n-1} \begin{pmatrix} 1 & 0 \end{pmatrix} P^j \begin{pmatrix} 0 \\ 1 \end{pmatrix} = p_{h_d} \begin{pmatrix} 1 & 0 \end{pmatrix} \frac{P^n - I}{P - I} \begin{pmatrix} 0 \\ 1 \end{pmatrix}$$

137

From the earlier recurrence for DG;

$$DG_{n+1} = DG_n + p_g DH_{d;n}$$

we therefore obtain

$$DG_n = p_g p_{h_d} \sum_{j=0}^{n-1} \begin{pmatrix} 1 & 0 \end{pmatrix} \frac{P^j - I}{P - I} \begin{pmatrix} 0 \\ 1 \end{pmatrix} = p_g p_{h_d} \begin{pmatrix} 1 & 0 \end{pmatrix} \frac{P^n - I - n(P - I)}{(P - I)^2} \begin{pmatrix} 0 \\ 1 \end{pmatrix}$$

which is our final result for the expected number of amplicons *arising from the g genomic strand*.

Note that if all the amplification probabilities are equal to 1, we obtain:

$$P^n = \begin{pmatrix} 1 & 1 \\ 1 & 1 \end{pmatrix}^n = \begin{pmatrix} 2^{n-1} & 2^{n-1} \\ 2^{n-1} & 2^{n-1} \end{pmatrix}$$

which leads to $DG_n = 2^{n-1} - n$ obtained earlier.

We now need to do a similar calculation for the g_d strand.

B.1.2 DG_d

We may substitute 1 for every component, except t_{a_d} which we set to t, in the joint **PGF** recurrence relations. Assume this is done. Then differentiating with respect to t and substituting $t = 1$ we obtain the following recurrence relations:

$$\begin{aligned}
DG_{d;n+1} &= (1 - p_{g_d})DG_{d;n} + p_{g_d}(DG_{d;n} + DH_n) \\
&= DG_{d;n} + p_{g_d}DH_n \\
DH_{n+1} &= (1 - p_h)DH_n + p_h(DH_n + DA_{d;n}) \\
&= DH_n + p_h DA_{d;n} \\
DA_{n+1} &= (1 - p_a)DA_n + p_a(DA_n + DA_{d;n}) \\
&= DA_n + p_a DA_{d;n} \\
DA_{d;n+1} &= (1 - p_{a_d})DA_{d;n} + p_{a_d}(DA_{d;n} + DA_n) \\
&= DA_{d;n} + p_{a_d} DA_n
\end{aligned}$$

with initial conditions $DG_0 = DH_{d;0} = DA_0 = 0$ and $DA_{d;0} = 1$. Note that the last two coupled equations are as before for DG, and so have the same solution as given above:

$$\begin{pmatrix} DA_n \\ DA_{d;n} \end{pmatrix} = \begin{pmatrix} 1 & p_a \\ p_{a_d} & 1 \end{pmatrix}^n \begin{pmatrix} 0 \\ 1 \end{pmatrix} = P^n \begin{pmatrix} 0 \\ 1 \end{pmatrix}$$

The equation for H reads:

$$H_{n+1} = DH_n + p_h DA_{d;n}$$

but

$$DA_{d;n} = \begin{pmatrix} 0 & 1 \end{pmatrix} P^n \begin{pmatrix} 0 \\ 1 \end{pmatrix}$$

Hence

$$DH_n = p_h \sum_{j=0}^{n-1} \begin{pmatrix} 0 & 1 \end{pmatrix} P^j \begin{pmatrix} 0 \\ 1 \end{pmatrix} = p_h \begin{pmatrix} 0 & 1 \end{pmatrix} \frac{P^n - I}{P - I} \begin{pmatrix} 0 \\ 1 \end{pmatrix}$$

Finally from the recurrence for DG_d:

$$DG_{d;n+1} = DG_{d;n} + p_{g_d} DH_n$$

we obtain

$$DG_{d;n} = p_{g_d} p_h \sum_{j=0}^{n-1} \begin{pmatrix} 0 & 1 \end{pmatrix} \frac{P^j - I}{P - I} \begin{pmatrix} 0 \\ 1 \end{pmatrix} = p_{g_d} p_h \begin{pmatrix} 0 & 1 \end{pmatrix} \frac{P^n - I - n(P - I)}{(P - I)^2} \begin{pmatrix} 0 \\ 1 \end{pmatrix}$$

which is our final result for the expected number of amplicons *arising from the g_d genomic strand.*

Note that is all amplification efficiencies are equal to 1, then we obtain $DG_{d;n} = 2^{n-1} - 1$ obtained earlier.

B.1.3   *DG* and *DG_d* combined

The mean number of tagged amplicons is given by the sum of the two results obtained above, which may be written in the form:

$$\begin{pmatrix} p_g p_{h_d}, & p_{g_d} p_h \end{pmatrix} \frac{P^n - I - n(P - I)}{(P - I)^2} \begin{pmatrix} 0 \\ 1 \end{pmatrix}$$

If $p_g p_{h_d} = p_{g_d} p_h$, which will happen if $p_g = p_{g_d}$ and $p_{h_d} = p_h$, this simplifies to:

$$p_g p_h \begin{pmatrix} 1 & 1 \end{pmatrix} \frac{P^n - I - n(P - I)}{(P - I)^2} \begin{pmatrix} 0 \\ 1 \end{pmatrix}$$

with

$$P = \begin{pmatrix} 1 & p_a \\ p_{a_d} & 1 \end{pmatrix}$$

If $p_a = p_{a_d} = p$ then

$$P = \begin{pmatrix} 1 & p \\ p & 1 \end{pmatrix}$$

then

$$P^n = \frac{1}{2} \begin{pmatrix} (1 + p)^n + (1 - p)^n & (1 + p)^n - (1 - p)^n \\ (1 + p)^n - (1 - p)^n & (1 + p)^n + (1 - p)^n \end{pmatrix}$$

and

$$(P - I)^{-2} = \begin{pmatrix} p^{-2} & 0 \\ 0 & p^{-2} \end{pmatrix} = \frac{1}{p^2} I$$

After a little matrix algebra we obtain that the mean number of tagged amplicons is given by

$$EA_d = \frac{p_g p_h}{p^2}((1 + p)^n - np - 1)$$

Note that if $p_g = p_h = p = 1$ this reduces to $2^n - n - 1$ obtained earlier for the Eulerian numbers. If we have instead $p_g = p_h = p$ we obtain

$$EA_d = (1 + p)^n - np - 1,$$

which can be compared to the value $(1 + p)^n$ of the simple **PCR** model that starts with a single amplicon.

Note that, if starting with m amplicons these mean values are simply multiplied by m.

Returning to the more general result:

$$\begin{pmatrix} p_g p_{h_d}, & p_{g_d} p_h \end{pmatrix} \frac{P^n - I - n(P - I)}{(P - I)^2} \begin{pmatrix} 0 \\ 1 \end{pmatrix}$$

with

$$P = \begin{pmatrix} 1 & p_a \\ p_{a_d} & 1 \end{pmatrix}$$

The eigenvalues of P are $1 + \sqrt{p_a p_{a_d}}$ and $1 - \sqrt{p_a p_{a_d}}$, and it can be shown that:

$$P^n = \frac{1}{2} \begin{pmatrix} (1 + \sqrt{p_a p_{a_d}})^n + (1 - \sqrt{p_a p_{a_d}})^n & , & \sqrt{\frac{p_a}{p_{a_d}}}((1 + \sqrt{p_a p_{a_d}})^n - (1 - \sqrt{p_a p_{a_d}})^n) \\ \sqrt{\frac{p_{a_d}}{p_a}}((1 + \sqrt{p_a p_{a_d}})^n - (1 - \sqrt{p_a p_{a_d}})^n) & , & (1 + \sqrt{p_a p_{a_d}})^n + (1 - \sqrt{p_a p_{a_d}})^n \end{pmatrix}$$

and

$$(P - I)^{-2} = \frac{1}{p_a p_{a_d}} I$$

More matrix algebra shows that

$$(P^n - I - n(P - I)) \begin{pmatrix} 0 \\ 1 \end{pmatrix} = \begin{pmatrix} \sqrt{\frac{p_a}{p_{a_d}}}[(1 + \sqrt{p_a p_{a_d}})^n - (1 - \sqrt{p_a p_{a_d}})^n]/2 - np_a \\ [(1 + \sqrt{p_a p_{a_d}})^n + (1 - \sqrt{p_a p_{a_d}})^n]/2 - 1 \end{pmatrix}$$

Hence the mean number of amplicons for the general case is given by the row and column matrix inner product:

$$\begin{pmatrix} \frac{p_g p_{h_d}}{p_a p_{a_d}}, & \frac{p_{g_d} p_h}{p_a p_{a_d}} \end{pmatrix} \begin{pmatrix} \sqrt{\frac{p_a}{p_{a_d}}}[(1 + \sqrt{p_a p_{a_d}})^n - (1 - \sqrt{p_a p_{a_d}})^n]/2 - np_a \\ [(1 + \sqrt{p_a p_{a_d}})^n + (1 - \sqrt{p_a p_{a_d}})^n]/2 - 1 \end{pmatrix}$$

that is:

$$\frac{p_g p_{h_d}}{p_a p_{a_d}} \left(\sqrt{\frac{p_a}{p_{a_d}}} \frac{(1 + \sqrt{p_a p_{a_d}})^n - (1 - \sqrt{p_a p_{a_d}})^n}{2} - np_a \right) + \frac{p_{g_d} p_h}{p_a p_{a_d}} \left(\frac{(1 + \sqrt{p_a p_{a_d}})^n + (1 - \sqrt{p_a p_{a_d}})^n}{2} - 1 \right)$$

If $p_a = p_{a_d} = p$, this simplifies to:

$$\frac{p_g p_{h_d}}{p^2} \left(\frac{(1 + p)^n - (1 - p)^n}{2} - np \right) + \frac{p_{g_d} p_h}{p^2} \left(\frac{(1 + p)^n + (1 - p)^n}{2} - 1 \right)$$

B.1.4 Variance of the number of amplicons

Recall that if $F(t)$ is a **PGF** for a random variable X then

$$\mathbb{E}X = \frac{dF(t)}{dt}\Big|_{t=1} = F'(1)$$

$$\mathbb{E}X(X-1) = \frac{dF(t)}{dt}\Big|_{t=1} = F''(1)$$

$$\mathbb{V}X = F''(1) + F'(1) - (F'(1))^2$$

We can apply this to

$$F(t) = G_n(1,1,1,t)G_{d;n}(1,1,t,1),$$

however is is simpler to consider the variances of the number of tagged amplicons arising separately from the individual g and g_d strands and add them: because they amplify independently their variances will add to give the total variance of interest. This we now do.

Recall that our basic vectorial **PGF** has the form

$$G_{n+1} \to G_n(1 - p_g) + p_g G_n H_{d;n}$$

$$H_{d;n+1} \to H_{d;n}(1 - p_{h_d}) + p_{h_d} H_{d;n} A_n$$

$$A_{n+1} \to A_n(1 - p_a) + p_a A_n A_{d;n}$$

$$A_{d;n+1} \to A_{d;n}(1 - p_{a_d}) + p_{a_d} A_{d;n} A_n$$

with

$$G_0 = t_g$$

$$H_{d,0} = t_{h_d}$$

$$A_d = t_a$$

$$A_{d,0} = t_{a_d}$$

Differentiating each twice with respect to t_{a_d} and setting all the t's equal to 1 gives this set of linear recurrence relations

$$D^2 G_{n+1} = D^2 G_n + 2p_g DG_n DH_{d;n} + p_g D^2 H_{d;n}$$

$$D^2 H_{d;n+1} = D^2 H_{d;n} + 2p_{h_d} DH_{d;n} DA_n + p_{h_d} D^2 A_n$$

$$D^2 A_{n+1} = D^2 A_n + 2p_a DA_n DA_{d;n} + p_a D^2 A_{d;n}$$

$$D^2 A_{d;n+1} = D^2 A_{d;n} + 2p_{a_d} DA_{d;n} DA_n + p_{a_d} D^2 A_n$$

As before, we consider the last two coupled set of equations. These may be written in matrix form as follows:

$$\begin{pmatrix} D^2A_{n+1} \\ D^2A_{d;n+1} \end{pmatrix} \;=\; \begin{pmatrix} 1 & p_a \\ p_{a_d} & 1 \end{pmatrix}\begin{pmatrix} D^2A_n \\ D^2A_{d;n} \end{pmatrix} \;+\; 2\begin{pmatrix} p_a DA_n DA_{d;n} \\ p_{a_d} DA_{d;n} DA_n \end{pmatrix} \qquad (40)$$

Previously we had the first order solution

$$\begin{pmatrix} DA_n \\ DA_{d;n} \end{pmatrix} \;=\; \begin{pmatrix} 1 & p_a \\ p_{a_d} & 1 \end{pmatrix}^n \begin{pmatrix} 0 \\ 1 \end{pmatrix} \;=\; P^n \begin{pmatrix} 0 \\ 1 \end{pmatrix}$$

where

$$P^n = \frac{1}{2}\begin{pmatrix} (1 + \sqrt{p_a p_{a_d}})^n + (1 - \sqrt{p_a p_{a_d}})^n & , & \sqrt{\frac{p_a}{p_{a_d}}}\big((1 + \sqrt{p_a p_{a_d}})^n - (1 - \sqrt{p_a p_{a_d}})^n\big) \\ \sqrt{\frac{p_{a_d}}{p_a}}\big((1 + \sqrt{p_a p_{a_d}})^n - (1 - \sqrt{p_a p_{a_d}})^n\big) & , & (1 + \sqrt{p_a p_{a_d}})^n + (1 - \sqrt{p_a p_{a_d}})^n \end{pmatrix}$$

hence

$$\begin{pmatrix} DA_n \\ DA_{d;n} \end{pmatrix} \;=\; \frac{1}{2}\begin{pmatrix} \sqrt{\frac{p_a}{p_{a_d}}}\big((1 + \sqrt{p_a p_{a_d}})^n - (1 - \sqrt{p_a p_{a_d}})^n\big) \\ (1 + \sqrt{p_a p_{a_d}})^n + (1 - \sqrt{p_a p_{a_d}})^n \end{pmatrix}$$

and it follows that

$$DA_n DA_{d;n} = \frac{1}{2}\sqrt{\frac{p_{a_d}}{p_a}}\Big((1 + \sqrt{p_a p_{a_d}})^{2n} - (1 - \sqrt{p_a p_{a_d}})^{2n}\Big)$$

This could be substituted into (40) and the resulting in-homogeneous difference equation may be solved (initial conditions are that the second derivatives $D^2A_0 = D^2A_{d;0} = 0$). It gets a bit complicated, so it is simpler to work from the following scalar equation and the substitute matrices for scalar.

So consider the recurrence relation

$$y_{n+1} = p y_n + c(a^n - b^n)$$

where $y_0 = 0$. Iteration gives the solution sequence:

$$y_1 = 0$$
$$y_2 = (a - b)c$$
$$y_3 = p(a - b)c + (a^2 - b^2)c$$
$$y_4 = p^2(a - b)c + p(a^2 - b^2)c + (a^3 - b^3)c$$
$$\vdots$$
$$y_n = \sum_{i=0}^{n-2} p^{n-i}(a^{i+1} - b^{i+1})c$$
$$= \left(a \frac{p^{n-1} - a^{n-1}}{p - a} - b \frac{p^{n-1} - b^{n-1}}{p - b} \right) c$$

Referring back , we may substitute $c = \sqrt{p_{a_d}/p_a}\binom{p_a}{p_{a_d}}$, $a = (1 + \sqrt{p_{a_d}p_a})^2 I$, $b = (1 - \sqrt{p_{a_d}p_a})^2 I$, where I is the 2×2 identity matrix, and $p = P$, to recover a matrix formula for the solution of $y_n \equiv \binom{D^2 A_n}{D^2 A_{d;n}}$.

The result is a fairly complex matrix expression that has to be picked apart to substitute various terms into the equations to solve for the h and h_d, which themselves in turn have to be substituted into equations to solve for g and g_d. This could possibly be done using a computer algebra system, the results can be expected to be messy - even more so when we introduce stutter - so we stop the algebraic analysis here.

It seems appropriate therefore to generate matrix expressions at the outset which would be more amenable to numerical evaluation. We now follow this more direct approach. We could proceed by considering the matrix formulation for g and g_d separately, or by using a combined approach. We do the latter, they lead to the same results.

B.2   Moments from matrix analysis

B.2.1   First moment: Mean as matrix expression

The recurrence relation for the mean may be expressed as

$$
\begin{pmatrix} DG_{n+1} \\ DG_{d;n+1} \\ DH_{n+1} \\ DH_{d;n+1} \\ DA_{n+1} \\ DA_{d;n+1} \end{pmatrix}
=
\begin{pmatrix}
1 & 0 & 0 & p_g & 0 & 0 \\
0 & 1 & p_{g_d} & 0 & 0 & 0 \\
0 & 0 & 1 & 0 & 0 & p_h \\
0 & 0 & 0 & 1 & p_{h_d} & 0 \\
0 & 0 & 0 & 0 & 1 & p_a \\
0 & 0 & 0 & 0 & p_{a_d} & 1
\end{pmatrix}
\begin{pmatrix} DG_n \\ DG_{d;n} \\ DH_n \\ DH_{d;n} \\ DA_n \\ DA_{d;n} \end{pmatrix}
= P
\begin{pmatrix} DG_n \\ DG_{d;n} \\ DH_n \\ DH_{d;n} \\ DA_n \\ DA_{d;n} \end{pmatrix}
$$

where P is now the 6×6 matrix. If we denote the column matrix on the right by Y_n, then we have

$$ Y_{n+1} = PY_n \rightarrow Y_n = P^n Y_0 $$

where Y_0 is the transpose of the row vector $(0, 0, 0, 0, 0, 1)$, and the mean number of tagged amplicons is given by the sum of the elements in the first two rows of Y_n.

Numerically this is straightforward to extract given the values of the various amplification probabilities.

B.2.2 Second moment: as matrix expression

The matrix equation for the second moment follows the pattern of the first order moment matrix equation. Let Z_n denote the column vector of second derivatives, that is

$$
Z_n =
\begin{pmatrix}
D^2 G_n \\
D^2 G_{d;n} \\
D^2 H_n \\
D^2 H_{d;n} \\
D^2 A_n \\
D^2 A_{d;n}
\end{pmatrix}
$$

Then the recurrence equations for the second moments may be written as

$$
Z_{n+1} = PZ_n + 2
\begin{pmatrix}
p_g DG_n DH_{d;n} \\
p_{g_d} DG_{d;n} DH_n \\
p_h DH_n DA_{d;n} \\
p_{h_d} DH_{d;n} DA_n \\
p_a DA_n DA_{d;n} \\
p_{a_d} DA_{d;n} DA_n
\end{pmatrix}
= PZ_n + 2
\begin{pmatrix}
p_g Y_n(1) Y_n(4) \\
p_{g_d} Y_n(2) Y_n(3) \\
p_h Y_n(3) Y_n(6) \\
p_{h_d} Y_n(4) Y_n(5) \\
p_a Y_n(5) Y_n(6) \\
p_{a_d} Y_n(6) Y_n(5)
\end{pmatrix}
$$

where $Y_n(i)$ is the element in the ith row of the column vector Y_n. We have the initial condition $Z_0 = (0, 0, 0, 0, 0, 0)^T$.

Thus we can iterate to solve sequentially for the pairs of column vectors Y_1, Z_1; Y_2, Z_2; ... ; Y_n, Z_n.

Now $Y_n(1)$ will denote the mean number of tagged amplicons arising from the g strand, and $Z_n(1)$ will denote the corresponding expectation $EM(M-1)$ for the number of tagged amplicons arising for the g strand. Hence the variance of tagged amplicons arising form the g strand will be

$$Z_n(1) + Y_n(1) - Y_n^2(1)$$

Similarly the variance of tagged amplicons from the g_d strand will be

$$Z_n(2) + Y_n(2) - Y_n^2(2)$$

Hence the total variance of tagged amplicons will be

$$Z_n(1) + Y_n(1) - Y_n^2(1) + Z_n(2) + Y_n(2) - Y_n^2(2)$$

If there are m genomic strands to begin with, we simply multiply this variance expression by m to get the required total variance.

C   Derivation of moments for genomic model, single stutters

C.1   Moments

The combined set of iterative equations of the branching process is:

$$t_g \rightarrow t_g(1 - p_g) + p_g(1 - \xi)t_g t_{h_d} + p_g \xi t_g t_{h_{sd}}$$
$$t_{g_d} \rightarrow t_{g_d}(1 - p_{g_d}) + p_{g_d}(1 - \xi)t_{g_d}t_h + p_{g_d}\xi t_{g_d}t_{h_s}$$
$$t_{h_d} \rightarrow t_{h_d}(1 - p_{h_d}) + p_{h_d}(1 - \xi)t_{h_d}t_a + p_{h_d}\xi t_{h_d}t_{a_s}$$
$$t_{h_{sd}} \rightarrow t_{h_{sd}}(1 - p_{h_{sd}}) + p_{h_{sd}}t_{h_{sd}}t_{a_s}$$
$$t_h \rightarrow t_h(1 - p_h) + p_h(1 - \xi)t_h t_{a_d} + p_h \xi t_h t_{a_{sd}}$$
$$t_{h_s} \rightarrow t_{h_s}(1 - p_{h_s}) + p_{h_s}t_{h_s}t_{a_s}$$
$$t_a \rightarrow t_a(1 - p_a) + p_a(1 - \xi)t_a t_{a_d} + p_a \xi t_a t_{a_{sd}}$$
$$t_{a_d} \rightarrow t_{a_d}(1 - p_{a_d}) + p_{a_d}(1 - \xi)t_{a_d}t_a + p_{a_d}\xi t_{a_d}t_{a_s}$$
$$t_{a_s} \rightarrow t_{a_s}(1 - p_{a_s}) + p_{a_s}t_{a_s}t_{a_{sd}}$$
$$t_{a_{sd}} \rightarrow t_{a_{sd}}(1 - p_{a_{sd}}) + p_{a_{sd}}t_{a_{sd}}t_{a_s}$$

which lead directly to the coupled set of equations for the vectorial generating function:

$$G_{n+1} = G_n[(1 - p_g) + p_g(1 - \xi)H_{n;d} + p_g \xi H_{n;sd}]$$
$$G_{n+1;d} = G_{n;d}[(1 - p_{g_d}) + p_{g_d}(1 - \xi)H_n + p_{g_d}\xi H_{n;s}]$$
$$H_{n+1} = H_n[(1 - p_h) + p_h(1 - \xi)A_{n;d} + p_h \xi A_{n;sd}]$$
$$H_{n+1;d} = H_{n;d}[(1 - p_{h_d}) + p_{h_d}(1 - \xi)A_n + p_{h_d}\xi A_{n;s}]$$
$$H_{n+1;s} = H_{n+1;s}[(1 - p_{h_s}) + p_{h_s}A_{n;sd}]$$
$$H_{n+1;sd} = H_{n;sd}[(1 - p_{h_{sd}}) + p_{h_{sd}}A_{n;s}]$$
$$A_{n+1} = A_n[(1 - p_a) + p_a(1 - \xi)A_{n;d} + p_a \xi A_{n;sd}]$$
$$A_{n+1;d} = A_{n;d}[(1 - p_{a_d}) + p_{a_d}(1 - \xi)A_n + p_{a_d}\xi A_{n;s}]$$
$$A_{n+1;s} = A_{n;s}[(1 - p_{a_s}) + p_{a_s}A_{n;sd}]$$
$$A_{n+1;sd} = A_{n;sd}[(1 - p_{a_{sd}}) + p_{a_{sd}}A_{n;s}]$$

147

Differentiating once for the mean, we obtain the matrix equation

$$
\begin{pmatrix} DG_{n+1} \\ DG_{n+1;d} \\ DH_{n+1} \\ DH_{n+1;d} \\ DH_{n+1;s} \\ DH_{n+1;sd} \\ DA_{n+1} \\ DA_{n+1;d} \\ DA_{n+1;s} \\ DA_{n+1;sd} \end{pmatrix} =
\begin{pmatrix}
1 & 0 & 0 & p_g(1-\xi) & 0 & p_g\xi & 0 & 0 & 0 & 0 \\
0 & 1 & p_{g_d}(1-\xi) & 0 & p_{g_d}\xi & 0 & 0 & 0 & 0 & 0 \\
0 & 0 & 1 & 0 & 0 & 0 & 0 & p_h(1-\xi) & 0 & p_h\xi \\
0 & 0 & 0 & 1 & 0 & 0 & p_{h_d}(1-\xi) & 0 & p_{h_d}\xi & 0 \\
0 & 0 & 0 & 0 & 1 & 0 & 0 & 0 & 0 & p_{h_s} \\
0 & 0 & 0 & 0 & 0 & 1 & 0 & 0 & p_{h_{sd}} & 0 \\
0 & 0 & 0 & 0 & 0 & 0 & 1 & p_a(1-\xi) & 0 & p_a\xi \\
0 & 0 & 0 & 0 & 0 & 0 & p_{a_d}(1-\xi) & 1 & p_{a_d}\xi & 0 \\
0 & 0 & 0 & 0 & 0 & 0 & 0 & 0 & 1 & p_{a_s} \\
0 & 0 & 0 & 0 & 0 & 0 & 0 & 0 & p_{a_{sd}} & 1
\end{pmatrix}
\begin{pmatrix} DG_n \\ DG_{n;d} \\ DH_n \\ DH_{n;d} \\ DH_{n;s} \\ DH_{n;sd} \\ DA_n \\ DA_{n;d} \\ DA_{n;s} \\ DA_{n;sd} \end{pmatrix}
$$

Denoting the 10×10 square matrix by P, and the column matrix on the right by Y_n, then we have

$$Y_{n+1} = PY_n \rightarrow Y_n = P^n Y_0$$

where Y_0 is the transpose of the row vector $(0, 0, 0, 0, 0, 0, 0, 0, 0, 1)$, and the mean number of tagged amplicons is given by the sum of the elements in the first two rows of Y_n. This will be equal to $P^n[1, 10] + P^n[2, 10]$.

Let Z denote the column of second derivatives, then we have the following in-homogeneous matrix recurrence relation that is readily solved numerically by iteration:

$$
Z_{n+1} = PZ_n + 2
\begin{pmatrix}
p_g DG_n[(1-\xi)DH_{n;d} + \xi DH_{n;sd}] \\
p_{g_d} DG_{n;d}[(1-\xi)DH_n + \xi DH_{n;s}] \\
p_h DH_n[(1-\xi)DA_{n;d} + \xi DA_{n;sd}] \\
p_{h_d} DH_{n;d}[(1-\xi)DA_n + \xi DA_{n;s}] \\
p_{h_s} DH_{n;s} DA_{n;sd} \\
p_{h_{sd}} DH_{n;sd} DA_{n;s} \\
p_a DA_n[(1-\xi)DA_{n;d} + \xi DA_{n;sd}] \\
p_{a_d} DA_{n;d}[(1-\xi)DA_n + \xi DA_{n;s}] \\
p_{a_s} DA_{n;s} DA_{n;sd} \\
p_{a_{sd}} DA_{n;sd} DA_{n;s}
\end{pmatrix}
$$

and similarly to before, the total variance of tagged amplicons in stutter position is given by

$$Z_n(1) + Y_n(1) - Y_n^2(1) + Z_n(2) + Y_n(2) - Y_n^2(2)$$

148

C.2 Covariance with main peak

The vectorial generating function may be used to find the mean and variance of the main peak, and also the covariance between main peak and stutter peak. For the main peak, the mean height is given by multiplying P^n into the column matrix that has zero everywhere except for a 1 on the seventh row, and then adding the values in the first two rows of the resulting column matrix. The variance is similarly found.

The second derivatives obey the following recurrence relation.

$$
\begin{pmatrix}
DDsG_{n+1} \\
DDsG_{n+1;d} \\
DDsH_{n+1} \\
DDsH_{n+1;d} \\
DDsH_{n+1;s} \\
DDsH_{n+1;sd} \\
DDsA_{n+1} \\
DDsA_{n+1;d} \\
DDsA_{n+1;s} \\
DDsA_{n+1;sd}
\end{pmatrix}
= P
\begin{pmatrix}
DDsG_n \\
DDsG_{n;d} \\
DDsH_n \\
DDsH_{n;d} \\
DDsH_{n;s} \\
DDsH_{n;sd} \\
DDsA_n \\
DDsA_{n;d} \\
DDsA_{n;s} \\
DDsA_{n;sd}
\end{pmatrix}
+
\begin{pmatrix}
p_g DG_n[(1-\xi)DsH_{n:d}+\xi DsH_{n;sd}] \\
p_{g_d} DG_{n;d}[(1-\xi)DsH_n+\xi DsH_{n;s}] \\
p_h DH_n[(1-\xi)DsA_{n;d}+\xi DsA_{n;sd}] \\
p_{h_d} DH_{n;d}[(1-\xi)DsA_n+\xi DsA_{n;s}] \\
p_{h_s} DH_{n;s} DsA_{n;sd} \\
p_{h_{sd}} DH_{n;sd} DsA_{n;s} \\
p_a DA_n[(1-\xi)DsA_{n;d}+\xi DsA_{n;sd}] \\
p_{a_d} DA_{n;d}[(1-\xi)DsA_n+\xi DsA_{n;s}] \\
p_{a_s} DA_{n;s} DsA_{n;sd} \\
p_{a_{sd}} DA_{n;sd} DsA_{n;s}
\end{pmatrix}
+
\begin{pmatrix}
p_g DsG_n[(1-\xi)DH_{n:d}+\xi DH_{n;sd}] \\
p_{g_d} DsG_{n;d}[(1-\xi)DH_n+\xi DH_{n;s}] \\
p_h DsH_n[(1-\xi)DA_{n;d}+\xi DA_{n;sd}] \\
p_{h_d} DsH_{n;d}[(1-\xi)DA_n+\xi DA_{n;s}] \\
p_{h_s} DsH_{n;s} DA_{n;sd} \\
p_{h_{sd}} DsH_{n;sd} DA_{n;s} \\
p_a DsA_n[(1-\xi)DA_{n;d}+\xi DA_{n;sd}] \\
p_{a_d} DsA_{n;d}[(1-\xi)DA_n+\xi DA_{n;s}] \\
p_{a_s} DsA_{n;s} DA_{n;sd} \\
p_{a_{sd}} DsA_{n;sd} DA_{n;s}
\end{pmatrix}
$$

D A further look at target and stutter peak height correlations

In Bright et al. (2013) the authors looked at developing a model for the stutter ratio, defined as the ratio of the stutter peak to main peak, such that the mean stutter ratio is linearly dependent on the *longest uninterrupted sequence* (LUS) of repeats. They used controlled experimental single-source samples, 289 in all, with a target of 1ng of DNA and amplified with a 25 RFU detection limit. After discarding loci which had heterozygous loci one repeat apart, 2323 heterozygous loci were left for analysis.

It is important to note that they define stutter ratio as the ratio of the stutter peak height to the main peak height:

$$
SR_a = \frac{O_{a-1}}{O_a}
$$

They define the total allelic product to be

$$
T_a = O_{a-1} + O_a
$$

They propose a lognormal distribution for the ratio of observed to expected peak height for main and stutter peaks (they comment that a gamma model is not suitable because of the heavy tails). From their data they conclude that there is little evidence of correlation between the main and stutter peaks given the target amount of DNA. They write: "Unexpectedly the scatter plots in Fig. 8a and b indicate that there is no detectable correlation between stutter and allele in this biological model". They found a low correlation of around 0.11.

Now clearly having little to no correlation is quite at variance with the branching **PCR** model. We suggest that this is an artefact of grouping the data together within and across loci. First we recast their results. In their Appendix 2 they give the following table for the linear regression of their stutter ratio model (using the NGM SELect system), in which the stutter ratio of an allele i, having LUS L_i, from a locus is equal to $SR_i = a + b \times L_i$:

	Locus	Intercept a	Slope b
1	D10S1248	-0.0576	0.0089
2	D12S391	-0.0571	0.0107
3	D16S539	-0.0502	0.0088
4	D18S51	-0.0297	0.0066
5	D19S433	-0.0302	0.0074
6	D1S1656	-0.0699	0.0106
7	D21S11	-0.0079	0.0059
8	D22S1045	-0.0881	0.0139
9	D2S1338	-0.0073	0.0062
10	D2S441	0.0004	0.0031
11	D3S1358	-0.0455	0.0092
12	D8S1179	-0.0148	0.0062
13	FGA	-0.0344	0.0066
14	SE33	0.0129	0.0041
15	TH01	-0.0208	0.0052
16	vWA	-0.0354	0.0078

Now from the simple amplicon model, with amplification probability p and conditional stutter probability ξ, the expected number of amplicons heights for main and stutter peaks given k cycles and starting from n_0 amplicons, are given by

$$ET = n_0(1 + p(1 - \xi))^k$$
$$ES = n_0[(1 + p)^k - (1 + p(1 - \xi))^k]$$

Thus we can approximate, with ξ dependent on L:

$$SR = a + bL \approx \frac{ES}{ET} = \left(\frac{1 + p}{(1 + p(1 - \xi))}\right)^k - 1 \approx \frac{kp}{1 + p}\xi + \frac{k(k - 1)p^2}{2(1 + p)^2}\xi^2 + 0(\xi^3)$$

From this we obtain to a good approximation, by taking the linear term only, the incremental change in mean stutter ratio by a unit increase in LUS:

$$\Delta\xi = b\frac{1 + p}{kp}$$

For $p \in [0.8, 1]$, $(1 + p)/p$ varies between 2 and 2.25, hence to a good approximation $\Delta\xi = 2b/k$.

So now we can collect results. Given the nature of the experimental setup, with a target DNA amount of 1ng, (corresponding to around 152 cells) we may take the number of alleles from a heterozygous marker to be $Pois(152)$. In addition the LUS in their plots varies from 10-15 for most markers, some having a larger range, some smaller. So for simplicity we shall simulate LUS values from the same range for each of the 16 markers, (also corresponding therefore to a uniform distribution of alleles). The following table collects individual marker correlations, based on around 2000 simulations on each marker, under various scenarios, but using the ξ values for each marker using the SR formula above; we take $k = 28$ and $p = 0.85$ in all simulations.

Locus	LUS=12 $n_0 = 152$	LUS=12 $n_0 \sim Pois(152)$	LUS~Unif[8,15] $n_0 = 152$	LUS~Unif[8,15] $n_0 \sim Pois(152)$
D10S1248	0.2005406	0.7255809	-0.5541554	-0.07269729
D12S391	0.2290437	0.773266	-0.6050955	-0.04926867
D16S539	0.2054748	0.7379974	-0.5366395	-0.03364616
D18S51	0.1665038	0.7108246	-0.4260814	0.06089547
D19S433	0.248041	0.7182632	-0.4844209	0.06972643
D1S1656	0.1848627	0.7401926	-0.6481533	-0.0976838
D21S11	0.1952987	0.7507546	-0.3596321	0.2097556
D22S1045	0.217241	0.7738013	-0.7170921	-0.1489542
D2S1338	0.2145392	0.7708068	-0.3787377	0.1656755
D2S441	0.1509088	0.6713596	-0.1463518	0.2585785
D3S1358	0.2333797	0.7477239	-0.5480802	-0.03041745
D8S1179	0.2451524	0.731677	-0.3884186	0.1381175
FGA	0.1308529	0.6779035	-0.4587745	0.06434562
SE33	0.1765904	0.6558634	-0.2304545	0.1803573
TH01	0.1666116	0.6661396	-0.3677087	0.1420518
vWA	0.1850046	0.7455873	-0.5083684	0.0339069

We see that keeping LUS and n_0 fixed we get moderate correlations as in earlier chapter. Making the starting number of alleles Poisson distributed and keeping LUS fixed leads to high correlation between the stutter and peak amplicon numbers, also as found earlier. Now making LUS random (to simulate a range of genotypes) but keeping n_0 fixed the correlations are negative. Combining the randomization of LUS and making $n_0 \sim Pois(132)$ yields the correlations in the final column, which are largely quite small with some positive and some negative.

Finally we do a simulation in which we aggregate the various loci simulations: here are 16 runs of such a simulation which mirrors the experimental data of Bright et al. (2013). We see that all the correlations are negative, but very close to zero.

|			
-0.003916072	-0.02691701	-0.0257117	-0.03113958
-0.02115133	-0.02109356	-0.02308784	-0.05802165
-0.02720094	-0.0288306	-0.0345473	-0.07301637
-0.01966967	-0.031646	-0.0649325	-0.02202189

The following scatterplot was obtained from one simulation, in which we plot the log of the sumulated number of amplicons divided by their expected number

(itself estimated from simulation) for the target and stutter alleles, so that it corresponds to the quantities plotted in Figure 8b of Bright et al. (2013). The plot below has a smaller range than their Figure 8b, which could be because we have simulated from the amplicon model rather than the genomic model. The sample correlation of the points in the plot is 0.157, close to the figure of 0.11 they found from their experimental data.
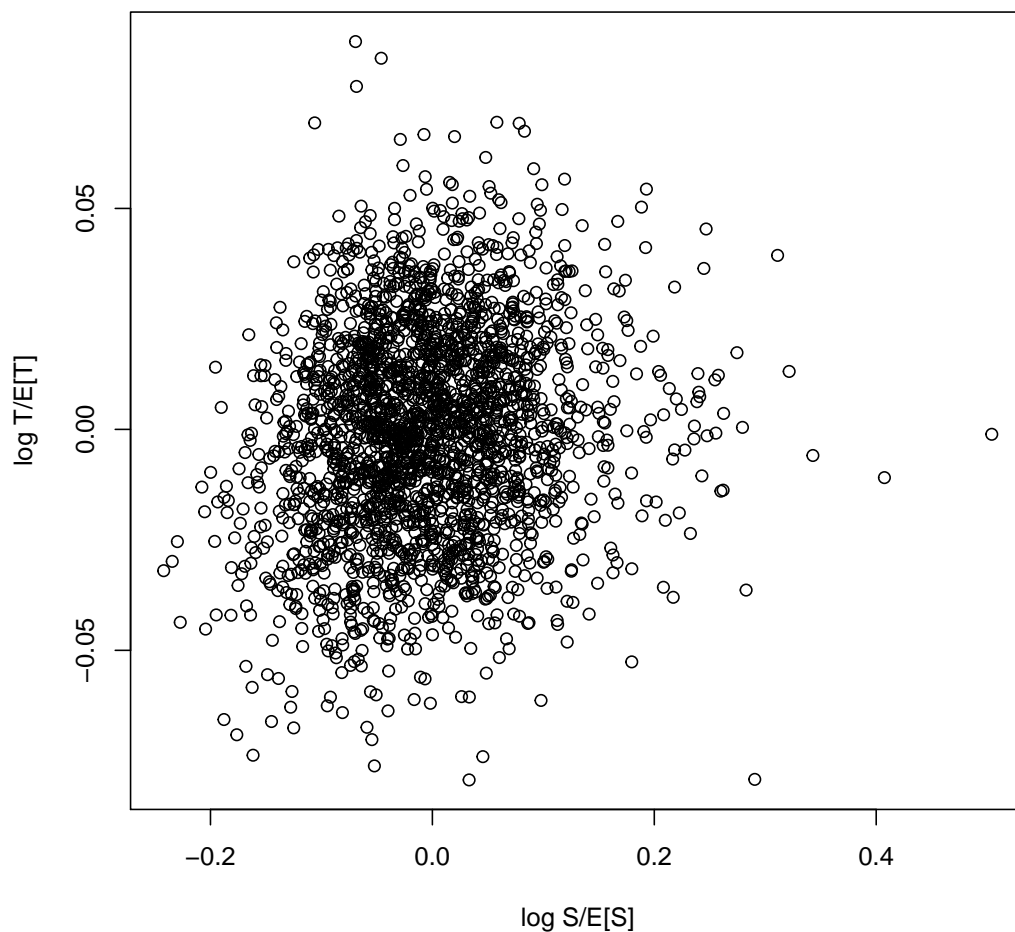
Hence, on the basis of this simulation, we deduce that the bivariate **PCR** branching process model showing high main allele and stutter-peak correlations

153

on individual alleles is compatible with the experimental results of Bright et al. (2013) which aggregates observations of alleles within and between loci.

Support for this may be found in a dataset of experimental single source and mixed profiles released by Boston University in 2012[7] These were samples prepared from extracted DNA from 4 anonymous individuals (labelled A,B,C and D) diluted to prepare controlled DNA amounts, and amplified for four kits. In the single source samples there many independent amplifications of each individual's DNA, allowing the target-stutter peak height data to be found for individual alleles for a given amount of initial DNA, making sure that neither are "contaminated" by neighbouring alleles. Looking at the genotypes , we see that for person A allele 25 on the locus D2D1338 is a possible target allele. Taking all the single source samples on 1ng and 10 seconds injection time for person A amplified with the Identifiler^{TM}kit (chosen here because it yields the most number of data points), the author extracted target (25) and stutter (24) peak height values to produce the following scatterplot , having a sample correlation of 0.929.
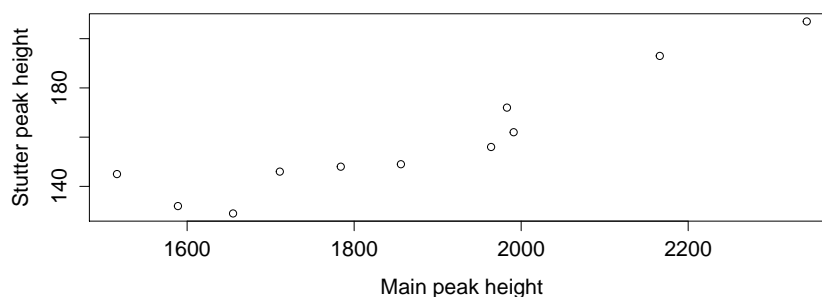
Bearing in mind the way the samples were prepared, we should expect Poisson sampling for the initial number of amplicons prior to **PCR**, and hence expect a high correlation to result as found. Looking at the stutter proportions (stutter/total) which average around 0.08 for the 11 data points, we see that the results are very consistent with **PCR** branching modelling approach for stutter.

In conclusion, we suggest that the combined effects of aggregating across loci and alleles might be giving a misleading impression that there is no significant correlation. Dedicated experiments concentrating on specific alleles and their stutter product, that do not aggregate data over different alleles either within or between loci, could be carried out to confirm or refute this.

---

[7]see `http://www.bu.edu/dnamixtures/pages/help/introduction/`

E   Sample code for generating distributions and plots

E.1   Python scripts

E.1.1   code for Figure 3.

```python
import numpy as np
import matplotlib.pyplot as plt
from scipy.stats.kde import gaussian_kde


K = 28
M=1
phi = 2.0/9
p = 0.8


N = np.ones(100000).astype(int)
N = N*M
n = np.random.binomial(N,phi)


for k in range(K):
    m = np.random.binomial(n, p)
    n = n+m


# find total dropout probability,
pdrop = float(len(n[n==0]))/len(n)
# remove zeros for the kernel density estimate
n = n[n != 0]


# find the kernel density estimate
pcr_dist = gaussian_kde(n)


# plot it out
x = np.linspace(1,3.0e7,1000)


fig = plt.figure()
plt.plot(x, pcr_dist(x),'r')
```

E.1.2 code for Figure 4

```python
import numpy as np
import matplotlib.pyplot as plt

def singleAmpliconPCR(p,K, M, phi):
    N = M*2**K
    a = np.zeros(N)
    a[1] = 1.0
    afft = np.fft.fft(a)
    for k in xrange(K):
        afft = (1-p)*afft + p*afft*afft
    afft = (1-phi + phi*afft)**M
    pn  = np.fft.ifft(afft)
    pn = pn.real
    return pn

pn = singleAmpliconPCR(p=0.8,K=28,M=1, phi=2.0/11)
n = range(len(pn))
pdrop = pn[0]
pn[0] = 0
plt.plot(n,pn,'-')
```

E.1.3 code for Algorithm 5.5

Algorithm E.1 [JOINT DISTRIBUTION FOR TARGET AND STUTTER AMPLICONS: PYTHON CODE]

```python
import numpy as np
from scipy.fftpack import fftn, ifftn

def ampliconStutterPCR(p, xi, K, M, phi):
    N = M*2**K
    NT = N
    NS = N
    F = np.zeros((NT,NS))
    F[1,0] = 1
    F = fftn(F)
```

```
        G = np.zeros(NS)
        G[1] = 1
        G = fftn(G)
        for k in xrange(K):
            for g in xrange(NS):
                for  f in xrange(NT) :
                    F[f,g] = F[f,g]*(1-p + p*(1-xi)*F[f,g]+ p*xi*G[g])
                G[g] = G[g]*(1-p + p*G[g])
            F[f,g] = (1-phi + phi*F[f,g])**M
        F = ifftn(F)
        F = F.real
        return F                                                    □
```

Note that even for $M = 1$ and with a typical $K = 28$ cycles in **PCR**, the size of the 2-dimensional array F to hold the joint distribution will be $N = 2^{56} \approx 7.2 \times 10^{16}$, which is far in excess of the memory of any computer. To fill the array with double precision values would require approximation 4.2 billion Gigabytes of Ram. Filling the array would also take an excessive amount of time. Hence this should be used only for small K and M values.

E.1.4   code for Algorithm 5.6

Algorithm E.2 [MARGINAL DISTRIBUTION FOR STUTTER AMPLICONS: PYTHON CODE]

```
import numpy as np
from scipy.fftpack import fftn, ifftn

def  ampliconStutterMarginalPCR(p, xi, K, M, phi):
    N = M*2**K
    F = np.zeros(N)
    F[0] = 1
    F = fftn(F)
    G = np.zeros(N)
    G[1] = 1
    G = fftn(G)
    for k in xrange(K):
        F *= 1-p + p*(1-xi)*F+ p*xi*G
        G *= 1-p + p*G
```

```
F = (1-phi + phi*F)**M
F = ifftn(F)
F = F.real
return F
```

□

E.2 R scripts

E.2.1 code for generating target marginal distribution, no stutters

R code for the distribution of the total number of amplicons arising from K amplification cycles, amplification probability p on each cycle, starting with M amplicons binomially sampled prior to amplification with probability ϕ. Note that R vector indices start at 1 instead of 0, hence on line 3 we set $F[2] = 1$ (rather than $F[1] = 1$).

Algorithm E.3 [AMPLICON PROBABILITY DISTRIBUTION USING R]

```
N = M*2**K
F = rep(0,N)
F[2] = 1
F = fft(F,inverse=FALSE)
for (k in 1:K) F = (1 - p)*F + p*F*F    # K amplifications cycles
F = (1-phi + phi*F)**M                  # binomial sampling
F = Re(fft(F,inverse=TRUE)) /N           # real part of inverse
```

□

E.2.2 code to generate Figure 6

```
K=15
Th= 40000
M = 200
phi = 0.1
p = 0.85
N = M*2**K
F = rep(0,N)
F[2] = 1
F = fft(F,inverse=FALSE)
for (k in 1:K) F = (1 - p)*F + p*F*F     # K amplifications cycles
Fphi = 1-phi + phi*F
pdhet = NULL
pdhom = NULL
for (m in 5:M){
# heterozygous
```

```
G = Fphi**m                        # binomial sampling
G = Re(fft(G,inverse=TRUE)) /N             # real part of inverse
G = cumsum(G)
pdhet = c(pdhet, G[Th])
# use double m for homozygous
G = Fphi**(2*m)
G = Re(fft(G,inverse=TRUE))  /N
G = cumsum(G)
pdhom = c(pdhom, sum(G[Th]))
cat ("m = ", m, "\n")
}
m = 5:M
plot(pdhet~m,log="x", ylim = c(0,1), typ="l", xlab = "Number of cells",
ylab = "Dropout probability P(D)")
par(new=T)
plot(pdhom~m, col="red", log="x", ylim=c(0,1), typ="l",
xlab = "Number of cells",  ylab = "Dropout probability P(D)")
```

E.2.3 code for generating marginal distributions for the genomic model, implementing Algorithm 6.1

```
N = M*2^K
  g = rep(0,N)
  g[1]=1
  g = FFT(g)

  gd = h = hd = hs = hsd  = a = ad = as = g
  asd = rep(0,N)
  asd[2]=1  # note use of index 2.
  asd = FFT(asd)

for (k in 1:K){
  g = g*(1-q + q*hd)
  gd = gd*(1-q + q*h)
  hd = hd*(1-p + p*a)
  h = h*(1-p + p*ad)
  at  = a     # temporary copy to break the cyclic dependency of a and ad
  atd = ad     # temporary copy to break the cyclic dependency of a and ad
```

```
  ad = atd*(1-p + p*at)
  a = at*(1-p + p*atd)
}

# the final probability distribution of interest.
pn = Re(IFFT( (1 -phi + phi*g*gd)^M ))
```

E.3 Julia scripts

E.3.1 code for generating Figure 19

Julia, like R, uses arrays with indices starting from 1. You will need to install the PyPlot package to run this script, and will require approximately 10Gb of free ram to do the full **FFT** evaluation with $K = 28$.

```julia
using PyPlot

# function for full fft analysis
function maindist(p::Float64, K::Int64)
    N = 2^K
    y= zeros(N)
    y[2] = 1
    y=fft(y)
    for i in 1:N
        for k in 1:K
            y[i] = y[i]*(1-p+p*y[i])
        end
    end
    y=ifft(y)
    return y
end

# truncated analysis
function maintrunc1(p::Float64, K::Int64, npos::Int64,  L::Int64)
    N = 2^K
    pn = 1.0
    for j in 2:L
        x = exp(-2pi*im*(j-1)/N)
        for k in 1:K
            x = x*(1-p + p*x)
        end
        x = x*exp(2pi*im*(npos-1)*(j-1)/N)
        pn = pn + 2*real(x)
    end
    return pn /N
end
```

```
p = 0.85
K = 28
cy = maindist(p, 28)

# pick a subset of points for the plot, to speed up the plotting
step = 60000
xv = [ i*step for i in 1:1000]
pnfull = [real(cy[i*step]) for i in 1:1000]
# generate the truncated values
pntruncated =  [maintrunc1(p, K, i*step,1024)    for i in 1:1000]

xlabel("Number of amplicons, n")
ylabel("P(n)")
fig, ax = subplots()
ax[:plot](xv,pnfull, label = "FFT")
ax[:plot](xv,pntruncated , label = "truncated")
ax[:legend]()
title("p = 0.85, K = 28")
```

References

L. E. Alfonse, A. D. Garrett, H. Swaminathan, K. C. Peters, G. Wellner, X. Yearwood-Garcia, L. M. Taranow, S. Lun, K. R. Duffy, M. Médard, et al. The development and release of a collection of computational tools and a large-scale empirical data set for validation: The PROVEDIt initiative. In *International Symposium on Human Identification*, 2016.

L. E. Alfonse, A. D. Garrett, D. S. Lun, K. R. Duffy, and C. M. Grgicak. A large-scale dataset of single and mixed-source short tandem repeat profiles to inform human identification strategies: PROVEDIt. *Forensic Science International: Genetics*, 32:62–70, 2018.

D. Balding. Evaluation of mixed-source, low-template DNA profiles in forensic science. *Proceedings of the National Academy of Sciences of the United States of America*, 110(30):12241–12246, 2013.

D. J. Balding. *Weight-of-evidence for Forensic DNA Profiles*. Statistics in Practice. Wiley, Chichester, UK, 2005.

D. J. Balding and C. D. Steele. *Weight-of-evidence for Forensic DNA Profiles*. John Wiley & Sons, 2015.

Ø. Bleka, G. Storvik, and P. Gill. Euroformix: an open source software based on a continuous model to evaluate str dna profiles from a mixture of contributors with artefacts. *Forensic Science International: Genetics*, 21:35–44, 2016.

Ø. Bleka, M. Eduardoff, C. Santos, C. Phillips, W. Parson, and P. Gill. Open source software euroformix can be used to analyse complex SNP mixtures. *Forensic Science International: Genetics*, 31:105–110, 2017.

M. Bodner, I. Bastisch, J. M. Butler, R. Fimmers, P. Gill, L. Gusmão, N. Morling, C. Phillips, M. Prinz, P. M. Schneider, et al. Recommendations of the dna commission of the international society for forensic genetics (isfg) on quality control of autosomal short tandem repeat allele frequency databasing (strider). *Forensic Science International: Genetics*, 24:97–102, 2016.

J.-A. Bright, D. Taylor, J. M. Curran, and J. S. Buckleton. Developing allelic and stutter peak height models for a continuous method of DNA interpretation. *Forensic Science International: Genetics*, 7(2):296–304, 2013.

J. M. Butler. *Forensic DNA Typing: Biology, Technology, and Genetics of STR Markers, Second Edition*. Elsevier Academic Press, 2005. ISBN 0121479528.

J. M. Butler. *Advanced topics in forensic DNA typing: methodology*. Academic Press, 2011.

J. M. Butler. *Advanced topics in forensic DNA typing: interpretation*. Academic Press, 2014.

J. M. Butler, R. Schoske, P. M. Vallone, J. W. Redman, and M. C. Kline. Allele frequencies for 15 autosomal loci on U.S. Caucasian, African American, and Hispanic populations. *Journal of Forensic Science*, 48(4):908–911, 2003. Available online at www.astm.org.

R. Cowell. Combining allele frequency uncertainty and population substructure corrections in forensic dna calculations. *Forensic Science International: Genetics*, 23:210–216, 2016.

R. Cowell, T. Graversen, S. Lauritzen, and J. Mortera. Analysis of forensic DNA mixtures with artefacts. *Journal of the Royal Statistical Society: Series C (Applied Statistics)*, 64(1):1–48, 2015.

R. G. Cowell. Validation of an STR peak area model. *Forensic Science International: Genetics*, 3(3):193–199, 2009. ISSN 1872-4973. doi: 10.1016/j.fsigen.2009.01.006. URL `http://www.sciencedirect.com/science/article/pii/S1872497309000088`.

K. Duffy, N. Gurram, K. C Peters, G. Wellner, and C. Grgicak. Exploring str signal in the single- and multi-copy number regimes: Deductions from an in silico model of the entire dna laboratory process. *Electrophoresis*, 38, 12 2016.

T. Egeland, I. Dalen, and P. F. Mostad. Estimating the number of contributors to a DNA profile. *International journal of legal medicine*, 117(5):271–275, 2003.

T. Egeland, D. Kling, and P. Mostad. *Relationship inference with familias and R: statistical methods in forensic genetics*. Academic Press, 2015.

I. W. Evett and B. S. Weir. *Interpreting DNA evidence: statistical genetics for forensic science*. Sunderland, Massachusetts, 1998.

I. Findlay, R. Frazier, A. Taylor, and A. Urquhart. Single cell DNA fingerprinting for forensic applications. *Nature*, 389:555–556, 1997.

P. Gill, J. Curran, and K. Elliot. A graphical simulation model of the entire DNA process associated with the analysis of short tandem repeat loci. *Nucleic Acids Research*, 33(2):632–643, 2005.

I. Good. The joint distribution for the sizes of the generations in a cascade process. In *Mathematical Proceedings of the Cambridge Philosophical Society*, volume 51, pages 240–242. Cambridge University Press, 1955.

I. J. Good. The number of individuals in a cascade process. *Proceedings of the Cambridge Philosophical Society*, 45:360–363, 1949.

I. J. Good. *Probability and the Weighing of Evidence*. C. Griffin London, 1950.

I. J. Good. Studies in the History of Probability and Statistics. XXXVII A. M. Turing's statistical work in World War II. *Biometrika*, 66(2):393–396, 1979.

T. Graversen and S. Lauritzen. Computational aspects of DNA mixture analysis. *Statistics and Computing*, 25(3):527–541, 2015.

K. Grisedale and A. van Daal. Method summary. *Biotechniques*, 56(3):145–147, 2014.

H. Haned. *forensim: Statistical tools for the interpretation of forensic DNA mixtures*, 2013. URL `https://CRAN.R-project.org/package=forensim`. R package version 4.3.

H. Haned, L. Pene, J. R. Lobry, A. B. Dufour, and D. Pontier. Estimating the number of contributors to forensic DNA mixtures: does maximum likelihood perform better than maximum allele count? *Journal of forensic sciences*, 56 (1):23–28, 2011.

M. Heideman, D. Johnson, and C. Burrus. Gauss and the history of the fast fourier transform. *IEEE ASSP Magazine*, 1(4):14–21, 1984.

A. J. Jeffreys, A. J. Wilson, and S. L. Thein. Individual specific 'fingerprints' of human DNA. *Nature*, 316:76–79, 1985.

S. L. Lauritzen and J. Mortera. Bounding the number of contributors to mixed DNA stains. *Forensic science international*, 130(2):125–126, 2002.

D. V. Lindley. A problem in forensic science. *Biometrika*, 64(2):207–213, 1977.

M. Perlin and B. Szabady. Linear mixture analysis: a mathematical approach to resolving mixed DNA samples. *Journal of Forensic Science*, 46:1372–1378, 2001.

R. Puch-Solis. A dropin peak height model. *Forensic Science International: Genetics*, 11:80–84, 2014.

R Core Team. *R: A Language and Environment for Statistical Computing*. R Foundation for Statistical Computing, Vienna, Austria, 2016. URL `https://www.R-project.org/`.

K. R. Rao, D. N. Kim, and J. J. Hwang. *Fast Fourier Transform-Algorithms and Applications*. Springer Science & Business Media, 2011.

T. F. Scientific. Ampflstr® identifiler® plus pcr amplification kit user's guide. *Waltham, MA, USA: Thermo Fisher Scientific*, 2012.

G. Stolovitzky and G. Cecchi. Efficiency of DNA replication in the polymerase chain reaction. *Proceedings of the National Academy of Sciences*, 93:12947–12952, 1996a.

G. Stolovitzky and G. Cecchi. Efficiency of DNA replication in the polymerase chain reaction. *Proceedings of the National Academy of Sciences*, 93(23):12947–12952, 1996b.

F. Sun. The polymerase chain reaction and branching processes. *Journal of Computational Biology*, 2(1):63–86, 1995.

H. Swaminathan, C. M. Grgicak, M. Medard, and D. S. Lun. Nocit: A computational method to infer the number of contributors to DNA samples analyzed by STR genotyping. *Forensic Science International: Genetics*, 16:172–180, 2015.

T. Tvedebrink, P. S. Eriksen, H. S. Mogensen, and N. Morling. Estimating the probability of allelic drop-out of STR alleles in forensic genetics. *Forensic Science International: Genetics*, 3(4):222–226, 2009.

T. Tvedebrink, P. S. Eriksen, H. S. Mogensen, and N. Morling. Evaluating the weight of evidence by using quantitative short tandem repeat data in DNA mixtures. *Applied Statistics*, 59(5):855 – 874, 2010.

T. Tvedebrink, P. S. Eriksen, M. Asplund, H. S. Mogensen, and N. Morling. Allelic drop-out probabilities estimated by logistic regression—further considerations and practical implementation. *Forensic Science International: Genetics*, 6(2):263–267, 2012a.

T. Tvedebrink, P. S. Eriksen, H. S. Mogensen, and N. Morling. Identifying contributors of DNA mixtures by means of quantitative information of STR typing. *Journal of Computational Biology*, 19(7):887–902, 2012b. doi: 10.1089/cmb.2010.0055.

P. S. Walsh, H. A. Erlich, and R. Higuchi. Preferential pcr amplification of alleles: mechanisms and solutions. *Genome Research*, 1(4):241–250, 1992.

T. Wang, N. Xue, and J. D. Birdwell. Least-square deconvolution: A framework for interpreting short tandem repeat mixtures. *Journal of Forensic Sciences*, 51 (6):1284–1297, 2006.

J. Weusten and J. Herbergs. A stochastic model of the processes in PCR based amplification of STR DNA in forensic applications. *Forensic Science International: Genetics*, 6(1):17–25, 2012. URL `doi:10.1016/j.fsigen.2011.01.003`.